# COMPLEX CHOLINERGIC SIGNALING IN THE MOUSE INTESTINAL EPITHELIUM

by
Kelli Johnson

A dissertation submitted to Johns Hopkins University in conformity with the requirements for the degree

of Doctor of Philosophy

Baltimore, Maryland
May 2021

# Abstract

Epithelial enteroids are an evolving *ex vivo* model of intestinal physiology and pathophysiology. As a model, the enteroids contain limited populations and restricted physiology, but the simpler system reduces the variables and confounding complexity of whole tissues or bodies during physiological research. Restoring small pieces of complexity in the form of physical traits, differentiation and development, or including additional populations allows for greater application of limited model systems. Here we describe methods to expand on the original mouse enteroid culture system in the form of differentiation of the cultures, generating monolayers, and co-culturing with the sub-mucosal plexus population of the enteric nervous system. The development and characterization of new *ex vivo* modelling of the enteroids revealed physiology previously unobserved that redefines our understanding of cholinergic signaling in the intestine and potentially other systems. The newly defined nicotinic component and increasing complexity of our understanding of cholinergic signaling has implications in both our fundamental understanding of cholinergic signaling and secretion in the intestinal epithelium, but also in clinical considerations of secretory pathophysiology such as various diarrheal diseases and their treatment. The enteroid monolayer model offers a system with which to further interrogate the complex mechanism of cholinergic signaling in the intestinal epithelium.


**Primary Reader and Advisor:** Dr. Mark Donowitz

**Secondary Reader:** Dr. Subhash Kulkarni

# Dedication

This work is dedicated to my family, by blood and choice,

who never doubted that a seven-year-old could cure cancer.

Thank you for believing in me.

# Contents

# List of Tables

# List of Figures

# I. Introduction

The study of living organisms is endlessly complicated. From small, single base pair changes in the DNA code to environmental factors, there are uncountable influences pushing and pulling on all organisms every day.

The study of intestinal physiology is advancing beyond reliance on cancer cell lines and animal models to now include the use of stem cell derived organoids, called enteroids and colonoids from various species—including humans—or intestinally differentiated induced pluripotent stem cells (iPSC)[1–5]. These are an *ex vivo* primary culture of normal--or diseased—intestine, derived from stem cells of the small intestine (enteroids) or colon (colonoids) which can self-renew indefinitely when provided the appropriate growth factors and conditions. The enteroid cultures can be maintained and passed for several years in an undifferentiated, crypt-like culture that contains stem cells (LGR5+[6–8]), transit amplifying cells, and Paneth cells. Since the model was first described derived from the mouse small intestine and stomach[9,10], similar methods have been used to generate *ex vivo* primary models for many species and organs, from the brain, cornea, and inner ear to liver, lung, and all segments of the GI tract[11]. Such cultures are not limited to cells from healthy individuals either, isolation and maintenance of cultures from individuals with genetic defects have been used to screen for diseases and drug effectiveness. An example of such cultures is the successful generation of cystic fibrosis intestinal enteroids to test various drugs for specific patients to improve the quality of life of those with CF[12,13].

Specifically in the case of the intestine, enteroids have been used to model intestinal ion transport, barrier function, and enteric host-pathogen interactions such as rotavirus, cholera, *Enterohemorrhagic Escherichia coli* (EHEC), *Clostridium difficile*, Human noroviruses, various *Salmonella* strains, and *Cryptosporidium* infection[14,15,24–26,16–23].

The swift spread of the organoid style model system through such a widespread variety of fields and applications is testament to the robustness, application, and versatility of the model. However, even the original mouse small intestinal enteroid protocol has room for improvement. The original model is of

3-dimensional, multi-lobed spheroids embedded in a matrix that consists of the stem cell population rather than structured mix of undifferentiated and differentiated cells that makes up an adult organ system. Another limitation of the system is the inability to form a 2-dimensional culture for access to both the apical and basolateral surfaces. As a reductionist model, it lacks the surrounding and supporting cells that are constantly providing and receiving assorted signals to maintain the entire organism in response to diverse stimuli. Different models have different methods to address these issues in culture and part of the following work is in improving the mouse small intestinal enteroid system as a physiological model by developing a robust and reproducible 2-dimensional model, inducing differentiation into the assorted cell types of the small intestinal villus, and incorporating one of the supporting cell populations, the sub-mucosal plexus of the enteric nervous system, into culture with the enteroids.

Once the enteroid system had been altered successfully, characterization of the new culture system to validate its use as a model of intestinal physiology was paramount. As such, in addition to generating new models, the remainder of the following work consists of the validation of the various systems and the characterization of the undefined physiology revealed by the enteroids that was previously unobserved in cell culture, tissue, or organism studies.

# II. Cholinergic Signaling in the Intestinal Epithelium

The intestine serves as an extended surface area specialized for transfer of nutrients, ions, and fluid into and out of the body. Absorption and secretion of various substances occurs differentially both segmentally from the duodenum to the distal colon and across the crypt/villus or crypt/surface axes. One of the most common manifestations of pathophysiology in the gut is disrupted fluid transport which results in either diarrhea, when too much fluid is lost; or constipation when not enough fluid is secreted. The delicate balance of the ion and fluid status of the body is sustained by many signaling pathways integrating together to maintain and protect the body's internal environment[27].

Cholinergic signaling is a widespread method of paracrine signaling, often involving cholinergic neurons (those that use the neurotransmitter acetylcholine) to convey action potentials or to stimulate a response in terminal tissues. The localization of nerves fibers in close proximity to the intestinal epithelium has been a known part of the system for decades, and their role in intestinal function has been under investigation just as long.

Cholinergic stimulation of intestinal secretion was first confirmed in the rat jejunum, where not only a pro-secretory role for acetylcholine was described, but it was also determined that this function was likely mediated by muscarinic receptors—at the time more commonly known as post-junctional receptors[28]. Determining the secretory role of the intestinal crypt and that the villus/surface served as primarily an absorptive site was done by selectively damaging either the surface or the crypt of intestinal tissue before stimulation with acetylcholine[29]. The role of calcium in transport function of the intestine was first observed early on in rabbit ileum, where it was observed that serosal extracellular calcium is involved in intestinal electrolyte absorption and secretion, but mucosal calcium did not appear to be involved in basal or neuroendocrine-stimulated transport function[30–32].

The cellular processes behind cholinergic signaling in the intestinal epithelium were largely worked out in the T84 cell model, which is a human colon cancer model that exhibits endogenous transport activity that largely mimics intestinal tissue behavior[33].

The role of potassium ions in intestinal transport, and the proteins and mechanism involved, were defined first in the context of VIP-induced secretion, a cAMP-coupled mechanism of chloride secretion where the role of electroneutral NKCC1 and the Na/K-ATPase in chloride secretion of the intestine were confirmed[34]. In fact, T84 cells demonstrated a complex role of potassium ions in epithelial chloride secretion, with early studies that described the possibility of cAMP and calcium signaling activating two different types of basolateral potassium transport systems in addition to stimulating chloride transport[35–37]. The possibility that the common link between cAMP-induced secretion and calcium-induced secretion is the activation of two different basolateral potassium channels rather than the activation of different apical chloride channels was supported by differing sensitivities of VIP-induced chloride secretion and calcium ionophore A23187-induced secretion to inhibition by basolateral barium excess[35,37].

The general process determined for either cAMP- or calcium-induced chloride secretion includes net uptake of $Na^+$, $K^+$, and $Cl^-$ through the basolateral membrane via the bumetanide-sensitive NKCC1 cotransporter, with $Na^+$ and $K^+$ being recycled at the basolateral membrane through $Na^+/K^+$-ATPase and the $K^+$-channels, respectively. This allows for the accumulation of $Cl^-$ intracellularly above electrochemical equilibrium, generating part of the driving force for passive, net apical secretion of $Cl^-$. The remainder of the driving force behind chloride secretion is a result of the inside the cell being electronegative.

Not only is the potassium channel involved in chloride loading different in cAMP and calcium activated secretion, but the apical chloride channel may also be different based on the second messenger generated in response to the secretogogue[36]. In the case of acetylcholine, that would mean that the two points that that mediate chloride secretion consist of 1) a calcium activated potassium channel on the basolateral membrane and 2) a calcium activated chloride channel on the apical membrane.

Acetylcholine and it's analogue carbachol have been shown to act on the intestinal epithelium not through cyclic nucleotide signaling, but through increasing intracellular calcium[38–42]. Early on, T84 cells were determined to respond to carbachol in a pathway independent of cAMP as the carbachol response was synergistic to VIP and PGE2 stimulated responses, both agonists known to activate cAMP-induced

secretion[35,36]. It has also been demonstrated that increases in intracellular calcium alone are sufficient to induce an increase in $I_{sc}$ in the intestinal epithelium in an extracellular calcium-dependent manner without input from other signaling pathways by using reagents like thapsigargan—which increases cytosolic calcium but demonstrates effects on no other signaling pathways[42].

The pathway responsible for cholinergic-induced elevation of cytosolic calcium has been worked out extensively in many systems, defining the muscarinic receptors and the G-proteins they couple to in the context of many functions. In the intestinal epithelia and many other secretory tissues, acetylcholine is known to bind to muscarinic receptors and stimulate net secretion through the $G_{q/11}$ signaling pathway[43,44]. This signaling pathway involves the M3 muscarinic receptor in the human intestinal epithelium (in the mouse intestine the M1 receptor is also involved[45]) stimulating the $G_{q/11}$ pathway, activating PLC, increasing $IP_3$, and depleting ER calcium to increase the cytosolic calcium concentration. The resulting increase in intracellular calcium causes apical calcium activated anion channels and basolateral calcium activated potassium channels to open, and results in a net efflux of chloride into the lumen followed passively by sodium and fluid through the paracellular pathway[43]. In addition to the characteristic chloride secretion, basolateral potassium secretion is important to maintain the electrical gradient required for chloride loading into the cell through the electrochemically coupled $Na^+/K^+$-ATPase/NKCC1/KCNN4 transporters. Muscarinic regulation of basolateral potassium channels is therefore just as important as activation of the apical chloride channels in conducting cholinergic secretion.

The cholinergic-induced secretory response is rapid and transient, a contrast to the often sustained response to cyclic nucleotide stimulation, that indicates a swift, internal mechanism for downregulating the calcium-induced response even in the presence of continued exposure to both stimulus and elevated intracellular calcium[40]. The pathway involved in downregulating cholinergic-induced secretion was determined by a series of studies in T84 cells. The most obvious candidate to mediate the response was PKC, which was known to be activated in response to carbachol, but was determined to be unnecessary for chloride secretion as inhibition of the enzyme had no effect on epithelial chloride secretion[46]. Instead, it was determined that EGF signaling and the downstream tyrosine kinase activation played a role in

inhibiting cholinergic chloride secretion via PI3K activation with no effect on the rise in intracellular calcium[47]. In addition to the unrelated effects of EGF signaling, carbachol itself was shown to cause transactivation of the EGF receptor via $G_q$ signaling which resulted in activation of MAP kinase ERK. Specifically, inhibition of ERK led to the potentiation of the chloride secretory response to carbachol, and inhibition of the M3 receptor abolished the carbachol effects on ERK activation. This indicates a role for the enzyme in downregulation of cholinergic chloride secretion that is dependent on cholinergic activation[48].

The contributions from two different inhibitory pathways to downregulation of cholinergic secretion by EGF and carbachol are not particularly clear cut, as in addition to the major mode of action through PI3K activation and generation of lipid products, residual activation of PLC and generation of IP4 has been shown to occur in response to EGF signaling. Since carbachol demonstrated PLC/IP4 mediated inactivation of secretion, whether PI3 kinase alone was sufficient to downregulate cholinergic secretion required investigation. Using insulin and IGF to activate PI3 kinase without generating IP4 demonstrated that PI3K activation was sufficient to down-regulate cholinergic secretion, and that insulin and IGF are also able to downregulate cholinergic secretion[49]. A third distinct regulatory pathway was characterized involving EGFR activation, Src kinases, and p38 MAP kinase. Increases in intracellular calcium via carbachol or thapsigargan stimulated p38 phosphorylation in an EGFR and Src kinase dependent manner, and inhibition of p38 phosphorylation caused carbachol-induced secretion to be potentiated[50]. The many methods of negative regulation employed to keep cholinergic secretion in check highlights how important it is for the intestinal epithelium to keep tight control over fluid transport. Having many potential off-switches that are both self-regulated by muscarinic signaling and externally regulated by physiologically relevant signals like EGF, insulin, and IGF; offers a ‘fail-safe’ for the system to prevent dysregulation that could all too easily lead to potentially severe pathophysiology like diarrhea.

As a well-defined signaling pathway that involves both the neuronal-specific nicotinic receptors and the epithelial-specific muscarinic receptors that has an easily quantifiable, functional readout in the form of chloride secretion, the cholinergic signaling pathway was selected to serve as the method of

validation for the enteroid cultures after differentiation, as monolayers, and in co-culture with the sub-mucosal plexus. It was through validating our new enteroid culture systems that the observation was made that cholinergic signaling in the intestinal epithelia is not as simple as it is currently understood, as there is a significant nicotinic component in the epithelial response in the absence of a neuronal population that had previously been undefined. It was by characterizing this new nicotinic aspect, independent of muscarinic signaling, that the complexity of cholinergic signaling in the enteroids became apparent, revealing a variety of nicotinic receptor subunits in the epithelium and a secondary pathway upstream of intracellular calcium involved in mediating cholinergic anion secretion. Our contribution only scratches the surface of the previously undefined complexity of cholinergic signaling and leaves many questions still unanswered, but the culture systems defined in the process provides a means to systematically address those questions.

# III. Materials and Methods

## A. Mouse Enteroid Isolation and Culture

Mouse enteroids were prepared from the jejunum of adult male (>1yo) *Lifeact-EGFP* transgenic mice[51]. The isolation and propagation of these mouse enteroid cultures was performed using a modified version of the method developed by Sato et al, as previously described[9,52–55]. Briefly, mice were euthanized via isoflurane inhalation followed by cervical dislocation and a portion of the mid-jejunum ~2cm long was removed and bathed in ice cold PBS with 200U/mL pen/strep at 4°C for 45 minutes. Isolated crypts obtained after EGTA chelation for 1 hour were embedded in Matrigel (Corning, 356231) in 24-well plates (Corning) and maintained in medium similar to that proposed by Sato et al[9,11] consisting of a base medium (CMGF-; Advanced DMEM/F12 with 100U/mL penicillin/streptomycin, 10 mmol/L HEPES, and 1x GlutaMAX) with 50% WNT3A conditioned medium (produced by L-WNT3A cell line, ATCC CRL-2647), 15% R-SPONDIN1–conditioned medium (produced by HEK293T cell line stably expressing mouse R-SPONDIN1; generously provided by Dr. Calvin Kuo, Stanford University, Stanford, CA), 10% NOGGIN conditioned medium (produced by HEK293T cell line stably expressing mouse Noggin[56]), 1 × B27 supplement (Life Technologies), 1 mmol/L N-acetylcysteine (Sigma-Aldrich, St. Louis, MO), 50 ng/mL human epidermal growth factor (Life Technologies), and 100 μg/mL primocin (InvivoGen, San Diego, CA) (**Table 1**). Enteroids were cultured in a 5% $CO_2$ atmosphere at 37°C and are passaged via mechanical trituration every 3-7 days.

Enteroid cultures at passage 40 and passage 112 showed no significant difference morphologically or functionally, and so cultures from passage 40-155 were used. Enteroids used for the bulk of this study were generated from a single mouse, with preliminary cholinergic secretion experiments in enteroids isolated from 2 other male mice of different lineage and age at the time of isolation, but the same genetic background (C57BL/6) to verify the results across multiple individuals before more detailed studies were undertaken.

Mice used in these experiments were housed in the main animal facility at the Johns Hopkins School of Medicine. Full time veterinary care at Johns Hopkins University is provided by the division of Research Animal Resources and the Director of Laboratory Animal Medicine. The protocol was approved by the Hopkins Animal Care and Use Committee (protocol: M019M118).

## B. Monolayer Cultures

Mouse enteroid monolayer cultures were produced by adapting methods previously described for human enteroid monolayers[15,57]. Briefly, Transwell inserts (polyester membrane with 0.4μm pore, Corning, 3470) were coated with 200μg/mL rat tail collagen I (Corning, 354236) and incubated at 37°C overnight. Filters were washed with base conditioned medium without growth factors (CMGF-) prior to plating. Mouse enteroids were freed from Matrigel and mechanically triturated before being plated in suspension above the filter and maintained in culture with 150μL medium in the apical well and 600μL in the bottom well, changed every other day. Monolayers were cultured in a 5% $CO_2$ atmosphere at 37°C. Monolayer progression and confluence was estimated via trans-epithelial electrical resistance (TER; EVOM2 Voltohmmeter, World Precision Instruments).

## C. Mouse Enteroid Differentiation

Enteroid cultures were expanded after passaging before the proliferation medium was replaced with various test formulations. The successful differentiation protocol was based on a protocol developed by Kozuka et. al. in a development project at Ardylex[58]. Mouse proliferation medium was switched to mouse differentiation medium; CMGF- with addition of 10% Noggin, 300ng/mL recombinant murine BMP4 (Peprotech 315-27-10μg), 2.5μM Thiazovivin (Sigma SML1045), 1 × B27 supplement, 1 mmol/L N-acetylcysteine, and 100 μg/mL primocin) for two days (**Table 1**). The enteroids that underwent differentiation were analyzed via qRT-PCR to confirm the loss of stem cell markers and an induction of markers of differentiated cell types, and then studied in various applications.

| CMGF- | Sato[1,2] | Minimal or ND | DF[20] | PS120 | Caco-2 Complete | SCM | SCM+GF |
|---|---|---|---|---|---|---|---|
| Advanced DMEM/F12 | CMGF- | CMGF- | CMGF- | DMEM/F12 | DMEM | Neurobasal media | Neurobasal media |
| Pen/Strep | WNT3A conditioned media | WNT3A conditioned media | NOGGIN conditioned media | FBS | NaHCO3 | B27 | B27 |
| HEPES | RSPONDIN-1 conditioned media | RSPONDIN-1 conditioned media | B27 | Pen/Strep | Nonessential Amino Acids | BSA | BSA |
| GlutaMAX | NOGGIN conditioned media | NOGGIN conditioned media | n-AC | | FBS | GlutaMAX | GlutaMAX |
| | B27 | B27 | Murine BMP4 | | Glutamine | Antibiotic/Antimycotic | Antibiotic/Antimycotic |
| | n-AC | n-AC | Thiazovivin | | Pen/Strep | β-mecaptoethanol | β-mecaptoethanol |
| | hEGF | hEGF | Primocin | | Blastocidin | | bFGF |
| | A83-01 | Primocin | | | Puromycin | | EGF |
| | Gastrin | | | | | | GDNF |
| | SB202190 | | | | | | |
| | Primocin | | | | | | |

**Table 1: Media formulations used in cell culture**
Media compositions to maintain and differentiate various cell types in culture
Abbreviations: Pen/Strep; Penicillin and Streptomycin, nAC; n-acetylcysteine, BMP4; bone morphogenic protein isoform 4, FBS; fetal bovine serum, BSA; bovine serum albumin, bFGF; beta Fibroblast Growth Factor, EGF; epidermal growth factor, GDNF; glial derived growth factor

| Antibody | Name | Antibody/Label | Source | Dilution |
|---|---|---|---|---|
| **Na+/K+ ATPase (ATP1A1)** | Sodium/Potassium ATPase | a5 (mouse monoclonal) | DSHB [59] | [1:100] |
| **SGLT1** | Sodium-Glucose Cotransporter 1 | 07-1417 (rabbit polyclonal) | Millipore [60,61] | [1:100] |
| **DCLK1** | Doublecortin Like Kinase 1 | Ab37994 (rabbit polyclonal) | Abcam | [1:100] |
| **ChgnA** | Chromogranin A | Ab15160 (rabbit polyclonal) | Abcam | [1:100] |
| **ChAT** | Choline O-acyltransferase | Ab70219 (rabbit polyclonal) | Abcam | [1:2000] |
| **VIP** | Vasoactive intestinal peptide | Ab22736 (rabbit polyclonal) | Abcam | [1:2000] |
| **PGP9.5** | Protein Gene Product 9.5 | Ab108986 (rabbit monoclonal) | Abcam | [1:200] |
| **HuC/D** | Hu Antigen C/Hu Antigen D | Ab184267 (rabbit monoclonal) | Abcam | [1:1000] |
| **WGA 488** | Wheatgerm agglutinin | W11261 | Invitrogen | [1:100] |
| **PHLN 633** | Phalloidin | A22284 | Life Technologies | [1:100] |
| **Hoechst 405** | Hoechst 405 | 33342 | Sigma | [1:2000] |

**Table 2: Antibodies and labels used for immunofluorescence**

Primary antibodies and labels used for staining of cell culture and tissue. Short-hand used, target or label name, reference number, manufacturer, and dilution used when staining

## D. Immunofluorescence and Confocal Imaging of Monolayers

Monolayers were fixed in 4% paraformaldehyde (PFA; Electron Microscopy Sciences) for 30 minutes and 3D cultures for 1 hour at room temperature in the dark. After being washed 3 times with PBS for 10 minutes, permeabilization was carried out using 0.1% Saponin in 2% BSA/15% FBS for 1 hour or 0.1-0.5% TritonX-100 in 2% BSA/15% FBS for 20 minutes followed by blocking with 2% BSA/15% FBS for 40 minutes in a humidified chamber. Cells were washed with PBS and incubated overnight at 4°C with the appropriate primary antibody (**Table 2**). Cells were washed with PBS 5 times for 10 minutes each and then incubated at room temperature in the presence of secondary antibody, labelled marker, and/or Hoechst (**Table 2**). After incubation, cells were washed with PBS 5 times for 10 minutes each in the dark and monolayers were cut out of the Transwell inserts and mounted in FluorSave Reagent (Calbiochem).

Images of enteroid monolayers were obtained using an Olympus FV3000RS Confocal microscope (40x silicone immersion oil; 3.00x digital zoom; resonant scan with 16 frame average; 0.5µm

step size; NA= 1.25). Analysis was carried out using the Fluoview analysis and reconstruction software (FV31S-SW, v2.1.1.98).

## E. Ussing Chamber/Voltage Clamp Technique using Current Clamp Short-Circuit Current Measurements

The protocol used to quantitate anion secretion data was previously published in detail[62]. In summary, Transwell inserts with confluent enteroid monolayers were mounted in Ussing chambers and electrogenic ion transport determined using a voltage clamp (VCC MC6 Multichannel Voltage/current Clamp using P2302T sliders; Physiologic Instruments). The apical and basolateral chambers (P2300 Ussing chamber in a EM-CSYS-6 system) were filled with bathing solution that was gassed continuously with 95% $O_2$/5% $CO_2$, maintained at 37°C, and connected to the voltage-current clamp via Ag/AgCl electrodes and 3 mol/L KCl agar bridges. Bathing solution consisted of 120mM NaCl, 25mM $NaHCO_3$, 3.3mM $KH_2PO_4$, 0.8mM $K_2HPO_4$, 1.2mM $CaCl_2$, and 1.2mM $MgCl_2$, gassed with 5% $CO_2$, at pH 7.4. In addition, bathing solution in the basolateral chamber was supplemented with 4mM glucose as an energy

| Compound | Abbreviation | Manufacturer | Final Concentration | Application |
|---|---|---|---|---|
| **Forskolin** | Fsk | Sigma | 5μM | Basolateral |
| **Carbamoylcholine Chloride** | CCh | Sigma | 10μM[63,64] | Basolateral |
| **Hexamethonium Bromide** | Hex | Sigma | 10μM | Basolateral |
| **Atropine** | Atro | Sigma | 1μM | Basolateral |
| **Bethanechol Chloride** | BCh | Calbiochem | 10-300μM | Basolateral |
| **(-)-Nicotine hydrogen tartrate salt** | Nico | Sigma | 3-30μM | Basolateral |
| **(R)-benzopyrimido-pyrrolo-oxazinedione [(R)-BPO27]** | BPO27 | MedChem Express | 25μM | Apical+Basolateral |
| **Calcium-activated Chloride Channel inhibitor A01 ($CaCC_{inh}$-A01)** | A01 | | 10μM | Apical+Basolateral |
| **BAPTA-AM** | BAPTA-AM | Invitrogen | 25μM | Apical+Basolateral |
| **Clotrimazole** | Clotrimazole | Sigma | 30μM | Apical or Basolateral |
| **Ethylene glycol-bis(β-aminoethyl ether)-N,N,N′,N′-tetraacetic acid** | EGTA | Sigma | 1.4mM | Apical or Basolateral |

**Table 3: Compounds for transport and calcium experiments**

Table summarizing the reagents used in transport analysis or intracellular calcium measurements using the mouse enteroid or Caco-2 monolayers. Compound name, shorthand used, manufacturer, and concentration(s) applied in various experiments

substrate; while the apical chamber was supplemented with 4mM mannitol to maintain osmotic balance. Reagents are listed in **Table 3**. Current clamping was used and short-circuit current ($I_{sc}$) and TER were recorded by the Acquire and Analyze software (ver. 2.2.2, Physiologic Instruments 2005). Data were normalized to the surface area of the monolayer (0.33cm$^2$) in Microsoft Excel before being analyzed and graphed in GraphPad Prism8/9.

## F. Quantitative Real-Time Polymerase Chain Reaction

Expression of mRNA was determined according to the protocol previously published[62]. Total RNA was extracted from three different passages of mouse jejunal enteroids plated as monolayers using the PureLinkRNA Mini Kit (Life Technologies) according to the manufacturer's protocol. Complementary DNA (cDNA) was synthesized from 1µg of mRNA using SuperScript VILO MasterMix (Life Technologies). Quantitative real-time polymerase chain reaction (qRT-PCR) was done using Power SYBER Green Master Mix (Life Technologies) and a QuantStudio 12k Flex real-time PCR system (Applied Biosystems). Samples were run in triplicate using 5ng of cDNA for each reaction. Gene specific primer sequences are listed in **Table 4**. Ribosomal RNA 18S (*Rn18s*) was used as the internal control for normalization.

qRT-PCR was performed on monolayers grown under both non-differentiated and differentiation conditions to verify cell identity in the monolayer. Expression of the various muscarinic receptors and nicotinic receptor subunits was determined under both non-differentiated and differentiated conditions.

| Gene | Abbv. | Fwd | Rev | Product (bp) |
|---|---|---|---|---|
| **Primers used to verify mouse monolayer identity and differentiation** | | | | |
| *Leucine Rich Repeat Containing G Protein-Coupled Receptor 5* | *Lgr5* | CGAGCCTTACAGAGCCTGATACC | TTGCCGTCGTCTTTATTCCATTGG | 143 |
| *$Na^+$-$K^+$-2 $Cl^-$ Channel* | *Nkcc1* | TGCGAGAAGGTGCACAATAC | TGTTTGGCTTCATACGACCA | 60 |
| *Sucrase Isomaltase* | *Si* | GCTATCGCTCTTGTTGTGGTT | TTCCAGGACTAGGGGTTGAAG | 85 |
| *Villin* | *Vil1* | TCAAAGGCTCTCTCAACATCAC | AGCAGTCACCATCGAAGAAGC | 114 |
| *Mucin 2* | *Muc2* | TGCCCAGAGAGTTTGGAGAG | CCTCACATGTGGTCTGGTTG | 123 |
| *Double Corticotropin-like Kinase 1* | *Dclk1* | TCCACCGGAATTGAACTCGG | GGGAGCGAACAGTCTCAGA | 65 |
| *Slc26a3* | *Dra* | TAAGAAGACGCACAGACATCAC | GGAACAAAGACAGGGCGATTT | 101 |

| | | | | |
|---|---|---|---|---|
| *$Na^+/H^+$ Exchanger 3 (Slc9a3)* | *Nhe3* | TCCATGAGCTGAATTTGAAGG | TACTTGGGGAGCGAATGAAG | 87 |
| *Cystic Fibrosis Transmembrane Conductance Regulator (Abcc7)* | *Cftr* | CCCTTCGGCGATGCTTTTTC | AAGCCTATGCCAAGGTAAATGG | 166 |
| **Primers used to identify the presence of cholinergic receptors** | | | | |
| *Cholinergic Receptor Muscarinic 1* | *Chrm1* | AGTCCCAACATCACCGTCTTG | CAGGTTGCCTGTCACTGTAGC | 105 |
| *Cholinergic Receptor Muscarinic 2* | *Chrm2* | TGGTTTGGCTATTACCAGTCCT | CTGAAGGTGGCGGTTGACTT | 136 |
| *Cholinergic Receptor Muscarinic 3* | *Chrm3* | CCTCGCCTTTGTTTCCCAAC | TTGAGGAGAAATTCCCAGAGGT | 129 |
| *Cholinergic Receptor Muscarinic 4* | *Chrm4* | ATGGCGAACTTCACACCTGTC | CTGTCGCAATGAACACCATCT | 109 |
| *Cholinergic Receptor Muscarinic 5* | *Chrm5* | GACCACTGACATACCGAGCC | ATGGCGGTCCCAAAAGTGATG | 196 |
| *Cholinergic Receptor Nicotinic Alpha 1 Subunit* | *Chrna1* | ACCAATGTACGTCTGAAACAGC | TTTTCCGAGGGGATGTGAATTTT | 98 |
| *Cholinergic Receptor Nicotinic Alpha 2 Subunit* | *Chrna2* | TTATCTCTGGTGTCTGCTTCTGA | CCCAGCGATTGTAGCCTCC | 110 |
| *Cholinergic Receptor Nicotinic Alpha 3 Subunit* | *Chrna3* | TCCAGTTTGAGGTGTCTATGTCT | TGGTAGTCAGAGGGTTTCCATTT | 127 |
| *Cholinergic Receptor Nicotinic Alpha 4 Subunit* | *Chrna4* | CTAGCAGCCACATAGAGACCC | GACAAGCCAAAGCGGACAAG | 130 |
| *Cholinergic Receptor Nicotinic Alpha 5 Subunit* | *Chrna5* | ATCCTCTGCTGCAAAACATGA | TCCACGTCCACTAACTGAGAT | 141 |
| *Cholinergic Receptor Nicotinic Alpha 6 Subunit* | *Chrna6* | TAAAGGCAGTACAGGCTGTGA | AAAATGCACCGTGACGGGAT | 115 |
| *Cholinergic Receptor Nicotinic Alpha 7 Subunit* | *Chrna7* | AGTTTTAACCACCAACATTTGGC | TTTTCACTCCGGGGTACTCAG | 86 |
| *Cholinergic Receptor Nicotinic Alpha 9 Subunit* | *Chrna9* | GGAACCAGGTGGACATATTCAAT | GCAGCCGTAGGAGATGACG | 119 |
| *Cholinergic Receptor Nicotinic Alpha 10 Subunit* | *Chrna10* | ATGGATGAACGGAACCAAGTG | GTCCCAATGTAGGTAGGCGT | 78 |
| *Cholinergic Receptor Nicotinic Beta 1 Subunit* | *Chrnb1* | TGAAGAAATGAGCACAAAGGTG | TCCCAGCTTAACCTGTAGTCG | 63 |
| *Cholinergic Receptor Nicotinic Beta 2 Subunit* | *Chrnb2* | GAGGTGAAGCACTTCCCATTT | GCCACATCGCTTTTGAGCAC | 104 |

| | | | | |
|---|---|---|---|---|
| *Cholinergic Receptor Nicotinic Beta 3 Subunit* | *Chrnb3* | TGCTGACGGACGTTTTGAGG | GAGGAGTCCAACTGACGGT | 77 |
| *Cholinergic Receptor Nicotinic Beta 4 Subunit* | *Chrnb4* | GCTATGTGGACGTGACCTATG | CGACGTGATGAGCACACAAG | 92 |
| *Cholinergic Receptor Nicotinic Delta Subunit* | *Chrnd* | GAATGAGGAACAAAGGCTGATCC | GGTGAGACTTAGGGCGACAT | 112 |
| *Cholinergic Receptor Nicotinic Epsilon Subunit* | *Chrne* | CAGTTTGGAGTGGCCTACGAC | AGCGAAAAATGAGAGAGCAGTT | 148 |
| *Cholinergic Receptor Nicotinic Gamma Subunit* | *Chrng* | CTCCCTGAATGAACGAGAGGA | GGCCTTCGTAGTCTTTTGGGT | 101 |
| **Primers used to identify Adenylyl Cyclase Expression** | | | | |
| *Adenylyl Cyclase 1* | *Adcy1* | TTGGCAAGTTCGATGAGTTAGC | GGCGTGATCCGTCTTAGGC | 110 |
| *Adenylyl Cyclase 3* | *Adcy3* | ATGTCACCGTGGCAAACAAGA | GCAATGATGAGGTAGGTTTCGAT | |
| *Adenylyl Cyclase 6* | *Adcy6* | TGAGTCTTCTAGCCAGCTCTG | CAGCACCAAGTAGGTGAACCC | 92 |
| *Adenylyl Cyclase 8* | *Adcy8* | CGGAGGTAGTGATGAACGTGT | CCTTGAGAGGGTCCATTGGAG | 96 |
| **Primers used to identify Anoctamin Expression** | | | | |
| *Anoctamin1 (Tmem16A)* | *Ano1* | AGGAATATGAGGGCAACCTG | CGACACCATGGATTTTGGTA | 75 |
| *Anoctamin6 (Tmem16F)* | *Ano6* | GTATGAGGCCCAGTGCAATC | TTCCCACAGGTGGTAAATGG | 81 |
| **Primer used to identify expression of control genes** | | | | |
| *18s Ribosomal RNA* | *Rn18a* | GCAATTATTCCCCATGAACG | GGGACTTAATCAACGCAAGC | 68 |

**Table 4: Gene Specific Primer Sequences**
Sequence and expected product length of the amplification product for the primers used for qRT-PCR. qRT-PCR, real time quantitative reverse transcription polymerase chain reaction

## G. Mouse Enteroid Transduction

A selection of the plasmid-bearing Mission shRNA bacterial stock *E. coli* was purchased from Sigma, individual clones were picked and expanded in LB broth + Ampicilin [100µg/mL] on a shaker overnight at 200rpm and 37°C. Plasmids were isolated by MINIPrep according to the manufacturer's directions (QIAprep Spin Miniprep kit; 27106) and DNA was quantified. HEK293 cells were cultured in Dulbecco's modified Eagle medium/nutrient mixture F-12 supplemented with 10% fetal bovine serum, 100 U/mL penicillin, and 100 µg/mL streptomycin in a 5% $CO_2$/95% air atmosphere at 37°C. Two days after splitting, HEK cells were transfected with isolated plasmid [1µg] using Lipofectamine 2000 according to the manufacturer's protocol (Invitrogen, 11668-019). After overnight exposure, transfection medium was replaced and the cells were treated with medium supplemented with

| Gene | Abbv | TRCN# | Source | Product Type | Clone ID |
|---|---|---|---|---|---|
| Adenylyl Cyclase 6 (mouse) | *Adcy6* | 0000110755 | Sigma | SHCLNG-NM_007405 | NM_007405.1-3870s1c1 |
| | *Adcy6* | 0000110757 | Sigma | SHCLNG-NM_007405 | NM_007405.1-3041s1c1 |
| | *Adcy6* | 0000110759 | Sigma | SHCLNG-NM_007405 | NM_007405.1-2360s1c1 |
| Adenylyl Cyclase 8 (mouse) | *Adcy8* | 0000114956 | Sigma | SHCLNG-NM_009623 | NM_009623.1-1450s1c1 |
| | *Adcy8* | 0000114957 | Sigma | SHCLNG-NM_009623 | NM_009623.1-3899s1c1 |
| | *Adcy8* | 0000114958 | Sigma | SHCLNG-NM_009623 | NM_009623.1-2270s1c1 |
| | *Adcy8* | 0000114959 | Sigma | SHCLNG-NM_009623 | NM_009623.1-3677s1c1 |
| | *Adcy8* | 0000114960 | Sigma | SHCLNG-NM_009623 | NM_009623.1-2549s1c1 |

**Table 5: Lentiviral shRNA Sequences for knockdown in mouse enteroids**
Identity, TRCN#, and clone ID numbers for bacterial glycerol stocks from the Sigma MISSION shRNA library targeting the mouse sequences of the indicated target for knock-down

sodium butyrate [5mM] for at least eight hours. Medium was refreshed and the cells maintained for two days. Supernatant was then collected and filtered via syringe using a 0.20μm filter (Corning, 431229) and stored at -80°C until use.

Transduction of the mouse enteroids was performed by melting the Matrigel in Cell Recovery Solution at 4°C for 45 minutes mechanically triturating the enteroids 10-15 times with a multichannel pipettor, and diluting in CMGF- before spinning down at 1200rpm for 10 minutes at 4°C. Enteroid pellets were combined and re-divided into sterile Eppendorf tubes in 250μL mouse minimal medium with CHIR-99021 [10μM], Y-27632 [10μM], polybrene [8μg/mL], and individual lentivirus-containing supernatants **(Table 5)** (250μL) and transferred to a 24-well plate. Suspended enteroids were placed in a spinoculator (600g, VWR) at 32°C for 1 hour and then transferred to an incubator with 5% $CO_2$/95% air atmosphere at 37°C for a further 4 hours. Enteroids were spun down and washed gently in CMGF- three times before

| Gene | Plasmid | Source | ID# | Function |
|---|---|---|---|---|
| GCaMP6s | pGP-CMV-GCaMP6s | Addgene | 40753 | Cytosolic calcium sensor |
| CHRM3 | pLV-EF1aa IRES-3HA-CHRM3 | Addgene | 114189 | Cholinergic M3 receptor |

**Table 6: Lentiviral shRNA Sequences for Caco-2 cell overexpression**
Identity, plasmid, and source for Lentiviral plasmids for overexpression of the indicated human genes in Caco-2 cells

being plated in Matrigel with minimal medium supplemented with CHIR-99021 [10μM] and Y-27632 [10μM] for 24 hours. Medium was then replaced without the addition of the Y- and CHIR-compounds.

After the first few post-transduction passages, Puromycin [1.25μg/mL] was added to the minimal medium and maintained for selection. Enteroids were passaged as needed. Expression analysis for the various knock-down variants was performed via qRT-PCR compared to control enteroids.

## H. Caco-2/BBE cell culture

Caco-2 cells (C2BBe1) were cultured in Dulbecco's Modified Eagle Medium (DMEM) supplemented with 25 mmol/L $NaHCO_3$, 0.1 mmol/L nonessential amino acids, 10% fetal bovine serum, 4 mmol/L glutamine, 100 U/mL penicillin, and 100 μg/mL streptomycin in a 5% $CO_2$/95% air atmosphere at 37°C. Plasmid pGP-CMV-GCaMP6s (Addgene plasmid; no. 40753; http://addgene.org/40753) was cloned into lentiviral vector pCDH-EF1-MCS-IRES (puro) and lentiviral particles produced (**Table 6**). Caco-2 wild-type were transduced with GCaMP6s lentiviral particles and puromycin selected (10 mg/mL). Caco-2 cells stably expressing GCaMP6s were transduced with lentiviral particles produced from lentiviral vector pLV-EF1aa IRES-3HA-CHRM3 (Blasticidin) (M3-PAmCherry1, Addgene plasmid; no. 114189, cloned into lentiviral vector pLV-EFa-IRES) under standard protocol. Caco-2 cells stably expressing GCaMP6s and 3HA-CHRM3 were maintained under puromycin and blasticidin containing Caco-2 media. For calcium imaging, experiments Caco-2 cells were seeded into 12-well Transwell plates (1.2 X $10^5$ cells/ well). Cells were grown for 12–15 days post-confluence and were serum deprived for 2–3 hours before study.

## I. Calcium Measurements

Live images of GCaMP fluorescence for calcium measurements using the Caco-2/M3R/GcAMP6s monolayers were obtained with an Olympus FV3000RS confocal microscope (10x objective lens; 2.00x digital zoom; resonant scan with 16 frame average; 0.3μm step size; pinhole: 2.13 Airy units, NA= 0.40) at 37°C within a sealed environmental chamber (OkoLab stage top plus transparent shroud incubator) and the associated FluoView (FV31S, v2.1.1.98) acquisition software. Time lapse

images were taken approximately once every second for ten minutes. Average fluorescence for the entire frame at each time point was generated in MetaMorph Basic (v7.7.3.0) and transferred to Microsoft Excel for normalization before being transferred again to Prism8/9 for graphing and analysis.

## J. Submucosal Plexus Isolation and Culture

SMP Isolation was carried out using a slightly modified protocol[65,66]. *Wnt1-cre:tdTomato* mice (>3 weeks of age, female) were anesthetized with isoflurane and killed by cervical dislocation. A laparotomy was performed and the small intestine was removed and lavaged with PBS containing 3x Antibiotic-Antimycotic (Anti-Anti; Invitrogen), then cut into 2-cm-long segments and placed over a sterile plastic rod. The LM-MP was mechanically peeled off from the underlying tissue using a sterile cotton swab and discarded. The underlying tissue that remained, consisting of the epithelia and sub-mucosal layers, was slit open and transferred to Opti-MEM medium (Invitrogen) containing 2x antibiotic/antimycotic (Invitrogen) on ice.

The epithelial cells were removed through sequential washes in Citrate Buffer (50mM trisodium citrate, 95mM sodium chloride, 8mM potassium phosphate, 5.6mM sodium phosphate dibasic, 1.5mM potassium chloride). The first two washes (1x Citrate Buffer +1X antibiotic/antimycotic, +5% FBS) for 30 minutes at room temperature while shaken vigorously and the third (1x Citrate Buffer +1X antibiotic/antimycotic) agitated at 37°C for 30 minutes. Fragments were then transferred to digestion buffer.

The SMP was dissociated in a digestion buffer consisting of M199 medium (Invitrogen) containing 0.1% BSA, 1mM $CaCl_2$, 20mM HEPES, 150μM P188, 50U/mL DNase I (Worthington, LS0041746), 300U/mL collagenase type 2 (Worthington), and 5% D-+-Trehalose Dihydrate (MP Biomedical) rotated for 20-30 minutes at 37°C; until just before all the fragments are completely dissolved. The dissociated cells were washed in PBS then passed through a 70-μm and subsequently through a 40-μm nylon mesh cell strainer to yield single cells.

Cells were cultured for 1-2 days in stem cell medium (SCM +GFs) consisting of Neurobasal medium containing 1× B27, 0.7% BSA, 2 mM GlutaMAX, and 100 U/mL antibiotic/antimycotic, 0.1% 2-mercaptoethanol, plus 20 ng/mL recombinant human fibroblast growth factor (bFGF), 20 ng/mL recombinant human epidermal growth factor (EGF), and 20 ng/mL recombinant human glial cell-derived neurotrophic factor (GDNF) (Invitrogen) (**Table 1**).

Sorting the SMP neurons and glia from non-neuronal contamination was performed by negative cell sorting. Cultures were dissociated with Accutase (Millipore-Sigma) and DNAse I (20µL/mL) for 20 minutes at 37°C and then passed through a 40-µm nylon mesh cell strainer to yield single cells. Cells were washed with PBS and incubated with PE anti-mouse CD45 (clone 30F11; Biolegend 103105) for 20 minutes at 37°C then washed with PBS before incubation with Anti-PE microbeads (Miltenyi). Labelled cells were passed through at least 3 magnetic LS columns (Miltenyi) in succession. The CD45- fraction was cultured in SCM +GFs for 5 days.

CD45- cell cultures were plated on either glass coverslips (coated with 1:1 diluted Matrigel) or the bottom side of Transwell filters dual-coated with 1mg/mL rat tail collagen 1 (Corning, 354236) then 20µg/mL fibronectin (Santa Cruz; sc-29011) (apical coating: 200µg/mL rat tail collagen I) and allowed to adhere for 30-60 minutes at 37°C before being gently flipped into warm SCM –GFs and the cells were incubated at 37°C in 5% $CO_2$. Medium was gently refreshed every two days using a 1mL pipettor.

## K. SMP Culture Imaging: ChAT and VIP distribution

SMP cultures from five littermate mice combined and plated on slides coated with 1:1 diluted Matrigel on Millicell EZ slides (4-well glass; PEZGS0416) in triplicate and pre-differentiated in SCM for 6 days before being switched to one of five experimental medias. After 3 days in the experimental media, cultures were gently washed with PBS and then fixed in 1% PFA for 5 minutes in the dark at room temperature. Slides were then rinsed gently with PBS and stored in PBS in the dark at 4°C until stained.

Slides were permeabilized with 0.3% TX-100 / 10%BSA / 15%FBS for 30 minutes before being transferred to blocking solution without detergent (10%BSA / 15% FBS) for another 30

minutes. Slides were then incubated with either ChAT or VIP primary antibodies (**Table 2**) in blocking solution in a humidified chamber overnight at 4°C. The next day, slides were gently rinsed with PBS before being washed 3 times in the dark at room temperature for 10 minutes. Secondary antibodies and labels (**Table 2**) were incubated at room temperature in the dark in 10% BSA block for 45 minutes. Slides were gently rinsed, then washed 3 times with PBS (10 minutes each in the dark at RT) and mounted with FluoroSave before being sealed.

SMP culture images were captured using an LSM-510 META laser scanning confocal microscope (Zeiss; 20x objective lens; 1.00x digital zoom; 4 frame average) running ZEN 2012 (black edition) imaging software. Every Hoescht+ cell was imaged for each condition and cells were counted manually using the Hoechst nuclear stain to determine total cells. Data were recorded in Microsoft excel and transferred to Prism8 for graphing.

## L. Co-plating the SMP and enteroids in a 3-dimensional system

After SMP culture in neural differentiation condition (SCM –GFs) for 5-7 days on glass coverslips or 24-well plates, enteroids were dissociated according to standard passaging protocol and plated in 1:1 diluted Matrigel on top of the SMP cultures and allowed to polymerize for 10-15 minutes before the co-cultures were fed with Sato[1,2] enteroid-supporting medium (**Table 1**). Media was changed every two days.

## M. Forskolin-induced Swelling Assay

The FIS assay is modified from that previously described[12,13,20,67,68]. In short, 3D organoids have a closed, 'inside-in' morphology. Luminal secretion thus increases the volume of the enteroid. This change in volume can be observed post-stimulation (5μM Fsk) and was imaged post-incubation with Calcein Green AM (2μM, Invitrogen) using a Keyence All-in-one Fluorescence Microscope B7-X700 series with an incubation system to support live-cell imaging to obtain images every 3 to 5 minutes for 30 minutes. The cross-sectional area of each spherical enteroid over the time-course was then measured in ImageJ using a macro generously developed by Drs. Kremmers and de Jonge (Erasmus Medical Center,

Rotterdam) and normalized in Microsoft Excel to the initial cross-sectional area to generate a percent increase in size over time before being transferred to Prism8 for graphing and analysis.

To account for the possibility of a suppressive SMP effect on FIS in the enteroids, no minimal or maximal volume change cutoffs were applied when analyzing the co-culture data and associated controls. Enteroids were excluded from the analysis if in any image frame they: 1) were below size threshold, 2) touched the edge of the frame, 3) disappeared for more than one frame, 4) experienced a sudden, sharp (dependent on initial size, ex: >2% drop in enteroids under 1000 pixels$^2$) drop in cross-sectional area between two adjacent time points ('popped'), 5) when cross checked with the base image were not confirmed enteroids, or 6) when cross checked with the base image were actually 2 or more enteroids at least partially overlapping, but not fusing (enteroids in multiple z-planes overlapping, fused enteroids were included as long as their original cross-sectional areas were summed as well).

## N. Co-plating the SMP and enteroids in a 2-dimensional system

After culture in neural differentiation condition (SCM –GFs) for 5-7 days on the inverse side of dual-coated Transwell filters (0.4 μM pore, Corning, 3470 or 1μM pore; Millicell, MCRP24H48), Transwells were transferred to a new plate with warm enteroid medium (minimal media + various supplements) and enteroids were dissociated and plated in warm enteroid media in the apical well. Enteroid monolayer confluence was measured daily using an EVOM2 Voltohmmeter. Media was gently refreshed every two days.

## O. Immunofluorescence of 2D Co-cultures

Images of co-cultures on 1.0μM pore Transwell filters were obtained using an Olympus FV3000RS Confocal microscope (40x silicone immersion oil; 3.00x digital zoom; resonant scan with 16 frame average; 0.5μm step size; NA= 1.25). 3D reconstruction of the 2D co-culture was carried out using the CellSens module of Fluoview (FV31S, v2.1.1.98) to perform deconvolution on the images and reconstruct a volumetric rendering of the co-culture.

## P. Tissue Fixation and Processing to determine mouse SMP ChAT distribution

Small intestinal tissue from three female, littermate *ChAT-cre:tdTomato* mice wash flushed with PBS +3X antibiotic/antimycotic to remove luminal contents. The tissue was segmented into the duodenum, jejunum, and ileum, the longitudinal muscle/myenteric plexus (LMMP) was mechanically peeled away and the remaining tissue was slit open along the mesenteric border and then fixed in PFA for 3 hours at 4°C before being stored at 4°C in PBS.

When preparing for staining, the mucosa was removed using a pair of clean glass slides, one slide anchored one end of the tissue submerged in enough PBS to cover the tissue and keep hydrated in a $10cm^2$ dish while the other gently scraped off the mucosa. The tissue segments were further divided for staining with multiple antibodies. Tissue pieces were then washed with PBS and permeabilized for thirty minutes in 0.3% TritonX-100/10%BSA/15%FBS at room temperature in the dark before being changed to block without TritonX-100 for a further thirty-minute incubation. Primary antibodies (**Table 2**) were incubated over two nights at 15°C with shaking at 60rpm in 10% BSA block. The tissue was washed thoroughly with PBS before being incubated with secondary antibody (**Table 2**) in PBS at 15°C, 60rpm overnight. Tissues were washed thoroughly in PBS and mounted flat on a slide with Fluorsave mounting media and sealed.

Small intestinal tissue imaging was performed using a Leica SP8 confocal microscope (HC PL APO 20x objective lens; 2.25 digital zoom; 4 line average; 0.5µm step size, NA=0.75) and LAS X (Leica Application Suite X, ver. 3.5.5.19976) software. Depending on the segment, between 20 and 65 random fields with at least one HuC/D-positive (also known as ELAVL3 and ELAVL4 or Hu antigen C and D) cell body. Total cell bodies expressing HuC/D with or without ChAT were counted per segment. Distribution was not averaged to better display the variability between intestinal segments and littermates. Analysis was performed in Microsoft Excel and data were transferred to Prism8 for graphing.

## Q. Cryo Tissue Preparation and Processing: Identification of ChAT+ epithelial cells

Small intestinal tissue segments from *ChAT-cre:tdTomato* mice were flushed with PBS +3X antibiotic/antimycotic to remove luminal contents and the myenteric layers were mechanically peeled off. Tissue was submerged completely in 4% PFA at 4°C for 2 hours and then transferred to 30% sucrose and incubated at 4°C overnight. Tissue was then submerged in OCT (Optimal Cutting Temperature, 4583, Tissue-Tek) and frozen in liquid nitrogen. Blocks were stored at -80°C before being sectioned by the Hopkins Mouse Physiology Core.

To prepare for imaging, frozen slides were brought to room temperature in the dark (10 minutes). A short secondary fix (2% PFA for 10 minutes) was followed by 3 washes in PBS-Tween (10 minutes each). Tissues was then permeabilized with 0.3% TritonX-100 / 10% BSA for 20 minutes and then blocked with 10% BSA for a further 30 minutes. Primary antibodies against ChAT, DCLK1, and ChgnA were incubated overnight at 4°C in a humidified chamber in 2% BSA (**Table 2**).

The next day, slides were washed 7 times in PBS while rocking (dark, 10 minutes each) before the secondary antibodies were incubated for 1 hour in the dark at room temperature in a humidified chamber. Slides were then washed 5 times in PBS for 10 minutes each in the dark while rocking before coverslips were mounted using FluorSave mounting media. Slides were stored at 4°C until imaged.

Images of cryo-preserved jejunal slices were obtained using an Olympus FV3000RS Confocal microscope (40x silicone immersion oil; 4.00x digital zoom; galvano scan with 5 frame average; NA= 1.25; 2048x2048). Fluoview (FV31S, v2.1.1.98) imaging software was used to analyze and add scale bars.

## R. Confocal

Confocal imaging was carried out at the Fluorescence Imaging Core of the Hopkins Basic Research Digestive Disease Development Center. This work was supported by the NIH NIDDK Center Grant P30DK089502 and the NIH shared instrumentation grant 1S10OD025244.

## S. Statistical Analysis

qRT-PCR data was acquired using the QuantStudio program and analysis—normalizing to mouse *Rn18s* expression (ΔCt)—was performed in Microsoft Excel and graphed in Prism8. Expression differences between differentiated and non-differentiated monolayers was determined by the fold-change ($2^{-\Delta\Delta Ct}$) between ΔCt for each gene of interest with the non-differentiated cultures set to 1.00. Significance was determined via unpaired two-tailed Student's t-tests comparing expression in differentiated monolayers to expression in the non-differentiated monolayers (GraphPad Prism version 8.3.0).

Analysis of current clamp data were performed in Excel by normalizing the $I_{sc}$ to the surface area of the monolayer and subtracting the average $I_{sc}$ of the baseline current immediately prior to addition of the reagents, which was then compared to the peak $I_{sc}$. Significance for most experiments was determined via Student's unpaired t-tests to compare experimental conditions to the control responses, but as the experiments characterizing the differentiated monolayers were done without internal duplicates for each condition during each experiment the Student's paired t-test was used to determine significance for those experiments. Finally, One-way ANOVA with Tukey correction was used to determine significance for dose response curves as each condition was compared to every other condition rather than to a single control condition. The statistical analysis method used is indicated in each figure legend (GraphPad Prism version 8.3.0). Final graphs were generated using Prism8/9 with data from the individual traces included. Results are reported as mean ± SEM as either $\mu A/cm^2$ or percent of control response.

Kinetics for bethanechol and nicotine were determined in Microsoft Excel using the Lineweaver-Burk method. Each experiment counted as n=1 regardless of the number of monolayers studied.

Area under the curve (AUC) analysis of transport data were performed using the AUC function for XY analysis in Prism 8/9. Due to the rapid cholinergic response, peaks of a single point were included in the analysis.

The 'Time to Resolution' of various transport curves was determined by taking either the time at which $I_{sc}$ returned below baseline ($0\mu A/cm^2$) or the end of the experiment, whichever came first after addition of agonist, and subtracting the time it took to reach the maximum peak current to determine the

length of time after maximum $I_{sc}$ when the current returns to baseline. Data were then transferred to Prism 8/9 for graphing and statistical analysis.

Real-time live cell calcium analysis was performed using the Olympus FV3000RS confocal microscope to generate t-stacks at a rate of 1 second / image. These stacks were exported to Metamorph where a fluorescence intensity graph was generated for the average fluorescence of the entire frame for each time point and the numerical data were exported to Excel where it was normalized to the first 100 seconds (F0, baseline) or for the EGTA data the first 40s were averaged as the baseline. Normalized data were transferred to Prism8/9 to generate final graphs and calculate significance of both peak fluorescence and AUC measurements.

# IV. Mouse Jejunal Enteroid Monolayer and Differentiation Development and Characterization

## A. Background

Intestinal enteroids are a powerful model. The ability to isolate and propagate the primary stem cell population *ex vivo* indefinitely without introducing cancerous mutations that may alter other functions is a massive step forward for intestinal physiologic studies. The fact that these populations retain not only their organismal identity as conferred by their genetic and epigenetic sequences, but also their organ and local identities in that enteroids isolated from the duodenum retain their duodenal gene expression patterns in culture which are distinct from those of other intestinal segments like the stomach or colon. However, as incredible an advance as the system is, there is always room for improvement. In this case, the isolated crypts and intestinal enteroids are propagated and assayed as 3-dimensional spheroids or lobed structures that are embedded in a Matrigel matrix. This severely limits the types of assays that can be performed, introduces high levels of background—whether in the form of fluorescence by the Matrigel when imaging or excess extracellular matrix when protein is isolated—to the loss of numbers when trying to recover specimens for analysis, to the lack of easy access to both sides of the polarized epithelial layer, and finally issues of uneven distribution of reagents and dyes. The removal of the enteroids from the surrounding matrix to allow for a 2-dimensional monolayer to develop can solve many of these problems. Access to both the apical and basolateral surfaces is one of the biggest physiological weaknesses of the 3D system that is resolved by the monolayer culture in addition to the technical benefits. A successful monolayer protocol for human enteroids and colonoids was developed several years ago and has been utilized to great effect[22], however, when applied to the mouse enteroids, the cultures never reach confluence. The first aspect of this project was to determine the requisite conditions for successful culture of mouse jejunal enteroids as a monolayer and to differentiate the cultures to generate a more physiological model.

The intestinal epithelium is comprised of several major classes of epithelial cells that can further be divided based on specific markers or signaling molecules. Traditionally used cancerous cell lines do not represent the full scale of cell variety that the intestinal epithelium supports in normal physiology.

The intestinal epithelium is divided into two functional lineages during differentiation. Notch signaling and the downstream transcription factor ATOH1 has been shown to be the main determinant of cell fate in the intestinal epithelium, determining if differentiated cells become secretory (goblet[69], enteroendocrine[70–72], and paneth[73,74] cells) or absorptive (enterocytes[75])[76,77]. Interestingly, a rare cell type called tuft cells, recently determined to function in immune responses to type II parasite infections, do not appear to fit into this cell fate model[78–81].

Each cell type of the intestinal epithelium carries out a distinct function, and loss or disruption of these functions often causes pathology. Understanding the physiology and pathophysiology of the intestinal epithelium requires all aspects of the epithelia to be present. When a population is missing or over-represented, physiology due to the communication between cell populations is missing or altered, potentially blocking key aspects of the physiological response.

The early differentiation conditions for human enteroids consisted of the removal of WNT3A and the p38 MAPK inhibitor SB202190 from the medium for 5 days. Later RSPONDIN1 was also removed to generate the conditions currently used for differentiating human enteroids in culture. It has also been shown that differentiation of human enteroids in the presence of Notch inhibitor DBZ is sufficient to alter the cell fate ratio, significantly increasing the number of secretory cells in culture, a technique used to study physiology and pathophysiology of some of the rarer cell types[82].

The human enteroid differentiation process has since been thoroughly tested, inducing changes similar to those observed along the small intestinal crypt-villus or colonic crypt-surface axis, including an increase in monolayer TER and cell height, an increase in various differentiation and specific cell type markers, and a decrease in proliferative and stem cell markers[15,24,57,58,62]. However, differentiation of the mouse enteroid cultures has been elusive. Mouse cultures grown under the same conditions as the human-

derived cultures died by day four. Cutting the differentiation short to 2 or 3 days did not exhibit any marked reduction in proliferative markers that isn't accounted for by the increased cell death.

The three pathways most involved in intestinal differentiation are the Wnt, Notch, and Bone Morphogenetic Protein (BMP) pathways. Differentiation conditions including the Wnt antagonist dipkoff1, notch inhibitor DAPT, and removal of NOGGIN from the media (an endogenous BMP4 inhibitor), were tested to see if the cultures could be pushed into differentiating. Previous experiments in our lab testing the effects of these inhibitors alone in culture demonstrated a partial effect at best by qRT-PCR.

While our efforts did not succeed, in 2017 a group at Ardelyx published successful protocols for the generation of monolayers and differentiation of mouse and human small intestine and colon enteroids[58]. Mouse jejunal monolayers were differentiated and demonstrated increased numbers of *Muc2*+ goblet cells, *ChgnA*+ enteroendocrine cells, *ANPEP*+ absorptive cells, and *Lysozyme*+ Paneth cells via confocal microscopy and mRNA sequencing. Sequencing data further demonstrated an increase in sucrase-isomaltase, lactase, and NHE3 in addition to decreasing Ki67 (proliferation marker) and LGR5 (intestinal stem cell marker) expression. Ion transport analysis showed net $Na^+$ absorption and apical acidification in differentiated cultures. However, the TER of differentiated jejunum was not tested, nor were several other common markers of specific cell types included in the analysis of the cultures. Additionally, age matched, non-differentiated cultures were not present in their analysis, so it is inconclusive if their results are due to their differentiation media composition or to their proposed monolayer conditions. We proposed to more thoroughly characterize the differentiation protocol by analyzing mRNA expression of an expanded panel of intestinal proliferation and differentiation markers, recorded TER over time, and compared stimulated anion secretion in monolayers differentiated according to the proposed method and age matched undifferentiated jejunal monolayers.

## B. Results

### 1. A minimal media composition pushed mouse enteroids to a more proliferative state.

The minimal media condition developed to support mouse enteroid monolayers[83] appears to have the effect of driving the 3D mouse cultures to a more proliferative state, reducing the number of lobed enteroids in culture and increasing the average enteroid size in pair-matched wells (**Table 1, Figure 1, data not shown**). Comparatively, crypts isolated into the mouse minimal condition grew larger enteroids than the same isolation plated in the Sato condition, though the numbers of enteroids established were about equal in both wells (**data not shown**).

Using the mouse minimal media as a base, tests of differentiation conditions for mouse enteroids that were being published at the time led to cell death. Once the mouse monolayer platform was available, TER measurements were used as a real-time measure of differentiation to test several conditions which continued to result only in enteroid loss. The TER of differentiated intestinal monolayers of various cell types is increased compared to undifferentiated intestinal cultures, when our tested conditions did not increase the TER as expected but rather caused it to plummet within days indicating loss of the culture, the conditions were deemed a failure and further testing not conducted.

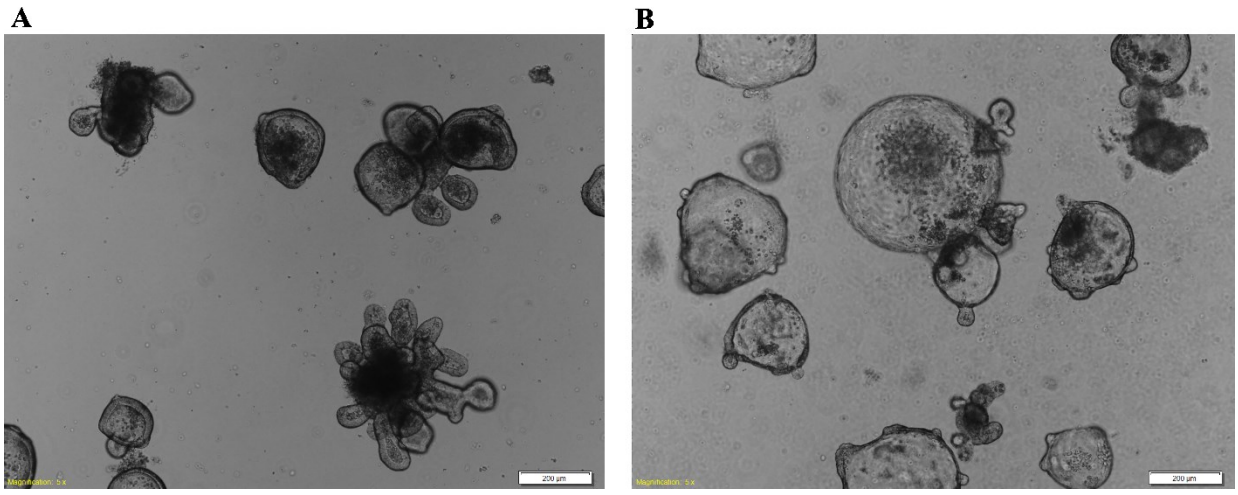


**Figure 1: Mouse jejunal enteroids plated in proliferative conditions**

**A)** Enteroids passaged in Sato media (3 days post-passage) are smaller and of a mixed-lobed morphology compared to paired enteroids passaged into **B)** minimal media for 3 days. Enteroids in both conditions were previously passaged together in Sato media for 32 passages before being divided into either Sato or minimal medium and imaged three days later. Enteroids grown in minimal media have a predominantly spherical morphology compared to the mixed spherical and lobed morphologies conventional to the Sato culture condition. Scale bar = 200μm.

## 2. Development of mouse jejunal monolayers and monolayer differentiation[83]

Using mouse enteroid lines isolated from the jejunum and the minimal media composition that produced enteroids that were predominantly non-differentiated (ND[53]), a protocol to generate confluent monolayers on Transwell filters was developed[83]. This protocol required making several key changes to the mouse enteroid and human monolayer systems: 1) Coating Transwell filters with a high concentration (200μg/mL) of rat tail collagen I instead of 34μg/mL of human placental collagen IV; 2) Removing the TGFβ1 receptor inhibitor A83-01 from the media, which prevented monolayer formation in mouse enteroids when present; and 3) Using non-enzymatic methods to passage the cultures, enzymatic digestion with TrypLE, Accutase, and Trypsin all prevented the formation of confluent monolayers even after several passages using mechanical disruption of the enteroids. The last two steps were necessary because A83-01 prevented the monolayers from becoming confluent, while using enzymatic dissociation to passage the mouse enteroids even once prevented monolayer formation for multiple passages.

Once the monolayers were confluent as determined via a TER over 100 $\Omega \cdot cm^2$, the monolayers were switched to a promising differentiation media published by the company Ardelyx which included the withdrawal of WNT3A/RSPONDIN-1 and the addition of BMP4 (300ng/mL) and Thiazovivin (2.5μM)[58]. These cultures exhibited a rapid and significant increase in TER over two days when compared to cultures maintained in ND media (**Figure 2A**) and all experiments were performed on cultures 2 days after switching to the differentiation media as suggested[58].

Confocal imaging was used to verify that the monolayers were 1) confluent as determined by a single layer of nuclei staining and 2) had apical-basolateral polarity based on confocal imaging with basolateral marker $Na^+/K^+$-ATPase and an apical marker WGA (used for non-differentiated cultures) or SGLT1 (used for differentiated cultures) (**Figure 2B, C**). The presence of intestinal cell types, including stem cells (*Lgr5*), enterocytes (*Si*), goblet cells (*Muc2*), and tuft cells (*Dclk1*) was determined by qRT-PCR (**Figure 2D, E**). The non-differentiated monolayers were composed of predominantly stem cells, with low but detectable levels of genes normally present in villus cells.

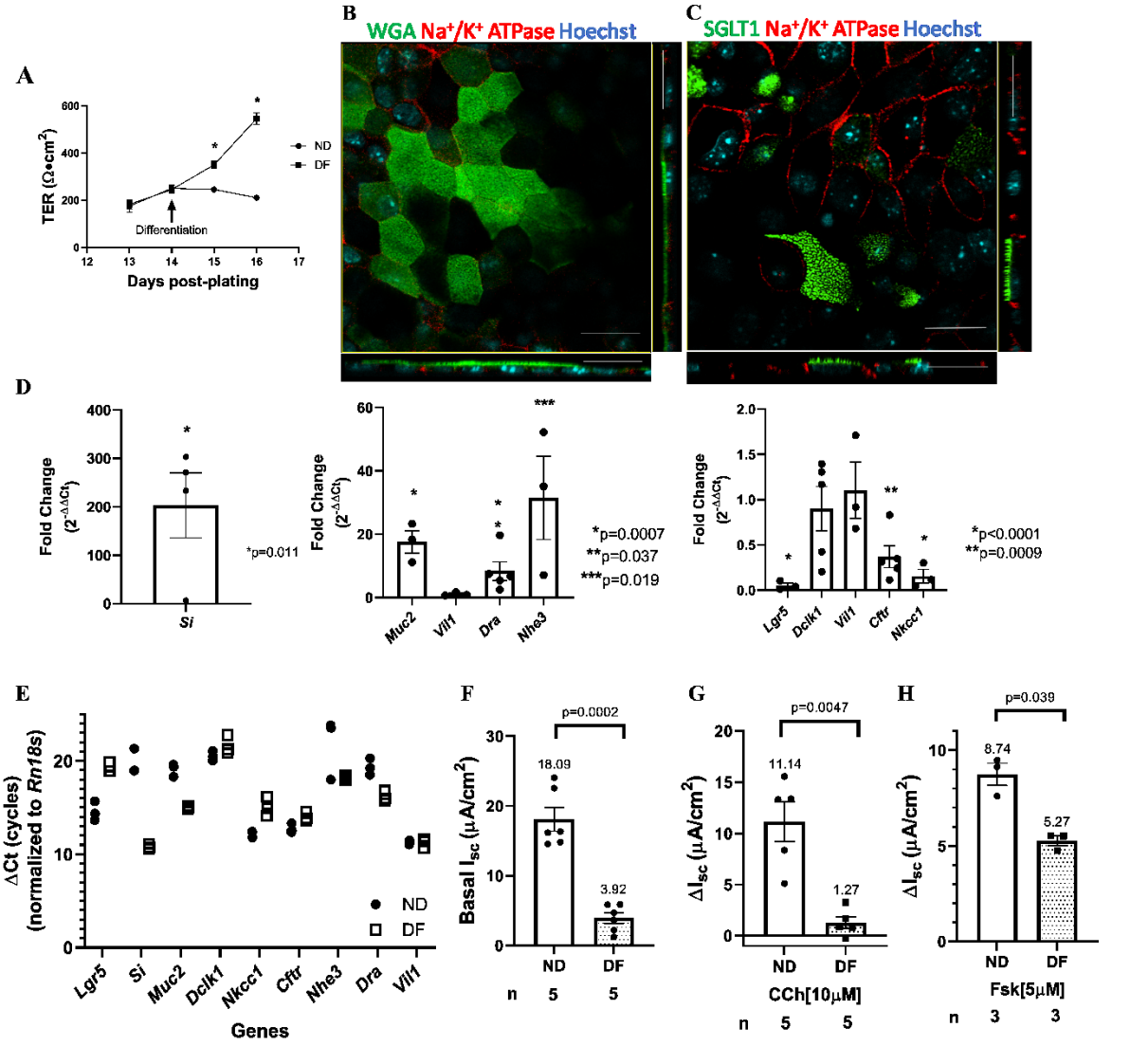


**Figure 2: Mouse Enteroid Monolayers**

**A)** Mouse jejunal monolayers display an increase in trans-epithelial electrical resistance (TER) that indicates confluence at values above 100 Ω•cm$^2$. The non-differentiated monolayers continue to increase in TER until a stable point is reached. Experiments are performed when TER is stable for at least two days. Non-differentiated mouse jejunal monolayers display a lower TER than differentiated monolayers. Results are mean ± SEM. p-values are comparison of non-differentiated and differentiated enteroids on the same day post-plating. Error bars not visible indicate an error smaller than the size of the point. *p<0.0001, n=4 monolayers/condition. **B-C)** Confocal images (single slice XY at the apical surface and XZ views) of a non-differentiated **(B)** and a differentiated **(C)** mouse jejunal monolayer. Monolayers are a single layer of cells that display apical (WGA or SGLT1)-basolateral ($Na^+/K^+$ATPase) polarity. Cyan: Hoechst. Scale bars = 20μm B) Green: WGA (apical), Red: $Na^+/K^+$ ATPase (basolateral), **C)** Green: SGLT1 (apical), Red: $Na^+/K^+$ ATPase (basolateral) **D)** Fold change in mRNA of differentiated enteroids normalized to Rn18s expression/ ND monolayers. **E)** ΔCt for the expression of markers and genes of interest in ND and DF monolayers. Lower ΔCt value indicates higher expression levels. Non-differentiated (ND) mouse jejunum monolayers display proliferation and crypt markers in addition to low but detectable levels of markers for several differentiated populations by qRT-PCR. Differentiated monolayers (2 days) lose stem cell and crypt markers (*Lgr5*, *Nkcc1*, and *Cftr*) and have increased expression of villus cell markers (sucrase-isomaltase (*Si*), mucin 2 (*Muc2*), and *Dra*). The tuft cell marker *Dclk1* and the intestinal epithelial marker villin (*Vil1*) are unaffected by differentiation. Normalized to *Rn18s* expression, n=3, points may overlap. **F)** Basal $I_{sc}$ in the non-differentiated jejunal monolayers is significantly higher than in the differentiated monolayers, p-value determined by Student's paired t-test. Number of experiments (n) indicated below the bars. **G-H)** Differentiated jejunal monolayers exhibited reduced anion secretory response to **G)** carbachol [10μM] and **H)** forskolin [5μM] compared to the non-differentiated monolayers. The number of experiments (n) is indicated under each bar, Student's paired t-test used for statistical comparison.

As expected, monolayers maintained in the non-differentiated condition expressed high levels of the stem cell marker *Lgr5,* while the differentiated enteroids expressed multiple villus brush boarder enterocyte genes including sucrase-isomaltase (*Si*) and the goblet cell marker *Muc2*. Interestingly, the tuft cell marker, *Dclk1,* was expressed similarly in the non-differentiated and differentiated monolayers. mRNA expression of differentially expressed transporters also supported the non-differentiated versus differentiated state of the monolayers. *Nkcc1* (a transporter expressed primarily in the crypts) and *Cftr* (expressed predominantly but not entirely in the intestinal crypt) exhibited reduced expression with differentiation. mRNA for transport proteins known to be expressed in the villi including the sodium/hydrogen exchanger 3 (*Nhe3*) and the chloride/bicarbonate exchanger downregulated in adenoma (*Dra*) were increased with differentiation (**Figure 2D, E**). The intestinal epithelial cell marker villin (*Vil1*) was unaffected by the differentiation status of the monolayers and confirmed that the monolayers did not lose their intestinal identity in culture. The increase in TER (**Figure 2A**) and changes in expression (**Figure 2D, E**) shows that these monolayers are differentiated and more similar to the jejunal villus while the non-differentiated monolayers are more representative of the intestinal crypt. It is interesting to note, that while mRNA expression displays the same directional trends in mouse jejunal enteroids as human duodenal enteroids, the average difference in expression between the two systems is different[62]. For example, in the mouse system, *Dra* expression is increased 10.5-fold with differentiation, but the average expression in human duodenum was over 20-fold increase with differentiation. Whether the differences in the change in expression are due to technical variation due to the differing primers used, differences caused by the culture and differentiation methods, or actual differences in expression between mouse and human tissues is unknown.

The functional characterization of ion transport by the monolayers in the Ussing Chamber/ Voltage Clamp was determined. Both non-differentiated and differentiated monolayers were studied using the Ussing Chamber/Voltage Clamp method with basal short-circuit current ($I_{sc}$) and response to forskolin [5μM] or carbachol [10μM][63,64] determined. Forskolin is an adenylate cyclase agonist and increases

intracellular cAMP. Carbachol on the other hand acts by activating $G_{q/11}$-coupled muscarinic receptors to increase intracellular calcium from the ER stores.

Basal $I_{sc}$ was significantly lower in differentiated monolayers compared to non-differentiated monolayers (DF = 3.9μA/cm$^2$ ± 0.8μA/cm$^2$ versus ND = 18.1μA/cm$^2$ ± 1.7μA/cm$^2$, p=0.0002, n=5) (**Figure 2F**). The agonists had divergent effects when applied to monolayers grown in the two conditions, the non-differentiated monolayers displayed a larger magnitude of increased anion secretion (11.1μA/cm$^2$ ± 1.9μA/cm$^2$, n=5) in response to carbachol [10μM] than the monolayers that underwent differentiation (1.3μA/cm$^2$ ± 0.58 μA/cm$^2$, 14.7% ± 4.4% of the response in ND monolayers, n=5, p=0.0047) (**Figure 2G**). Forskolin-induced current was also higher in non-differentiated monolayers (8.7μA/cm$^2$ ± 0.58μA/cm$^2$, n=3) when compared to differentiated monolayers (5.3μA/cm$^2$ ± 0.25μA/cm$^2$, 61.0% ± 3.8% % of the response in ND monolayers, p=0.039, n=3) (**Figure 2H**).

## C. Discussion

Mouse enteroid monolayers were generated by altering both the filter coating and media composition when compared to that used when generating human enteroid monolayers, which was used as a baseline to optimize the protocol[15]. The key modifications that allowed reproducible production of murine monolayers included: 1) Coating filters with a high concentration (200μg/mL) of rat tail collagen I instead of 34μg/mL of human placental collagen IV; 2) Removing the TGFβ1 receptor inhibitor A83-01, which prevents monolayer formation when present in the media; and 3) Using non-enzymatic methods to passage the cultures, as enzymatic digestion with TrypLE, Accutase, and Trypsin all prevented the formation of confluent monolayers. These monolayers could be maintained in a non-differentiated state or differentiated following the protocol published by Kozuka et. al.[58]

Mouse jejunal monolayers that underwent the defined differentiation protocol displayed several traits inherent to differentiated intestinal epithelium. Trans-epithelial resistance increased significantly after two days of differentiation. Molecular markers of differentiation cell types increased as did ion transport proteins native to the intestinal villus while genes of markers and transporters expressed in

proliferating and crypt ells were lost. Finally, transport behavior of the differentiated cultures displayed reduced secretory responses after stimulation with either forskolin or carbachol, a mark of differentiation in both tissue and other intestinal epithelium cell models. This demonstrates the validity of the differentiation model described for mouse enteroids as a model for the intestinal villus and the non-differentiated enteroids as a model of the intestinal crypt.

Mouse enteroids studied as confluent monolayers now can be used in a similar manner as human enteroids with the apical surface exposed to allow studies that include transcytosis of luminal or basolateral nutrients, separate effects of neurohumoral substances on the apical and basolateral surfaces, lumen specific effects of commensal or pathogenic organisms, and characteristics of separate transport processes present on the apical and basolateral surface.

# V. Cholinergic-induced anion secretion in mouse jejunal monolayers involves synergy between muscarinic and nicotinic pathways[83]

## A. Background

Cholinergic signaling is one of the most widespread signal-transduction pathways in the human body, acting through either the G protein-coupled receptor (GPCR) muscarinic receptors or the ligand-gated cation-channel nicotinic receptors[43,63,92–95,84–91]. The peripherally expressed muscarinic receptors have been thought responsible for terminal cholinergic effects, while the neuronal nicotinic receptors are thought to be involved with stimulating and transmitting action potentials.

The mouse intestinal cholinergic response has been attributed to M3 and to a lesser extent M1 muscarinic receptors[45]. Recently, however, nicotinic receptor subunit expression was identified in mouse intestinal enterocytes, the presence of which was confirmed at the message level in mouse enteroids[96–99]. Single cell mRNA sequencing of the mouse intestinal epithelium indicated that the previously published data were incomplete[97]. One example being that the nicotinic subunit *Chrnb1* was shown to be expressed at low levels by almost all cell types of the intestinal epithelia, but the subunit had previously been considered exclusive to neuromuscular junctions. Nicotinic subunit expression is also present in several intestinal cancer cell lines and other epithelia (mouse colonic epithelia[100,101], HT29[102], STC-1 cells[103], airway epithelia[104], skin keratinocytes[105]). The full spectrum of nicotinic subunit expression in intestinal epithelial cells is still undergoing evaluation.

Until recently, a physiological function of the nicotinic receptors in the intestinal epithelia was not reported. A link between nicotinic receptor activation and Wnt-signaling that regulates proliferation and differentiation of the intestinal epithelia was recently made using mouse enteroids, specifically the nicotinic antagonist Mecamylamine reduced growth of 3D organoids over 7 days[96], but other possible functions of nicotinic signaling in intestinal epithelial cells remain unexplored. The current paradigm of

nicotinic receptors being limited to the nervous system and specific cell types means that any data supporting nicotinic receptor function in terminal tissues is rare and may be mistakenly attributed to muscarinic receptor activation. This occurs since most studies model cholinergic regulation using the agonist carbachol, which activates both muscarinic and nicotinic receptors, and data are interpreted assuming the absence of nicotinic receptors.

The non-differentiated crypt model we developed was used for further analysis of cholinergic-induced anion secretion as the intestinal crypt where a majority of anion secretion is known to occur[62]. This is in contrast to whole tissue and animal models where the crypt and villus populations are both present during studies. One benefit of the enteroid cultures over these other models is that there are no contaminating cell populations so that epithelial contributions can be defined. As demonstrated by our following cholinergic findings, the enteroid monolayer system provides a unique platform to study physiology that may otherwise be masked by the complexity of whole tissues.

## B. Results

### 1. Cholinergic-induced anion secretion is partially hexamethonium sensitive

Since the differentiated monolayers have characteristics of the jejunal villus and display the expected low anion secretion in response to carbachol ($<2\mu A/cm^2$), the non-differentiated monolayers were used for analysis of cholinergic-induced secretion (**Figure 2G**). The cholinergic stimulation of anion secretion was initially evaluated in the jejunal enteroid monolayers using the mixed muscarinic and nicotinic agonist carbachol (CCh). Short-circuit current ($I_{sc}$) is a measure of electrogenic ion transport across an epithelium. As the measurement is dependent on the injection of voltage to maintain the current across the epithelium at 0, transport that results in electroneutral ion movement (such as the exchange of one $H^+$ for one $Na^+$ by NHEs) is invisible to this system. The direction of the current change is dependent on the order of electrodes and orientation of the sample. In our preparation, a positive deflection represents either electrogenic apical anion secretion or cation absorption. Based on the previously defined behavior of the intestinal epithelium in response to cholinergic signaling, it was assumed that anion

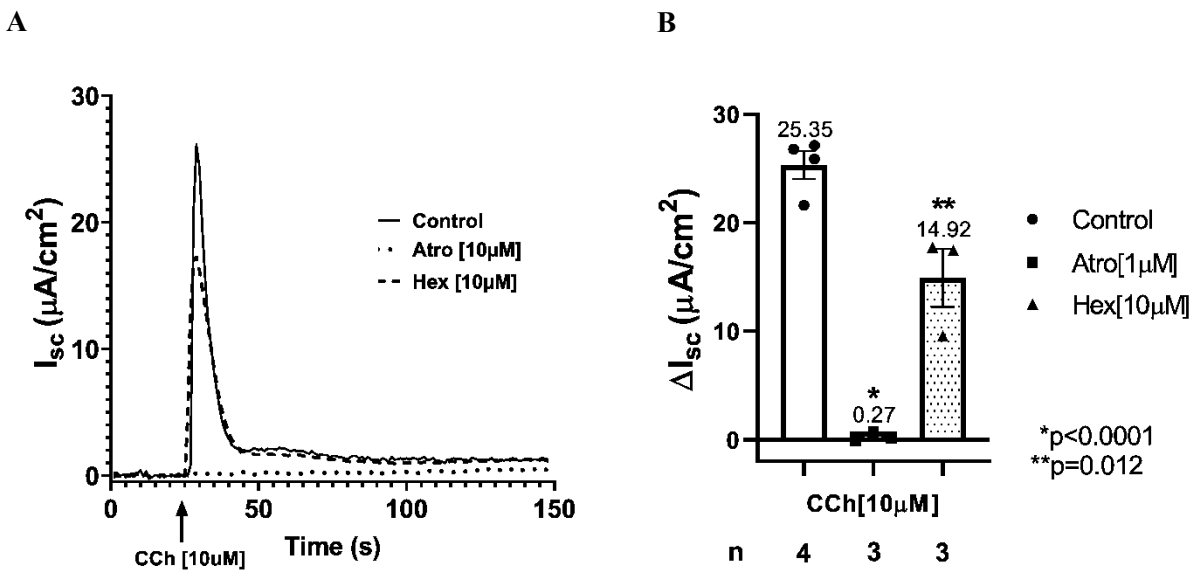


**Figure 3: Cholinergic Stimulation Increases $I_{sc}$ and is Atropine and Hexamethonium Sensitive**

**A)** Example traces of carbachol-induced anion secretion after 20 minute pre-incubation with hexamethonium [10μM] or atropine [1μM] in non-differentiated mouse jejunal enteroid monolayers. The arrow indicates addition of CCh [10μM]. **B)** The average increase in short circuit current ($I_{sc}$) after stimulation with 10μM carbachol ± SEMs. Points indicate average values for individual experiments. Total number of experiments (n) for each condition included in the labels below the bars. p-values were calculated using an unpaired Student's t-test between the carbachol [10μM] alone and pre-treatment with the cholinergic antagonists.

secretion (in particular chloride secretion) was being observed. Carbachol caused an increase in $I_{sc}$ that started immediately after addition to the serosal surface, peaked within 5 seconds, and lasted approximately 12 seconds total (**Figure 3A**). The effects of the cholinergic antagonists atropine (muscarinic) and hexamethonium (nicotinic) were evaluated on the carbachol response.

In non-differentiated monolayers, the response to carbachol [10μM] was 25.35μA/cm$^2$ ± 1.28μA/cm$^2$. Pretreatment with the muscarinic antagonist atropine [1μM] completely abolished the carbachol-induced secretion resulting in an increase in $I_{sc}$ of only 0.27μA/cm$^2$ ± 0.23 μA/cm$^2$ (1.0% ± 0.9% of the control response, $p<0.0001$, n=3). Surprisingly, the nicotinic antagonist hexamethonium [10μM] significantly reduced the carbachol-induced short-circuit current to 14.9μA/cm$^2$ ± 2.68μA/cm$^2$ (55.8% ± 9.4% of the control response, $p=0.012$, n=3) (**Figure 3B**). Based on this unexpected finding of a significant nicotinic component to the carbachol response, in the absence of a neuronal population in the preparation, the contribution was characterized further.

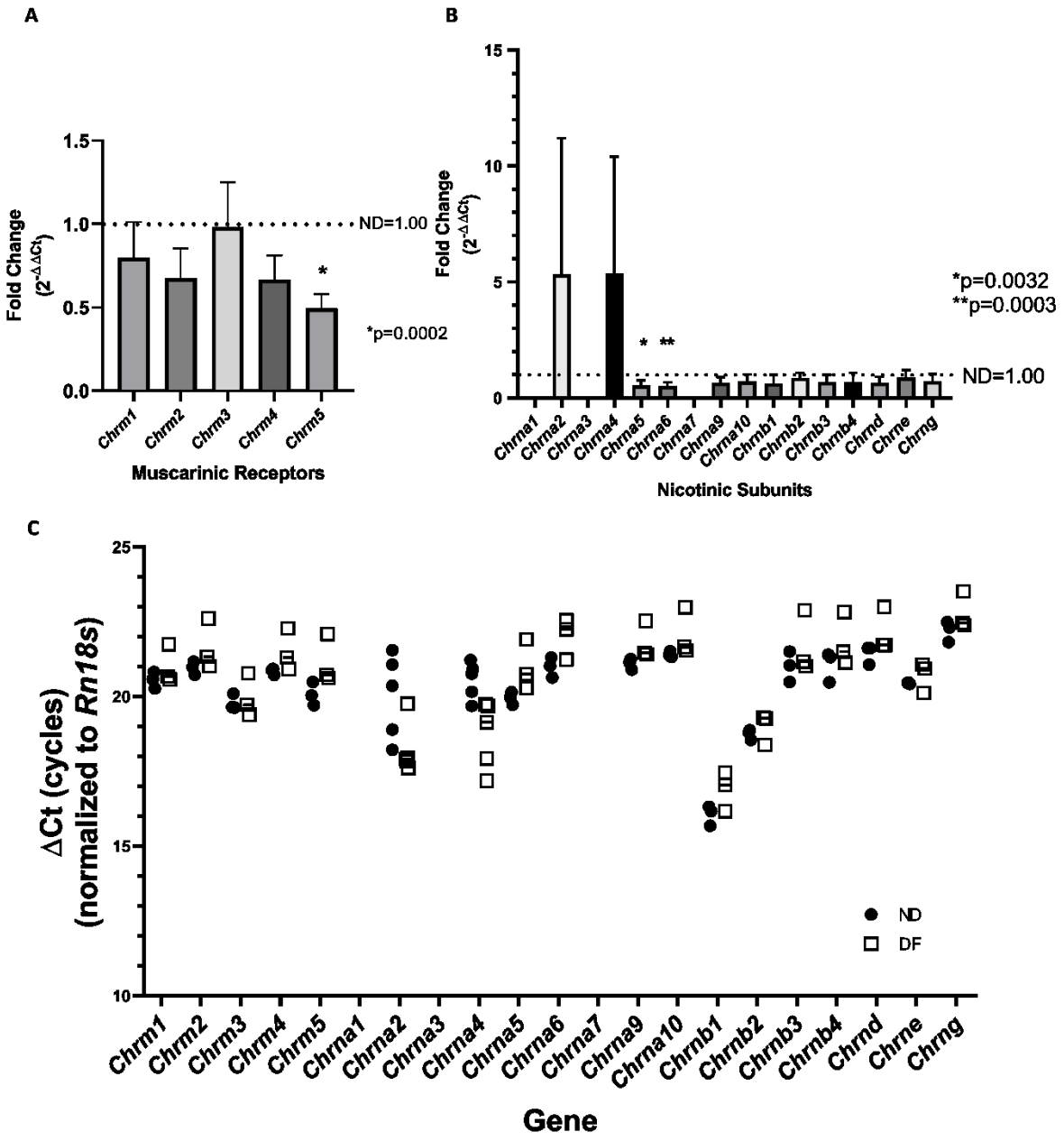


**Figure 4: Expression of Cholinergic Receptor Genes**

Fold change in mRNA expression of **A)** the muscarinic receptors and **B)** the nicotinic receptor subunits in mouse jejunal enteroid monolayers. Expression of non-differentiated monolayers set as 1.00 and expression in differentiated monolayers in comparison to non-differentiated presented as shaded bars. Expression of *Chrm5* is reduced in differentiated monolayers, the other four muscarinic receptors are unaffected. Nicotinic alpha subunits 1, 3, and 7 are not expressed in the jejunal monolayers at all, and alpha subunits 5 and 6 are reduced in differentiated cultures. **C)** Delta Ct showing approximate mRNA expression comparisons of the cholinergic receptors in non-differentiated and differentiated monolayers. Corrected to *Rn18s* endogenous control expression (n=3-6 different passages). p-values were calculated using an unpaired Student's t-test.

## 2. Expression of cholinergic receptors in mouse jejunal enteroid monolayers

The monolayers were tested for expression of nicotinic receptor subunits. Primers for each of the 21 mammalian cholinergic receptor genes (5 muscarinic and 16 nicotinic) were used for qRT-PCR with cDNA isolated from both non-differentiated and differentiated mouse jejunal monolayers. All five muscarinic receptors were detectable in both differentiated and non-differentiated enteroids, although as previously reported, the $M_3$ receptor was most highly expressed and only the $M_5$ receptor was significantly altered with differentiation, being reduced to 49% $\pm$ 8.7% (p=0.0002) of expression in non-differentiated monolayers (**Figure 4A, C**). Only three nicotinic subunits were not expressed in non-differentiated or differentiated enteroids: cholinergic nicotinic subunit alpha 1 (*Chrna1*), nicotinic subunit alpha 3 (*Chrna3*), and nicotinic subunit alpha 7 (*Chrna7*). A majority of the receptors and subunits did not display a significant difference in mRNA expression between the non-differentiated and differentiated cultures. The nicotinic subunits that changed in expression upon differentiation, being lower in the differentiated enteroids were *Chrna5* (53% $\pm$ 14%, p=0.0032) and *Chrna6* (51% $\pm$ 9.1%, p=0.0003) (**Figure 4B**).

As a variety of nicotinic receptor subunits were present in our culture model, we hypothesized that there was a previously uncharacterized nicotinic component to cholinergic-induced anion secretion that was being inhibited by pre-treatment with hexamethonium.

## 3. Muscarinic stimulation is concentration dependent while nicotine has no effect on $I_{sc}$

In order to separate the contributions of the muscarinic and nicotinic components to cholinergic induced anion secretion, specific muscarinic (bethanechol) and nicotinic (nicotine) agonists were used. Stimulation of the mouse jejunal enteroid monolayers with the muscarinic-selective agonist bethanechol resulted in a concentration-dependent increase in $I_{sc}$ that mimicked the timescale and shape of the carbachol response **(Figure 5A)**. Kinetic analysis using the Lineweaver-Burk method revealed a $K_m$ of bethanechol in this system of 91.5μM (**Figure 5C**).

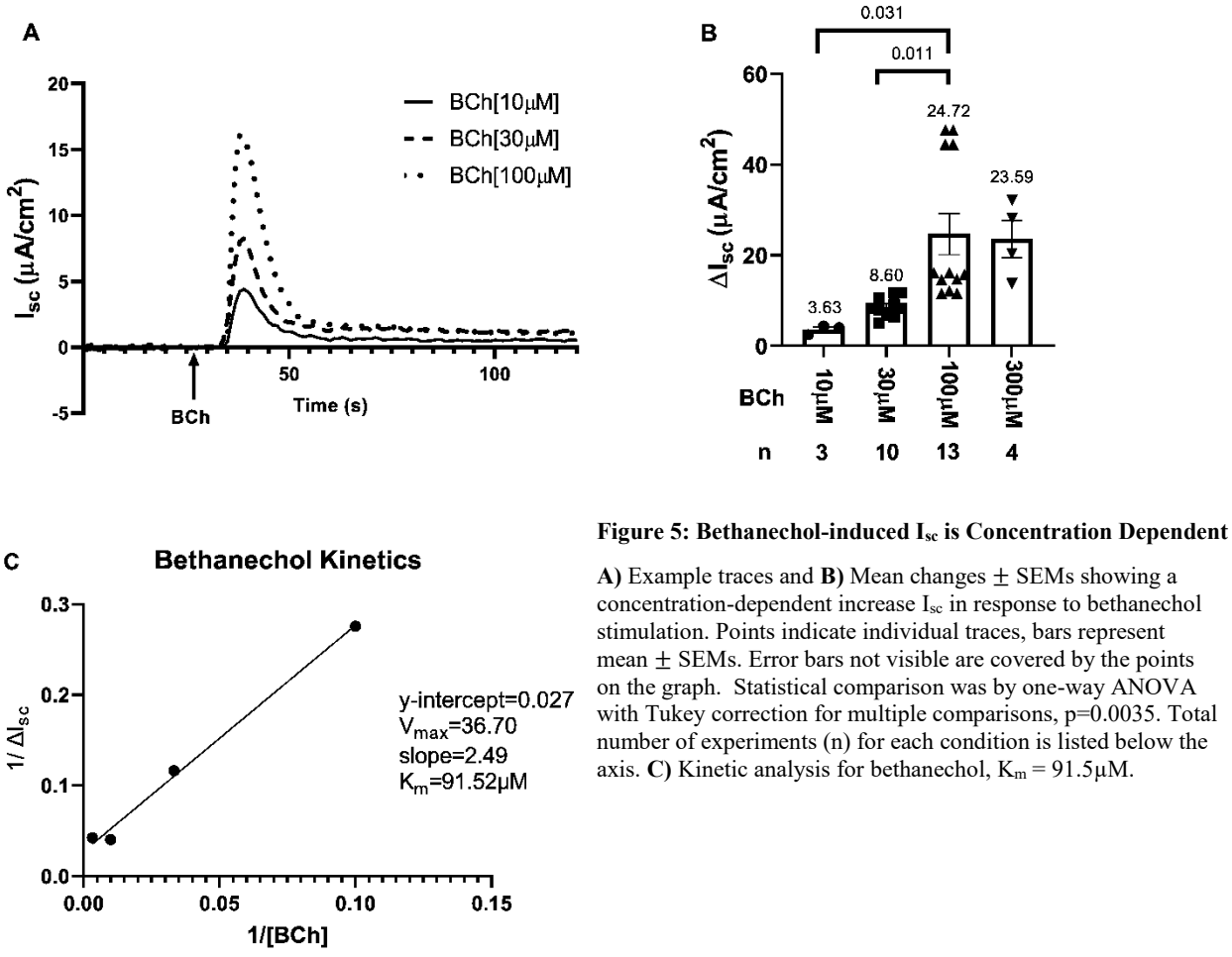


**Figure 5: Bethanechol-induced $I_{sc}$ is Concentration Dependent**

**A)** Example traces and **B)** Mean changes ± SEMs showing a concentration-dependent increase $I_{sc}$ in response to bethanechol stimulation. Points indicate individual traces, bars represent mean ± SEMs. Error bars not visible are covered by the points on the graph. Statistical comparison was by one-way ANOVA with Tukey correction for multiple comparisons, p=0.0035. Total number of experiments (n) for each condition is listed below the axis. **C)** Kinetic analysis for bethanechol, $K_m$ = 91.5μM.

In contrast, the addition of nicotine alone at concentrations from 3-30μM to the basolateral chamber did not significantly alter $I_{sc}$ **(Figure 6A)**, and at high concentrations (≥100μM) there was a hexamethonium-insensitive drop in $I_{sc}$ that was attributed to toxicity (**data not shown**).

## 4. Nicotine increases $I_{sc}$ when co-applied with bethanechol

To determine if nicotine enhanced the muscarinic response, as indicated by the hexamethonium sensitivity of carbachol, the reconstruction of the carbachol response was tested by co-administering bethanechol and nicotine at various concentrations. Bethanechol (BCh) and nicotine (Nico) were applied to the basolateral surface of jejunal monolayers both separately and together. When applied together with 30μM BCh, the addition of increasing concentrations of nicotine that were below the toxic dose resulted in an increased $I_{sc}$ compared to 30μM BCh alone **(Figure 6B-D)**. The nicotine component was

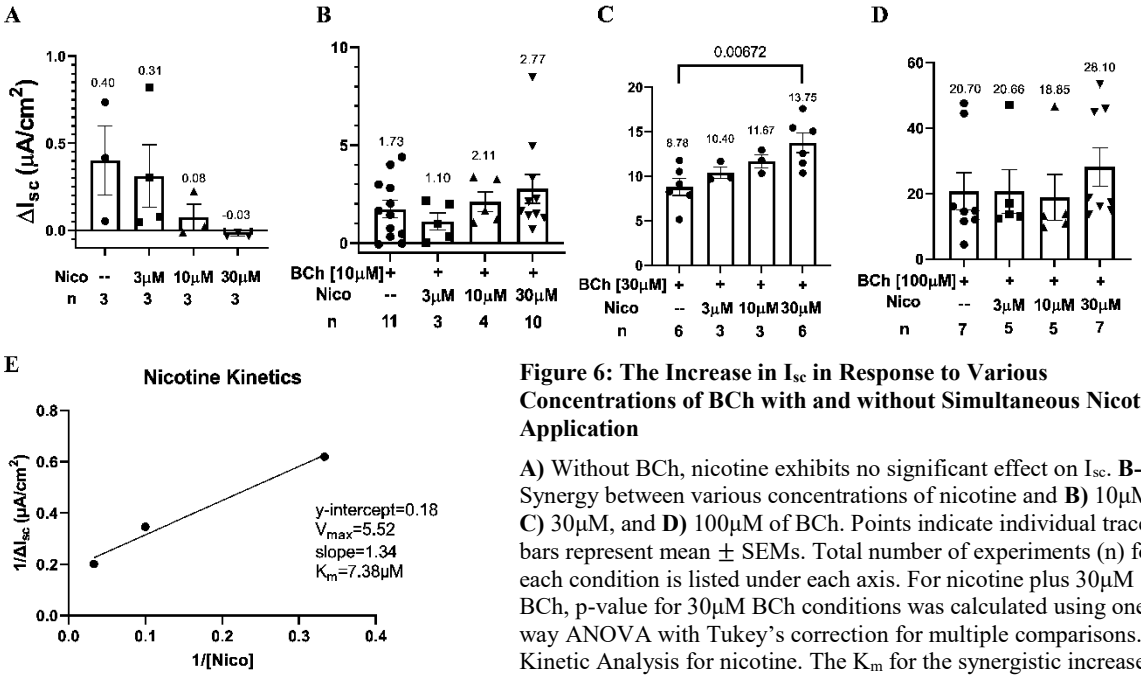


**Figure 6: The Increase in $I_{sc}$ in Response to Various Concentrations of BCh with and without Simultaneous Nicotine Application**

**A)** Without BCh, nicotine exhibits no significant effect on $I_{sc}$. **B-D)** Synergy between various concentrations of nicotine and **B)** 10μM, **C)** 30μM, and **D)** 100μM of BCh. Points indicate individual traces, bars represent mean ± SEMs. Total number of experiments (n) for each condition is listed under each axis. For nicotine plus 30μM BCh, p-value for 30μM BCh conditions was calculated using one-way ANOVA with Tukey's correction for multiple comparisons. **E)** Kinetic Analysis for nicotine. The $K_m$ for the synergistic increase in $I_{sc}$ caused by nicotine (calculated as the increase in $I_{sc}$ caused by BCh [30μM] plus nicotine [0-30μM], minus the increase in $I_{sc}$ by BCh alone [30μM]) = 7.4μM.

concentration dependent at this BCh concentration only. Kinetic analysis of the nicotine-induced increase in BCh-induced $I_{sc}$ for 30μM bethanechol (corrected by subtracting the bethanechol response without nicotine application before analysis with the Lineweaver-Burk method) indicated a $K_m$ of the nicotine component of 7.4μM (**Figure 6E**). Of note, a significant effect due to the addition of nicotine was not detected when applied with either 10μM or 100μM bethanechol.

## 5. Muscarinic and nicotinic synergy is hexamethonium sensitive

To demonstrate that the muscarinic and nicotinic components were mediated by the muscarinic and nicotinic receptors rather than an off-target response to the agonists, the combination of bethanechol and nicotine was tested for sensitivity to the antagonists atropine [1μM] and hexamethonium [10μM]. Pre-incubation with hexamethonium [10μM] reduced the synergistically-induced $I_{sc}$ to the same level as BCh [30μM] alone, and pre-incubation with atropine completely abolished the anion-induced secretion as expected (**Figure 7**). This indicates that the synergy is mediated through both types of receptors rather than a non-receptor mediated pathway.

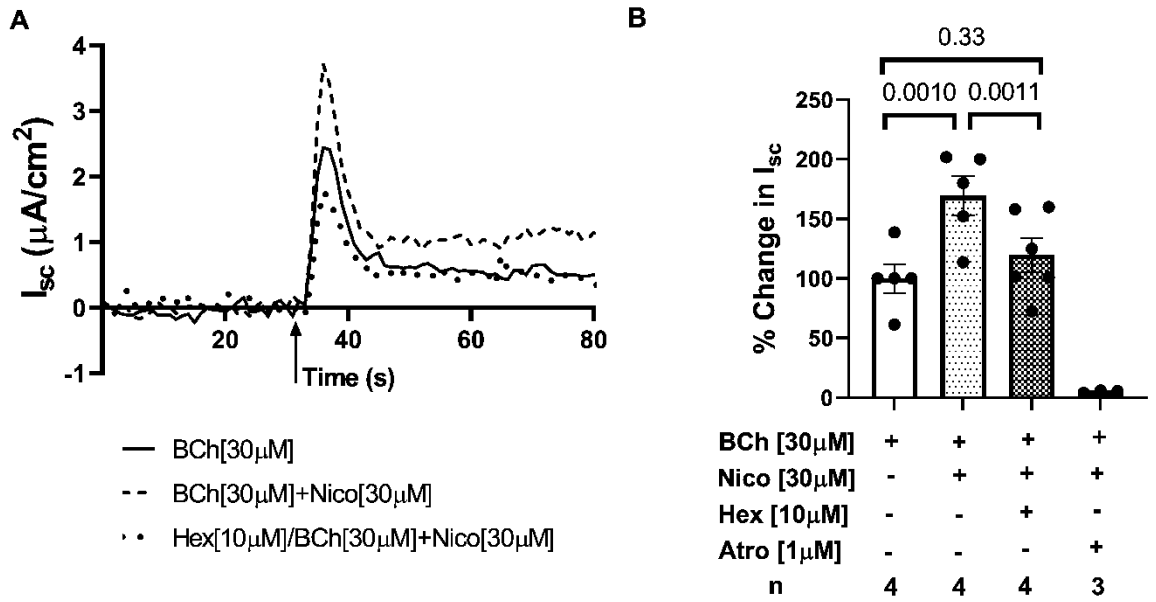


**Figure 7: Nicotine Synergy with Bethanechol Acts through the Nicotinic Receptor**
**A)** Traces from a single experiment (arrow indicates addition of agonist) and **B)** The mean maximum increase in $I_{sc}$ in the presence and absence of simultaneous administration of nicotine; in some cases after pre-treatment (20 min) with serosal hexamethonium [10μM] or atropine [1μM]. Hexamethonium eliminated the synergistic increase in $I_{sc}$ caused by BCh and nicotine. The elimination of the nicotinic component restored anion secretion to levels comparable to when stimulated with bethanechol[30μM] alone. Bars represent mean ± SEMs. p-values calculated by unpaired Student's t-tests between indicated conditions. Total number of experiments (n) for each condition listed under each bar.

## C. Discussion

The present study offers two significant findings: first is the observation of a previously uncharacterized component of cholinergic signaling in the intestinal epithelia through nicotinic ligand-gated cation channels and second is the development and characterization of a mouse enteroid monolayer system. While human enteroid monolayer studies have advanced gastrointestinal physiology and pathophysiology, problems with generating mouse enteroid monolayers have held the field back. Here we demonstrate successful, reproducible generation of confluent monolayer cultures using mouse enteroids. These cultures reveal a previously uncharacterized aspect of cholinergic-induced anion secretion, offering an important tool to further advance the field of gastrointestinal physiology.

This study applies the newly developed mouse enteroid monolayers to identify and characterize a functional nicotinic component of epithelial cholinergic-induced anion secretion that was previously masked by both the systems available and the assumptions made by the community. In challenging the current dogma regarding the presence of functional nicotinic receptors outside of select cell populations

and functions, we open the door to investigation of potential localization and functions in even more cell populations. Due to the widespread nature of nicotinic receptors within the body, there is clinical application in determining the extent of localization and function to address potential diseases, treatments, and side effects that may have been overlooked due to the masked nicotinic component of cholinergic signaling.

In the intestinal epithelia, it has been well documented that muscarinic receptor $M_3$ is responsible for a large outward current in response to acetylcholine, causing an efflux of chloride and fluid into the lumen of the intestine. In the mouse, this is supplemented by the $M_1$ receptor[45], but in the human small intestine only $M_3$ mediates anion secretion. The current model of intestinal cholinergic-induced anion secretion involves muscarinic receptors activating the $G_{q/11}$ signaling cascade to initially increase intracellular calcium release from ER stores to open apical chloride channels and activate plasma membrane $K^+$ channels. Our results do not contradict this model but identified that cholinergic anion secretion also involves nicotinic receptors in the intestinal epithelial cells. This conclusion is based on studies using mouse enteroids that are an exclusively epithelial cell model that lacks any component of the enteric nervous system or underlying muscle.

The current results demonstrate that multiple nicotinic receptor subunits are expressed in mouse jejunal enterocytes. Expression of the full panel of nicotinic receptors has not previously been reported in the mouse jejunum, and the majority of nicotinic receptor studies have been done in colon cancer cells lines that express only a subset of the nicotinic subunits[100–103]. We demonstrated that a majority (13/16 subunits) of the nicotinic subunits were expressed by the mouse jejunal epithelial cells, allowing for a large array of potential nicotinic receptors to compliment the known expression of muscarinic receptors. The variety of nicotinic subunits expressed by the mouse intestinal epithelial monolayers indicates that there may be nicotinic-mediated effects on many processes that have not previously been considered[96,99,106]. Determining which nicotinic pentamer is responsible for the effect on anion secretion will be an important step in characterizing the response.

Recently, murine small intestinal epithelial single cell mRNA sequencing data was reported, which expanded our knowledge of the nicotinic receptor genes that are expressed by intestinal epithelium[97]. This study identified 5 out of 16 mammalian receptor subunits, *Chrna2*, *Chrnb1*, *Chrnb2*, *Chrnb4*, and *Chrne*. The mRNA expression data from the enteroid monolayers identifies an even larger pool of nicotinic subunits (13/16).

The unexpected and significant inhibitory effect of hexamethonium on carbachol-induced anion transport in the enteroid monolayers indicated a likely role for nicotinic receptors expressed by the intestinal epithelia having a modulatory role on muscarinic-induced $I_{sc}$. Nicotine-induced nicotinic signaling, although it had a significant effect on cholinergic-induced anion secretion when inhibited, did not have an effect on short-circuit current when nicotine was applied independently. Rather, muscarinic activation with bethanechol was required to reveal the effect of nicotine on $I_{sc}$, and the co-application of nicotine enhanced bethanechol-induced anion secretion in a concentration dependent manner, an effect that was hexamethonium sensitive and thus mediated through the nicotinic receptors. Why nicotine has a synergistic effect at only an intermediate bethanechol concentration is not understood; although the lack of any additional effect of nicotine at the maximal bethanechol concentration likely indicates saturation of some aspect of the anion secretory process involved.

Taken together, the partial inhibitory effect of hexamethonium and the lack of nicotine-induced $I_{sc}$ indicates that nicotinic signaling does not play a primary role in secretion, but rather a modulatory one. It appears to act to further increase anion secretion only if anion secretion is already occurring in response to muscarinic activation.

The cholinergic response of the intestinal epithelia was initially characterized in T84 cells[40,47,50,107–109], which has subsequently been used as a model of the anion secretory response. The current study shows that in mouse jejunal enteroids, the cholinergic signaling pathway is more complex, and opens the door to considerations that the cholinergic signaling pathways may be regulated in this more complex manner in additional tissues/organs, and provides a cell model system for further

mechanistic investigation. In addition, it is important to consider differences in normal intestinal models compared to studies using cancer cell lines.

The isolated jejunal epithelial population cultured as monolayers allowed us to establish that nicotinic receptors are expressed by mouse intestinal epithelial cells and are involved in regulating anion secretion in response to cholinergic stimulation. As demonstrated by our cholinergic findings, the enteroid monolayer system provides a unique platform to study physiology that may otherwise be masked by the complexity of whole tissues. Mouse enteroids studied as confluent monolayers now can be used in a similar manner as human enteroids with the apical surface exposed to allow studies that include transcytosis of luminal or basolateral nutrients, separate effects of neurohumoral substances on the apical and basolateral surfaces, lumen specific effects of commensal or pathogenic organisms, and characteristics of separate transport processes present on the apical and basolateral surface. Further mechanistic understanding of the synergistic interactions of the muscarinic-nicotinic signaling pathways will be undertaken using this model of murine enteroid monolayers.

# VI. Mechanism of cholinergic synergy in jejunal anion secretion

## A. Background

The previously described observation of a nicotinic component of anion secretion that is dependent on muscarinic-induced secretion leads to the conclusion that there must be cross-talk between the two pathways. The literature regarding nicotinic-modified anion secretion in the small intestine is limited by being a novel observation, but cross-talk between the two pathways in other systems is also poorly defined. The current dogma of muscarinic and nicotinic receptors being expressed by mutually exclusive cell types has recently been called into question by observations in many systems[100,102–105,110]; but any functional physiology involving the two is still newly observed and poorly defined. In order to characterize the intracellular signaling pathways that are involved in the cross-talk of cholinergic muscarinic and nicotinic receptors as involved with cholinergic-induced anion secretion, we continued to utilize our newly defined mouse enteroid monolayer system in order to 1) define the ions and transport proteins involved and 2) begin to define the mechanism by which the two pathways interact.

The cholinergic stimulation of secretion in the intestinal epithelium was previously defined in T84 cell monolayers. It was determined that not only are these cell responsive to carbachol, but the response was mediated by net chloride secretion and independent of an increase in intracellular cAMP, the pathway defined as responsible for VIP- and PGE-induced secretion[36,44]. Additionally, basolateral potassium was shown to play a key role both in chloride loading and maintaining the electronegativity of cells in both pathways[35].

It was thought that the activation of cholinergic-induced secretion was fairly straightforward due to the assumption of muscarinic signaling being responsible for activating an apical CaCC via ER calcium stores increasing intracellular calcium[111,112]. The identification of a nicotinic component does not directly conflict with this understanding, as it is a ligand gated calcium channel and activation of the pathway could simply further increase intracellular calcium from the extracellular pool(s) and result in increased

activation of CaCCs. However, confirming the mechanism by which the two pathways act to synergistically increase $I_{sc}$ is the next step.

In our earlier work we demonstrated that muscarinic and nicotinic signaling pathways are likely to converge rather than act in a parallel fashion as the response could be saturated by bethanechol alone with no further increase in response from the addition of nicotine to a maximal dose of bethanechol (**Figure 6D**). We also know that whatever pathways are involved, the nicotinic pathway does not stimulate anion secretion when applied alone, the concurrent addition of bethanechol is required to see any effect of nicotine on anion secretion, indicating that nicotinic signaling likely acts as a positive modifier of muscarinic-induced $I_{sc}$ (**Figure 6**). Starting with these two observations, we proposed to determine the mechanism of intracellular cross-talk between the muscarinic and nicotinic pathways.

Previous observations indicate that cholinergic-induced secretion in the intestine is a result of chloride efflux into the lumen. Currently, electrogenic chloride efflux can be attributed to contribution(s) from two different chloride channel classes expressed on the apical surface of the mouse jejunum; the cystic fibrosis transmembrane regulator (CFTR) and calcium-activated chloride channels (CaCCs)[111]. CFTR is a well-known channel involved in chloride secretion in many secretory tissues. On the other hand, the exact member of the CaCC family involved in anion secretion in the mouse jejunum is still debated, with early evidence pointing to different isoforms being dominant in different regions of the intestine in the mouse[113,114].

The two classes of chloride channel are moderated by different intracellular signaling pathways, and knowing which channel is involved with the muscarinic and nicotinic components of secretion will help identify the mechanism of intracellular cross-talk that mediates the nicotinic modulation of muscarinic-induced $I_{sc}$.

## B. Results

### 1. Inhibition of potassium channels abolishes CCh-induced $I_{sc}$

To confirm that cholinergic-induced $I_{sc}$ is generated as result of apical chloride efflux rather than movement of a different ion, we tested the effect of inhibiting basolateral potassium channels—responsible for potassium efflux that maintains electronegative status of the epithelial cells, facilitates chloride loading into the cell, and serves as a driving force for anion secretion, including chloride.

The initial peak of CCh-induced $I_{sc}$ ($24.00\mu A/cm^2 \pm 4.06\mu A/cm^2$) was completely abolished by inhibition of the basolateral potassium channels with Clotrimazole [30μM] $1.86\mu A/cm^2 \pm 1.37\mu A/cm^2$ ($p=0.0067$, $n=3$) (**Figure 8-Red**). Interestingly, the second phase of the response—the plateau phase—remained unaffected by basolateral potassium channel inhibition. Only when monolayers were treated with clotrimazole apically either alone or in combination with basolateral inhibition were both peaks abolished (**Table 7**).

Time-to-resolution analysis of the initial peak confirms that the second phase and return to baseline of the cholinergic response is unaffected by potassium channel inhibition in general (**Figure 8D**), while area-under-the-curve (AUC) analysis demonstrates that losing only the peak current with basolateral potassium channel inhibition leaves a majority of chloride secretion intact in the second phase (66.9% of CCh control).

When apical potassium channels are inhibited, both peaks are affected and only 32.6% of total chloride secretion remains. Inhibition of potassium channels on both the apical and basolateral membranes together had a slightly smaller effect on AUC, leaving 49.3% of chloride secretion remaining, likely due to higher variability in the dual-inhibited condition (**Figure 8E**). This supports the observation that apical chloride secretion is responsible for the cholinergic-induced $I_{sc}$ observed and demonstrates that rather than being driven by a single, basolateral potassium channel, chloride secretion has two phases mediated through two potassium channels located on opposite sides of the polarized cell. The novel observation of an apical potassium channel influencing apical chloride secretion and the 2-phase secretory

response we observed, indicates that our understanding of the mechanism of chloride secretion in the intestinal epithelium is incomplete.

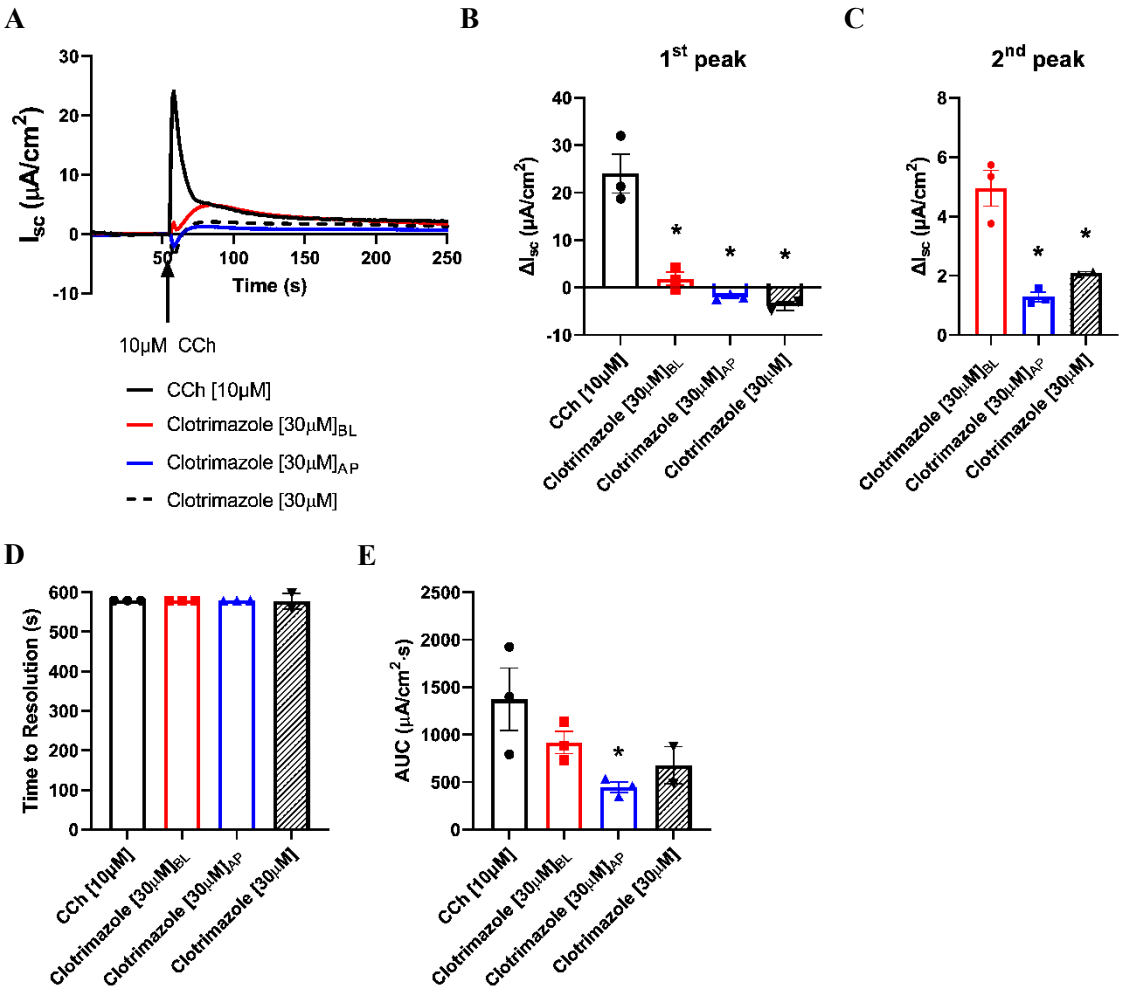


**Figure 8: Inhibition of potassium channels abolishes initial CCh-induced $I_{sc}$**

**A)** Average traces (arrow indicates addition of CCh[10μM]), and the mean maximum increase in **B)** the initial $I_{sc}$ peak and **C)** the second phase peak in the presence and absence of the potassium channel inhibitor Clotrimazole[30μM] applied serosally, mucosally, or both. **D)** The average amount of time before cholinergic-induced Isc returned to baseline. In all conditions, the experiment was ended before $I_{sc}$ returned to 0. **E)** The average AUC indicating total secretion post-crbachol stimulation. Only when apical potassium channels were inhibited was total secretion significantly reduced. Pre-incubation (15 minutes) with Clotrimazole[30μM] basolaterally abolished the initial peak of CCh-induced $I_{sc}$ but the plateau phase was unaffected. Pre-incubation with apical clotrimazole or the combination of apical and basolateral clotrimazole blocked both peaks. p-values were calculated using an unpaired Student's t-test comparing conditions to **B)** CCh alone or **C)** basolateral clotrimazole treatment. Points represent individual traces while bars denote the average and SEM for each condition. *p<0.05. n=2-3 experiments.

| Condition | Peak 1 | Peak 2 |
|---|---|---|
| Carbachol[10μM] | 24.00μA/cm$^2$ ± 4.06μA/cm$^2$ | N/A |
| Clotrimazole[30μM]$_{BL}$ | 1.86μA/cm$^2$ ± 1.37μA/cm$^2$ p=0.0067, n=3 | 4.95μA/cm$^2$ ± 0.61μA/cm$^2$ |
| Clotrimazole[30μM]$_{AP}$ | -1.97μA/cm$^2$ ± 0.30μA/cm$^2$ p=0.0031, n=3 | 1.30μA/cm$^2$ ± 0.16μA/cm$^2$ p=0.0043, n=3 |
| Clotrimazole[30μM] | -3.92μA/cm$^2$ ± 0.94μA/cm$^2$ p=0.013, n=2 | 2.10μA/cm$^2$ ± 0.05μA/cm$^2$ p=0.036, n=2 |

**Table 7: Inhibition of potassium channels abolishes initial CCh-induced $I_{sc}$**
Average maximum short-circuit current peaks for the initial peak and secondary peak post-carbachol[10μM] stimulation with and without clotrimazole[30μM] pre-incubation (15 minutes) as indicated.

## 2. Carbachol-induced anion secretion is mediated through CFTR and CaCC

The contribution of two different chloride channels to cholinergic-stimulated anion secretion was evaluated in the jejunal enteroid monolayers using the mixed muscarinic and nicotinic agonist carbachol (CCh), the muscarinic-specific agonist bethanechol (BCh), and the nicotinic-specific agonist nicotine (Nico). The inhibitor BPO27 was used to block any chloride secretion through CFTR. The CaCC inhibitor A01 was used to block contributions of this channel family to CCh-induced chloride secretion.

Inhibition of carbachol-induced chloride secretion using either the CFTR inhibitor BPO27 or the CaCC inhibitor A01 was used to determine the identity of the chloride channel(s) involved in the cholinergic-induced increase in $I_{sc}$. Carbachol caused an increase in $I_{sc}$ similar to that defined previously (**Figure 9**). The effects of chloride channel antagonists BPO27 and A01 were evaluated on the CCh response [10μM] in non-differentiated mouse jejunal monolayers. The carbachol response (27.46μA/cm$^2$ ± 5.5μA/cm$^2$, n=5) was blunted by 20 minute pre-treatment with the CFTR inhibitor BPO27 10.23μA/cm$^2$ ± 4.4μA/cm$^2$ (31.29% ± 8.0% of the control response, p<0.0001, n=3) or the CaCC inhibitor A01 9.9μA/cm$^2$ ± 1.7μA/cm$^2$ (44.5% ± 11.2% of the control response, p=0.0004, n=4). Application of both inhibitors abolished CCh-induced $I_{sc}$, 1.0μA/cm$^2$ ± 0.15μA/cm$^2$ (6.5% ± 0.4% of the control response, p<0.0001, n=3). Altogether, this data indicated that cholinergic-induced anion secretion is mediated by both CFTR and a CaCC.

## 3. Bethanechol- and nicotine-induced secretion is mediated through CFTR and CaCC

Inhibition of chloride secretion in response to the combination of BCh[30μM] + Nico[30μM] after pre-incubation with either the CFTR inhibitor BPO27 or the CaCC inhibitor A01 was tested to confirm that the combination of agonists is acting through the same channels as the mixed agonist carbachol. The combination of bethanechol and nicotine caused an increase in $I_{sc}$ (10.16μA/cm$^2$ ± 1.7μA/cm$^2$, n=9) that was greater than that of BCh alone (61.6% ± 10.0% of the control response, p<0.0001, n=5) and was blunted by 20 minute pre-treatment with the CFTR inhibitor BPO27 7.07μA/cm$^2$

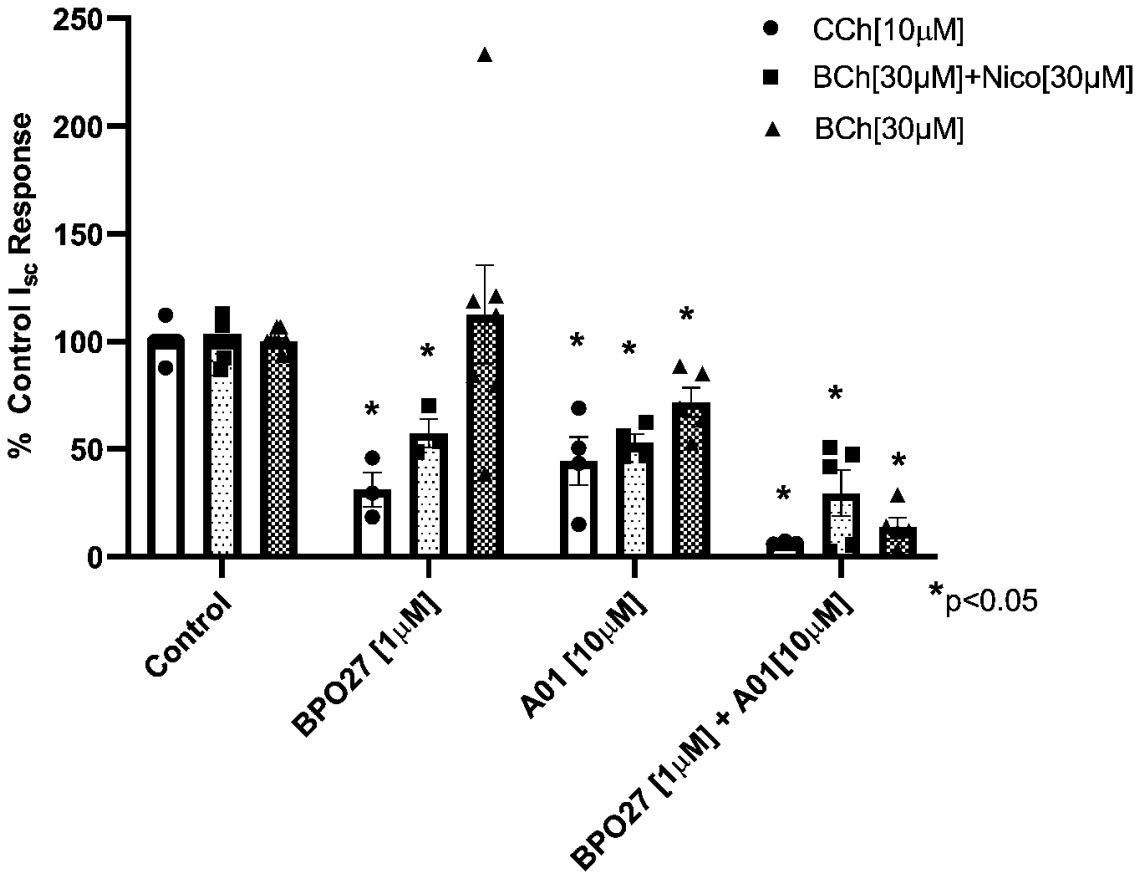


**Figure 9: Cholinergic-induced $I_{sc}$ is mediated through both CFTR and CaCC**
Stimulation of non-differentiated jejunal monolayers with a general cholinergic agonist (CCh[10μM]), muscarinic agonist (BCh[30μM]), or a combination of muscarinic and nicotinic agonists (BCh[30μM]+Nico[30μM]) after pre-incubation with either a CFTR inhibitor (BPO27) or a CaCC inhibitor (A01). Stimulation with CCh and BCh+Nico give similar inhibition profiles with BPO27 and A01 partially inhibiting $I_{sc}$ and pre-incubation with both abolishing $I_{sc}$. BCh-stimulated $I_{sc}$ is unaffected by BPO27 alone, but the CaCC inhibitor A01 only partially inhibits $I_{sc}$. Inhibition of both CaCC and CFTR abolished BCh-induced $I_{sc}$. p-values were calculated using an unpaired Student's t-test between the control condition of the agonist alone and pre-treatment with the chloride channel inhibitors, *p<0.05. Dots represent individual traces while bars denote the average and SEM for each condition.

$\pm$ 2.1μA/cm$^2$ (57.41% $\pm$ 6.6% of the control response, p<0.0001, n=3) or the CaCC inhibitor A01 7.0μA/cm$^2$ $\pm$ 0.5μA/cm$^2$ (53.0% $\pm$ 3.9% of the control response, p<0.0001, n=4). Application of both inhibitors abolished BCh+Nico-induced $I_{sc}$, 1.0μA/cm$^2$ $\pm$ 0.4μA/cm$^2$ (29.6% $\pm$ 10.6% of the control response, p<0.0001, n=5) (**Figure 9**). This data shows that the combination of muscarinic (bethanechol) and nicotinic (nicotine) agonists phenocopies the chloride response of the cholinergic agonist carbachol as expected, and that cholinergic-induced chloride secretion is mediated through both CFTR and a CaCC.

## 4. Bethanechol-induced secretion is primarily mediated through CaCC

Since nicotine does not elicit a change in $I_{sc}$ when applied alone, determining which channels are activated as a result of either muscarinic or nicotinic signaling must be done by comparing the responses of BCh-induced $I_{sc}$ to BCh+Nico-induced $I_{sc}$. Whatever is different between the two can be attributed to the action of nicotinic signaling while the BCh-induced current demonstrates the activity resultant from muscarinic signaling.

BCh-induced current (11.7μA/cm$^2$ $\pm$ 2.1μA/cm$^2$, n=7) was unaffected by pre-incubation with inhibitor BPO27 10.75μA/cm$^2$ $\pm$ 2.5μA/cm$^2$ (112.5% $\pm$ 23.0% of the control response, p=0.5445, n=6) and only partially inhibited by inhibitor A01 7.2μA/cm$^2$ $\pm$ 1.3μA/cm$^2$ (71.8% $\pm$ 6.7% of the control response, p=0.0002, n=5). Application of both inhibitors abolished BCh-induced $I_{sc}$, 1.2μA/cm$^2$ $\pm$ 0.3μA/cm$^2$ (14.0% $\pm$ 4.1% of the control response, p<0.0001, n=5) (**Figure 9**). The lack of a CFTR component in response to BCh stimulation alone indicates that the nicotinic pathway modifies muscarinic-induced $I_{sc}$ by regulating the activation of CFTR which possibly occurs via inducing cross-talk between $[Ca^{2+}]_i$ and cAMP. The incomplete abolishment of BCh-induced current by A01 indicates that a separate, secondary pathway may be involved when muscarinic-induced secretion fails—the cell partially activating CFTR in response to the inhibited CaCCs would explain why the CaCC-mediated current is only abolished when both of the chloride channels are inhibited.

## 5. Expression of chloride channels in mouse jejunal monolayers

As both CFTR and CaCCs appear to be involved in cholinergic induced anion secretion, we checked mRNA expression in both ND and DF mouse jejunal monolayers for *Cftr* and two CaCC isoforms previously shown to be involved in intestinal chloride secretion in the mouse[113–115]. In mouse jejunal monolayers, *Cftr* expression is reduced in DF monolayers compared to ND monolayers ($p<0.0001$), is higher than *Ano1/Tmem16A* expression in ND monolayers ($p<0.0001$) but is comparable to *Ano6/Tmem16F* in ND monolayers ($p=0.09$). In differentiated monolayers, *Cftr* expression is comparable to *Tmem16A* ($p=0.11$) but lower than *Tmem16F* ($p<0.0001$). In fact, while both *Cftr* ($p<0.0001$) and *Tmem16A* ($p=0.0011$) expression decreased with differentiation, *Tmem16F* increased with differentiation ($p=0.0008$) (**Figure 10**). Overall, *Tmem16F* is more highly expressed in the mouse jejunum than *Tmem16A*, though both appear to be expressed at levels that could result in an observable increase in chloride transport as they are expressed in comparable levels to *Cftr*. This is partially corroborated by

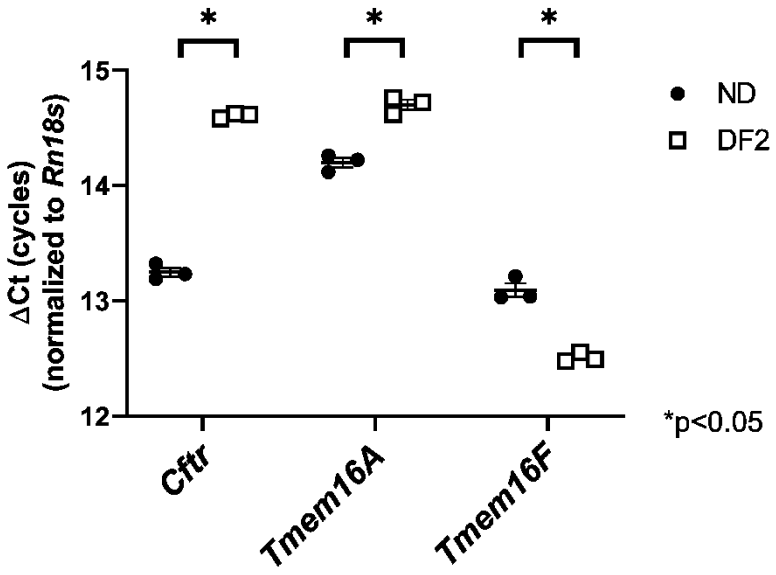


**Figure 10: Expression of Chloride Channels of Interest**

mRNA expression of apical chloride channels that may be involved in cholinergic secretion in mouse jejunal monolayers. CFTR is well defined as an apical chloride channel with functions in health and disease in the intestinal epithelia. TMEM16A and F are members of the calcium-activated chloride channel (CaCC) family that have been implicated in intestinal secretion. All three channels are expressed in both ND and DF mouse jejunal monolayers. Both *Cftr* and *Tmem16A* are reduced with differentiation ($p<0.05$, $n=3$) while *Tmem16F* expression is increased with differentiation of the jejunal monolayers ($p<0.05$, $n=3$). Mean and error bars indicating SEM not visible are covered by the points. Points indicate average expression (of 3 replicates).

studies in the literature describing segment specific expression of TMEM16 proteins in the intestine[113,114]. However, the lack of consensus regarding the validation of TMEM16 antibodies means that such studies should be considered carefully. Further confounding the situation is the fact that TMEM16F has several different functions reported. TMEM16F has been described as having flippase activity in platelets and mutations that result in the loss of flippase activity have been identified in patients with a rare bleeding disorder called Scott Syndrome[116,117]. Flippase function of TMEM16F in the intestine has not been investigated, but studies in other systems indicate that chloride channel activity and flippase functions may be independent of each other[118,119]. The literature regarding TMEM16F further confounds due to reports of cation channel function[120,121]. Thus we are faced with the possible conundrum of a single protein that acts as a flippase, an anion channel, and a cation channel all at once. Beyond TMEM16A, 16B, and 16F, the remaining TMEM16 family members remain largely uncharacterized and their functions debated, thus residual chloride current may even be attributed to another family member yet characterized as their tentative classifications are so far by sequence homology only[112].

## 6. Intracellular calcium chelation reduces, but does not abolish carbachol induced $I_{sc}$

Interestingly, chelation of intracellular calcium using BAPTA-AM led to a significant reduction, but not abolishment of CCh-induced $I_{sc}$ 15.3μA/cm$^2$ ± 4.0μA/cm$^2$ (35.8% ± 8.6% of the control response, $p<0.0001$, n=3) (**Figure 11A**). This was unexpected as we had hypothesized that $[Ca^{2+}]_i$ was the secondary signal responsible for the entirety of the response. The $I_{sc}$ remnant in the presence of BAPTA-AM indicated either 1) BAPTA-AM chelation was incomplete in the conditions we selected and there was residual calcium in the system, 2) there was another contributing pathway that was calcium independent, or 3) there was an effect—that due to either close localization or rapid temporal effects—was exerted on the system before the stimulated calcium could be chelated.

In order to be sure that the partial BAPTA-AM effect on $I_{sc}$ was not due to incomplete calcium chelation or due to calcium effects prior to chelation, Caco-2 M3R/GCaMP6s monolayers were pre-incubated with BAPTA-AM [25μM] before calcium was imaged. Using the same concentration and pre-

incubation time as when investigating transport, BAPTA-AM completely abolished both bethanechol- and bethanechol and nicotine-induced increases in intracellular calcium in the Caco-2 monolayers (**Figure 11B-C**). As intracellular calcium was successfully chelated and did not display any temporary increase in calcium levels, the residual $I_{sc}$ observed after chelation with BAPTA-AM is likely caused by a

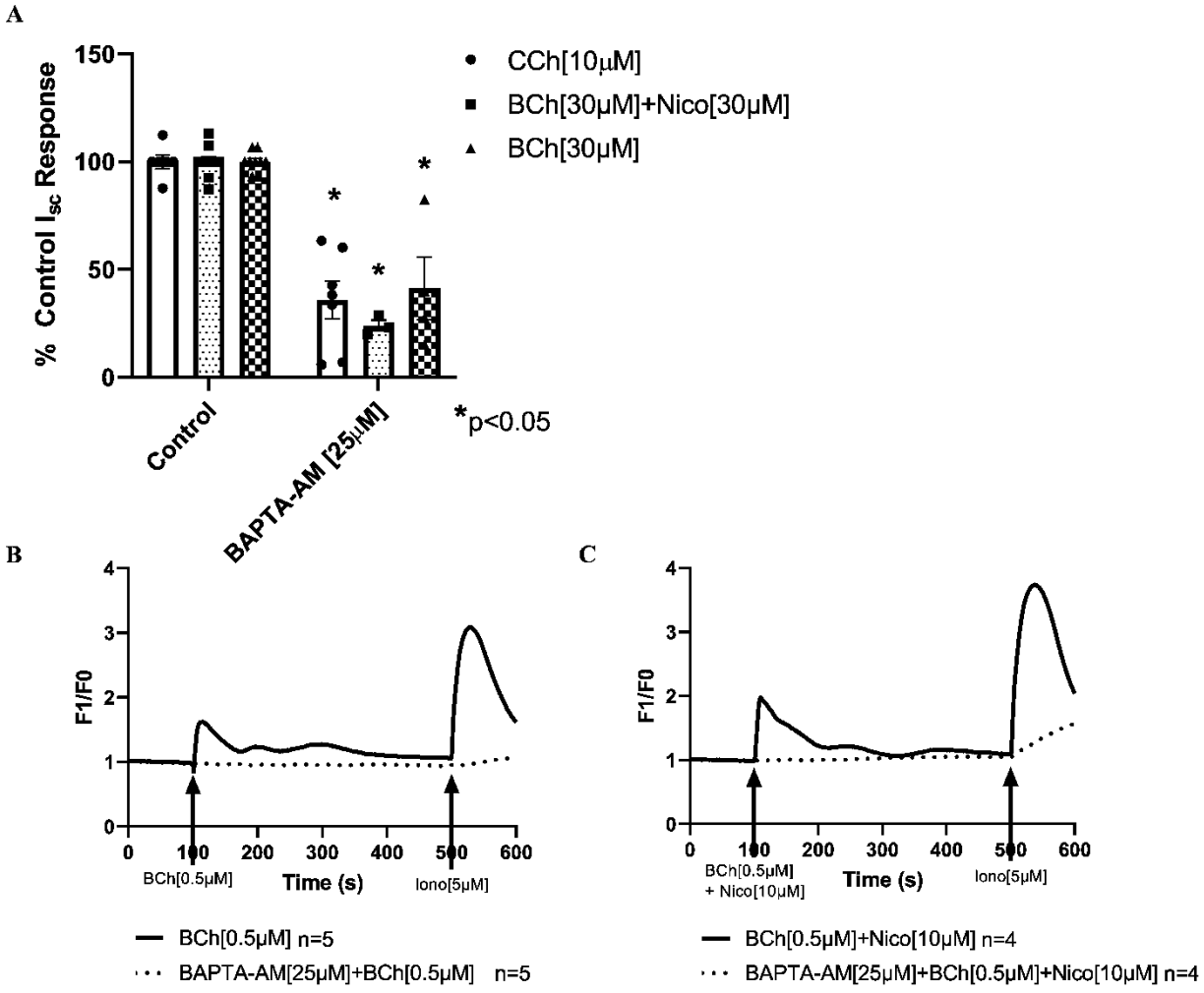


**Figure 11:Chelation of intracellular calcium reduces cholinergic-induced $I_{sc}$**

**A)** Stimulation of non-differentiated jejunal monolayers with a general cholinergic agonist (CCh[10μM]), muscarinic agonist (BCh[30μM]), or a combination of muscarinic and nicotinic agonists (BCh[30μM]+Nico[30μM]) after pre-incubation with the cell permeable calcium chelator BAPTA-AM [25μM] for 25 minutes. Stimulation with various cholinergic agonsits resulted in only partially inhibition of $I_{sc}$. p-values were calculated using an unpaired Student's t-test between the control condition of the agonist alone and pre-treatment with the chelator, *p<0.05. Dots represent individual traces while bars denote the average and SEM for each condition. **B-C)** The average traces of calcium-induced F1/F0 after for stimulation of Caco-2 M3R/GCaMP6s monolayers stimulated with **B)** BCh[0.5μM] or **C)** the combination of BCh[0.5μM]+Nico[10μM] either alone (**LINE**) or after 20 minutes pre-incubation with BAPTA-AM[25μM] (**DOTS**). The number of experiments averaged is indicated beneath each graph. Images acquired every second for 10.5 minutes and the entire frame averaged. Ionomycin[5μM] added after 500s as positive control.

secondary signaling pathway upstream of the increase in $[Ca^{2+}]_i$. This indicates a calcium-independent component of muscarinic-induced secretion that was unaccounted for in our current understanding and requires further investigation.

## 7. Nicotine has no effect on intracellular calcium

It is known that muscarinic induced $I_{sc}$ is generated through an increase in $[Ca^{2+}]_i$ from the ER stores through $IP_3R$ activation in response to $G_q$ signaling. It is also known that many nicotinic ligand-gated cation channels are strongly selective for calcium, though the exact selectivity is determined by the subunits which compose the final channel[106]. As such, we investigated whether there was a synergistic increase in $[Ca^{2+}]_i$ when both pathways were activated compared to muscarinic activation alone.

Overexpression of both the cytosolic calcium sensor GCaMP6s and the M3 receptor in Caco-2 cells (which do not endogenously express the M3 receptor) was used to image intracellular calcium in real time.

It was determined that a non-saturating concentration of BCh[0.5μM] combined with a concentration of nicotine[10μM] that resulted in no measurable increase in calcium on its own (**data not shown**) indicates that nicotinic activation has no effect on intracellular calcium (**Figure 11B and C, Figure 12A and B**). Rather than the expected synergy causing an increase in intracellular calcium due to two distinct sources of calcium being activated, there was no difference in the average traces with or without nicotine in any metric tested (**Figure 12C-F**) nor did nicotine alone cause a visible response.

It is possible that the mechanism regulating cross-talk between the two pathways involves a threshold of intracellular calcium that is met when both the M3 receptor and the nicotinic ligand-gated channels are activated while the nicotinic channels cause an increase in calcium that is undetectable by this sensor but that is unlikely. As a ligand-gated calcium channel, the nicotine-induced increase in the calcium response should in theory be near-immediate and very visible. Even discounting the fact that using the cytosolic GCaMP6S we were unable to detect an increase in $[Ca^{2+}]_i$ after stimulation with nicotine alone at any concentration, any nicotinic contribution to intracellular calcium increases should be

apparent in conjunction with muscarinic stimulation. This leads us to conclude that the nicotinic mechanism of action is likely independent of its function as a cation channel and any increases in intracellular calcium are by muscarinic signaling alone. Despite this, it is clear that there is a nicotinic

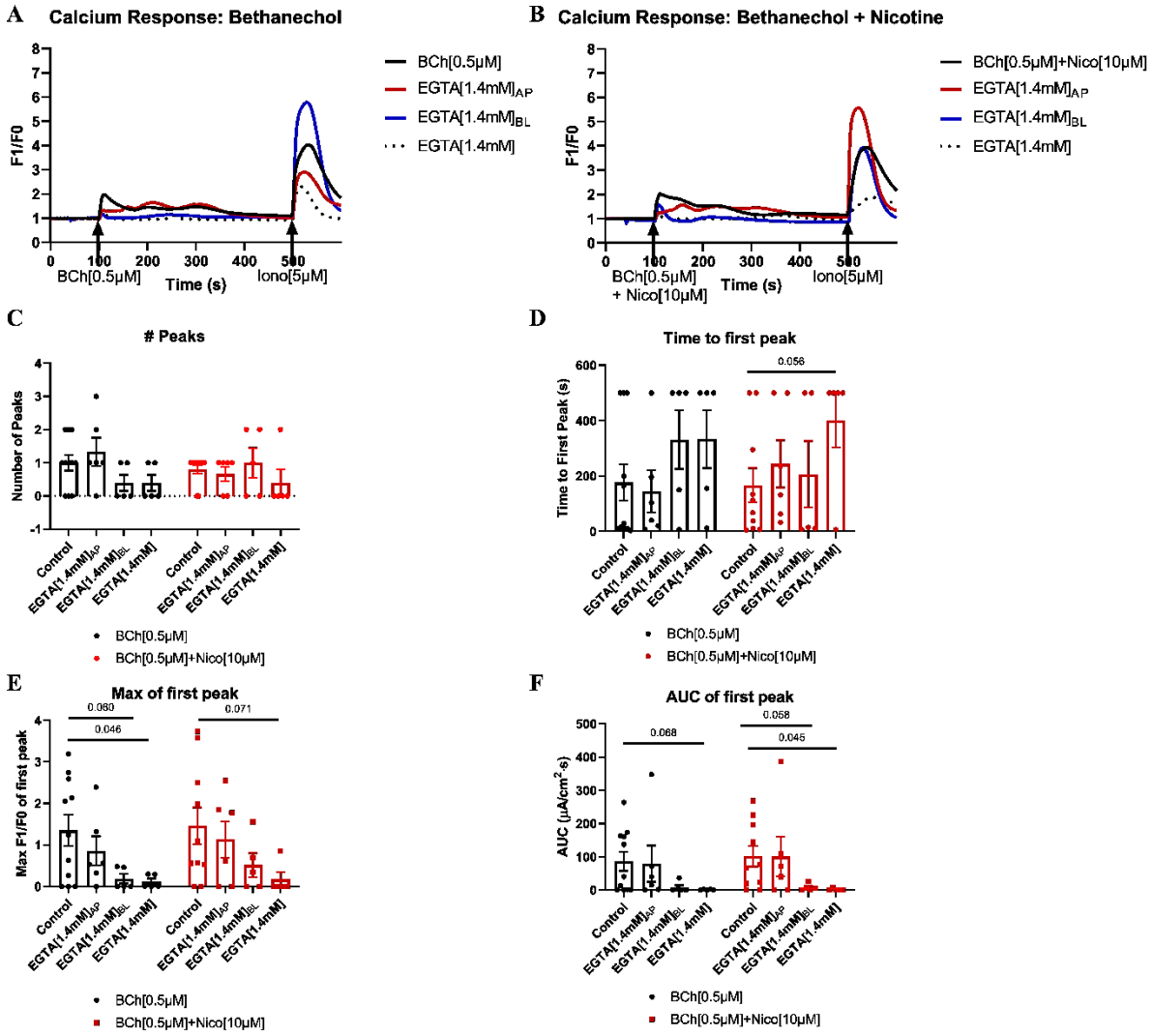


**Figure 12: Cholinergic intracellular calcium responses**

Average traces of fluorescence stimulated in response to increased cytosolic calcium increase in response to **A)** BCh[0.5μM] and **B)** BCh[0.5μM]+Nico[10μM] with and without chelation of extracellular calcium via pre-treatment for 60s with 1.4mM EGTA as indicated. **C)** The average number of calcium peaks observed as calculated using the AUC analysis method in Prism 8/9. **D)** The average number of seconds post stimulation with the indicated agonist it took to reach the first calcium-induced peak. **E)** The average amplitude of the first calcium peak. **F)** The average AUC indicating total calcium response for each condition. A number of replicates did not indicate a calcium response and are represented by time to peak = 500s (end of the experiment) and all other values = 0. Points indicate values from individual experiments. Bars indicate SEM. p-values were determined by Student's unpaired t-test and those trending ($p<0.1$) or significant ($p<0.05$) are included. n=5 experiments.

effect on $I_{sc}$ (**Figure 3, 6, and 7**) indicating a possible function of the nicotinic receptors independent of their role as cation channels.

## 8. Calcium sensitive adenylyl cyclase expression in mouse jejunal enteroids

Given that CFTR is regulated primarily by cAMP while CaCCs are regulated by $[Ca^{2+}]_i$, we investigated the possible cross-talk between the two pathways in calcium sensitive adenylyl cyclases. Links between adenylyl cyclase, calcium microdomains, and anion secretion have been made after observations in mammalian disease and cell culture, offering a promising starting point for investigation[122–128].

Adenylyl cyclases (AC) are a class of enzymes that catalyze the conversion from ATP to the signaling molecule cAMP. There are ten isoforms of the enzyme, AC1-9 are membrane bound and AC10 is cytosolic. AC1-9 are regulated through various methods, and several of them are known to be calcium inhibited or activated—either directly or through binding of calcium sensitive proteins like calmodulin[127,129–132]. Adenylyl cyclase 6 is the most highly abundant isoform in the intestinal epithelium and has been shown to be involved in intestinal secretion stimulated by both forskolin and cholera toxin[133,134], but AC6 is described in the literature as inhibited both by calcium and $G_{\alpha i}$ subunits[129]. As such, we tested the mouse jejunal monolayers for expression of the putatively calcium-activated isoforms *Adcy1*, *Adcy3*, and *Adcy8* in addition to *Adcy6* for reference (**Figure 13**). It was found that expression of the adenylyl cyclase isoforms does not differ between non-differentiated and differentiated monolayers. Adenylyl cyclases 1 and 3 are below the detection limit, but *Adcy8* is modestly expressed in the mouse jejunal enteroids while *Adcy6* is highly expressed as expected.

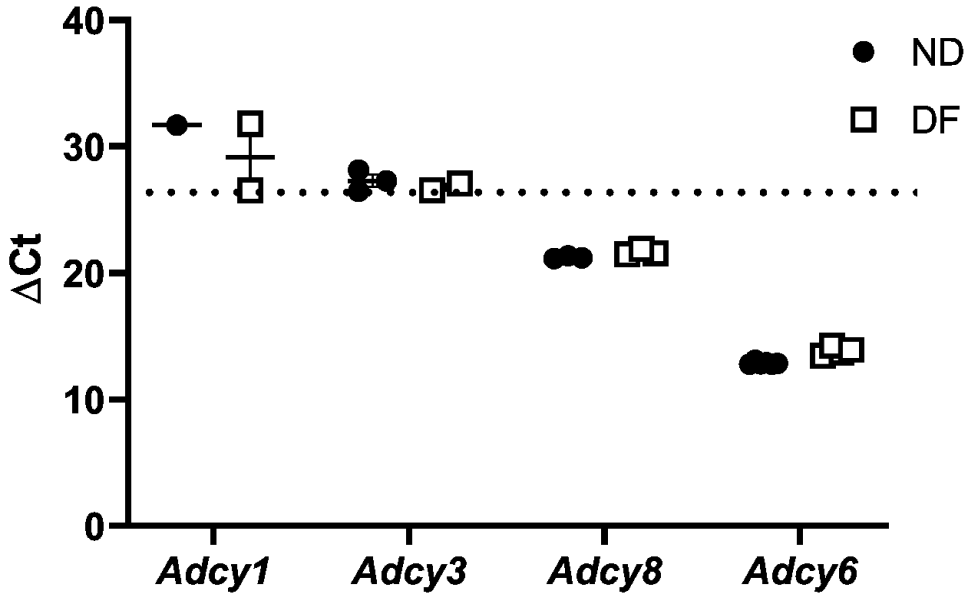


**Figure 13:Expression of calcium activated adenylyl cyclases in mouse jejunal enteroid monolayers**
mRNA expression of calcium activated adenylyl cyclases that may be involved in cAMP/calcium cross-talk in cholinergic secretion. *Adcy1* and *Adcy3* are below the detection limit, but *Adcy8* was found to be expressed in both ND (black) and DF (white) monolayers. *Adcy6* expression as a positive control in both conditions on the right. Expression normalized to *Rn18s* expression. The dotted line indicates the threshold of detection (normalized to *Rn18s* expression) for the system. Mean and error bars indicating SEM not visible are covered by the points. Points indicate average expression (of 3 replicates) in 3 different passages. Missing points indicate mRNA expression was not detected in the sample.

Confirmation of the role of AC6 and AC8 in forskolin and CCh induced anion secretion will require future genetic knock down of both adenylyl cyclases as there are no inhibitors or antibodies specific enough for this purpose.

## 9. Chelation of basolateral, but not apical, extracellular calcium blunts maximal CCh-induced $I_{sc}$

We hypothesized that not only were the intracellular ER calcium stores involved in regulating cholinergic-induced $I_{sc}$, but the linked store operated calcium entry (SOCE) pathway was also involved. SOCE is directly downstream of calcium depletion in the ER, with calcium sensors on the ER membrane re-localizing and dimerizing when $[Ca^{2+}]$ is low within the ER. These dimers re-localize to the ER-plasma membrane junctions and bind to calcium-release activated channels (CRAC) channels of the ORAI

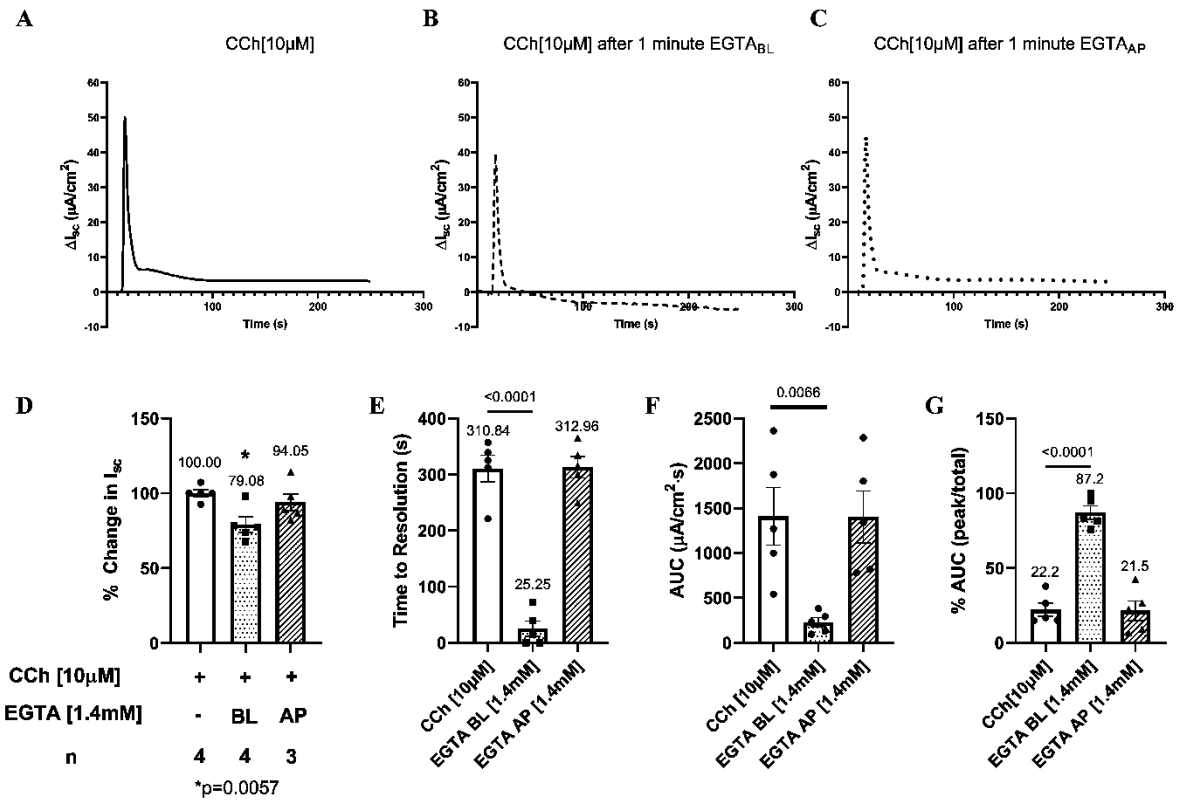


**Figure 14: EGTA chelation of basolateral extracellular calcium blunts peak CCh-induced $I_{sc}$**

Pre-incubation for 1 minute with EGTA [1.4mM] in either the apical or basolateral chamber before stimulation with CCh [10μM]. **A-C)** Average traces for mouse jejunal monolayers starting ten seconds before stimulation with carbachol and **D)** the mean peak increase ± SEM in $I_{sc}$. Chelation of basolateral calcium blunts CCh-induced $I_{sc}$ while chelation of apical calcium had no effect on peak $I_{sc}$. **E)** The average number of seconds it takes for $I_{sc}$ to return to baseline (y=0) after the CCh-induced peak ± SEM. **F)** The average total AUC of the cholinergic response indicating total chloride secretion for the duration of each experiment. **G)** The % AUC represented by the peak phase (defined as 0-26s with peaks aligned at 17s). p-values were calculated using unpaired Student's t-test to compare conditions pre-incubated with EGTA as indicated to CCh alone as the control. Points indicate individual traces, bars represent mean ± SEMs.

family. These channels on the extracellular membrane open and allow cations—primarily calcium—to enter the cell, further increasing cytosolic calcium[135–142].

Chelation of extracellular calcium with EGTA [1.4mM] had no effect on peak $I_{sc}$ when applied to the apical chamber, 45.05μA/cm$^2$ ± 9.9μA/cm$^2$ (94.1% ± 5.7% of the control response, p=0.36, n=4) when compared to control monolayers in normal calcium conditions, 49.6μA/cm$^2$ ± 8.2μA/cm$^2$ (100.0% ± 2.3% of the control response, n=4); however there was a significant decrease in peak $I_{sc}$ when EGTA was added to the basolateral chamber, but the peak is reduced only to 39.5μA/cm$^2$ ± 6.9μA/cm$^2$ (79.1% ± 5.1% of the control response, p=0.0057, n=4) of control $I_{sc}$ (**Figure 14A-D**). This is far less of an effect

than is observed when the nicotinic channels are inhibited by the antagonist hexamethonium (55.8%, **Figure 3**), contributing to the theory that the nicotinic mechanism is independent of its role as a calcium channel. However, this blunted effect is still less than expected based on the strong ties between the basolateral EGTA chelation inhibiting the muscarinic-induced increase in intracellular calcium and BAPTA-AM blunted $I_{sc}$ (**Figures 11 and 12**).

In some cell types, CRACs have been observed expressed on serosal or basolateral surfaces of polarized cell types rather than apical/luminal surfaces[143]. SOCE is most well characterized in non-polarized cells like lymphocytes and has not been well localized in native intestinal tissues yet. Due to the known localization of ER/PM interactions near the tight junctions, resolving the exact polarity of functional SOCE requires higher resolution than standard confocal methods. Co-expression analysis such as PLA assays (resolution to 40nm) and possibly even super-resolution methods may be required to definitely conclude the exact localization of the possible components, provided the sensors and channels involved are the same as defined for other SOCE activity. Functional analysis may be performed in the future using specific inhibitors of the various calcium channel families in the apical versus basolateral chambers to functional link $I_{sc}$ to both a specific channel type and confirm the polarity of distribution.

## 10. Basolateral calcium chelation reduces total secretion and the return to baseline after CCh-induced stimulation

In addition to the moderate reduction in peak current, there was a striking reduction in the time it took the CCh-induced current to return to baseline when basolateral calcium was chelated. A response that we had not observed in any of the previously tested conditions. To address this striking phenotype, alteration of the analysis method to include area-under-the-curve (AUC) and the time to resolution ($I_{sc} \leq 0$) was performed on the previously acquired dataset. As the data were acquired for analysis with a different method in mind, the data is incomplete, but does demonstrate several trends when applied to various datasets previously acquired.

| Initial Phase | Secondary Phase |
|---|---|
| Abolished by either apical or basolateral potassium channel inhibition (reduced 100%) | Reduced by apical potassium channel inhibition only (reduced 74%) |
| Reduced by BAPTA-AM (reduced 66%) | Unaffected by BAPTA-AM (reduced 0%) |
| Reduced by serosal EGTA (reduced 21%) | Reduced by serosal EGTA (reduced 84%) |

**Table 8: Cholinergic-induced $I_{sc}$ can be divided into two phases**
Summary of data supporting a two-phase cholinergic-induced change in $I_{sc}$

The new metrics considered were the time it took for stimulated secretion to resolve, that is the time it took after reaching maximum $I_{sc}$ for the response to return to baseline ($I_{sc} \leq 0$), and the total secretion calculated as AUC. As the maximal peak $I_{sc}$ was affected by many conditions tested, AUC was also normalized by dividing the peak AUC by the total AUC for each curve, generating a percentage of secretion attributed to both the peak and tail responses. When basolateral calcium was chelated with EGTA[1.4mM], the time to resolution was drastically reduced (25.3s $\pm$ 14s, $p<0.0001$, n=4) from the control traces which often did not reach resolution before the experiment was terminated (311s $\pm$ 24s , n=4) (**Figure 14E**). Similar to the control condition, chelation with apical EGTA[1.4mM] had no apparent effect on either phase under the tested parameters when compared to monolayers exposed to normal calcium conditions (313.0s $\pm$ 19s, p=0.9392, n=4). The AUC reflected this, chelation of basolateral calcium reduced total secretion and in particular it abolished the second phase, leaving a majority of secretion during basolateral EGTA chelation occurring during the initial, peak phase (87.2% $\pm$ 4.5% of total secretion, $p<0.0001$, n=4) whereas the bulk of secretion in the control and apically chelated conditions occurred during the tail phase (peak phase secretion--control: 22.2% $\pm$ 4.5%, n=4 and apical EGTA: 21.5% $\pm$ 6.4%, p=0.9258, n=4) (**Figure 14F and G**).

Overall, the proposed division of cholinergic secretion into two independent phases—an intracellular calcium dependent peak (**Figure 11**) and an extracellular $Ca^{2+}$-dependent tail (**Figure 14**)—has not previously been described in the intestinal epithelia and merits further investigation (**Table 8**).

## 11. Nicotinic signaling has an effect on the second secretory phase when chloride channels are blocked

To determine if any of the other conditions previously analyzed for maximal change in $I_{sc}$ display a quantifiable difference in either total secretion or in time to resolution, previous datasets were re-analyzed. In response to stimulation with carbachol [10μM] (282s ± 43s, AUC = 305 ± 39, % peak AUC = 61% ± 3.1%, n=9): it was found that chloride channel inhibition of either CFTR (155s ± 40s, p=0.047; AUC = 174 ± 29, p=0.019; % peak AUC = 67% ± 4.8%, n=9), CaCC's (173s± 38s, p=0.077, AUC = 90 ± 18, p=0.0002; % peak AUC = 61% ± 4.1%, n=9), or the combination (115s ± 47s, p=0.021; AUC = 23 ± 4, p<0.0001; % peak AUC = 34% ± 5.3%, p=0.0002, n=7) reduced the time it took to return to baseline and reduced total AUC (**Figure 15A-C**). Inhibition of CFTR or CaCCs alone had no significant effect on the initial peak AUC when data was normalized to account for the reduced maximum peak $I_{sc}$, but the combination of CFTR and CaCC inhibitors resulted in a significantly reduced initial peak AUC that could not be entirely explained by the reduction of the initial peak.

Supporting the hypothesis that extracellular calcium is responsible for the second phase effect, chelation of intracellular calcium with BAPTA-AM[25μM] did not appear to have any effect on either total secretion or time to return to baseline (284s ± 30s, p=0.9609; AUC= 204 ± 42; % AUC peak = 57% ± 4.4%, p=0.7314, n=7), whereas BAPTA-AM chelation demonstrated the ability to significantly reduce initial peak $I_{sc}$ with an intracellular calcium independent remnant (**Figures 11 and 14**).

Interestingly, these effects seem to be dependent on the activation of the nicotinic pathway, as monolayers stimulated with bethanechol [30μM] alone did not display the same trends in any condition. Inhibition of CFTR (343s ± 7.6s, AUC = , 158 ± 35, % AUC peak = 45% ± 3.9%, n=5), CaCC's (322s ± 16s, AUC = 151 ± 43, % AUC peak = 49% ± 4.8%, n=5), the combination (330s ± 9.8s, AUC = 132 ± 40, % AUC peak = 47% ± 6.7%, n=4), or chelation of intracellular calcium (318s ± 47s, AUC = 113 ± 26, % AUC peak = 42% ± 2.6%, n=2) had no apparent effect on either return to baseline or AUC when

compared to control monolayers (335s ± 39s, AUC = 166 ± 29, % AUC peak = 47% ± 3.5%, n=5) (**Figure 15 D-F**).

Based on this data, it can be theorized that the nicotinic pathway influences more than just maximum peak $I_{sc}$ in cholinergic-induced secretion, but also influences the secondary phase. Specifically, the time it takes to return to baseline and total AUC demonstrate nicotinic-dependent effects on the second phase only after chloride channel inhibition, though the exact pathways involved in this regulation

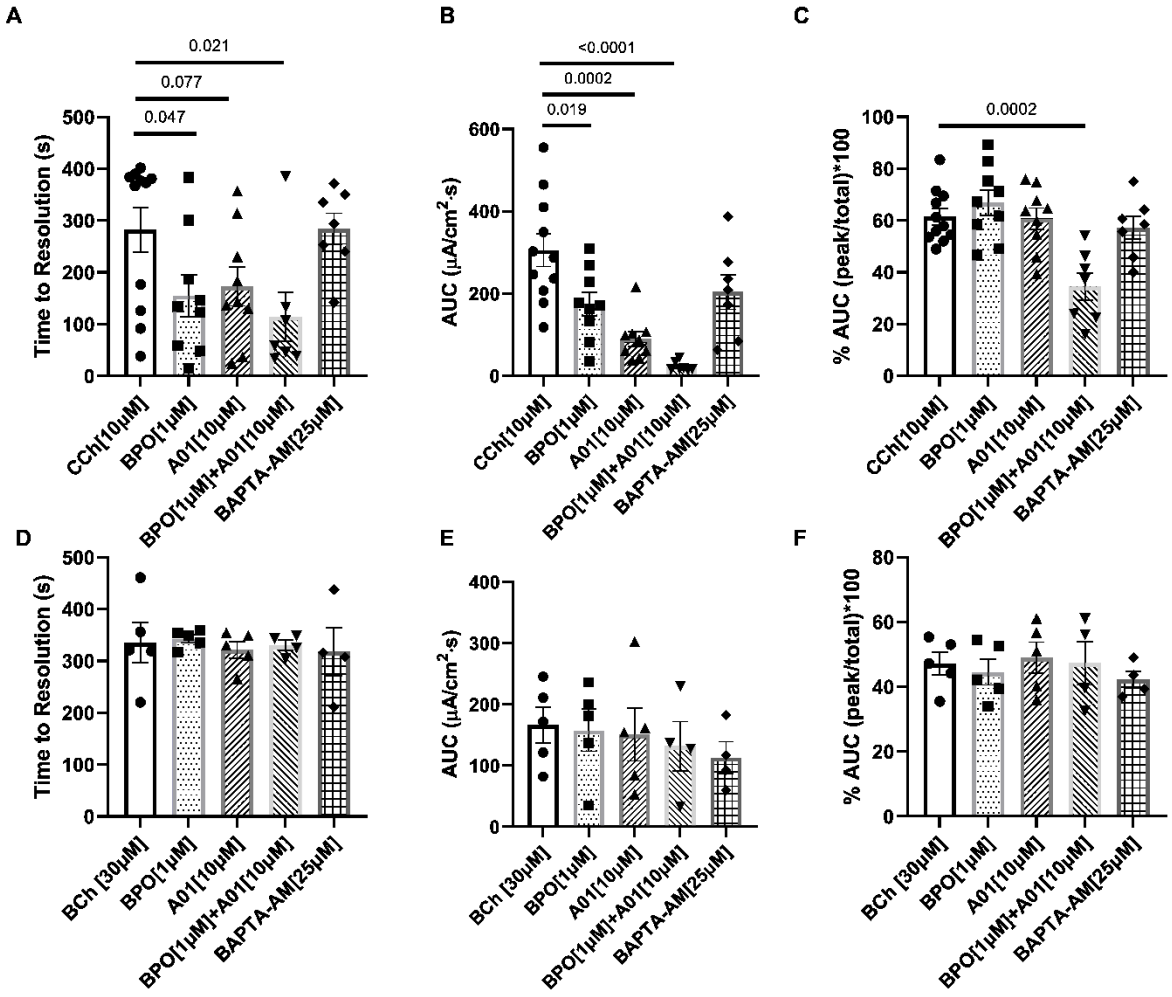


**Figure 15: Nicotinic signaling has an effect on the second secretory phase when chloride channels are blocked**
Pre-incubation for 25 minutes with the indicated inhibitor/combination before stimulation with CCh [10µM] **(A and B)** or BCh [30µM] **(C and D)**. **A)** The average number of seconds it takes for $I_{sc}$ to return to baseline (y=0) after the CCh-induced peak ± SEM. **B)** The % AUC represented by the peak phase (defined as 0-26s with peaks aligned at 17s) divided by total AUC to normalize for variation in maximum peak response after CCh stimulation. **C)** The average number of seconds it takes for $I_{sc}$ to return to baseline (y=0) after the BCh-induced peak ± SEM. **D)** The % AUC represented by the peak phase (defined as 0-26s with peaks aligned at 17s) after BCh stimulation. p-value calculated using Unpaired Student's t-tests compared to CCh or BCh alone as the control. Points indicate individual traces, bars represent mean ± SEMs.

are unknown at this time. Further studies would require investigating the possible role of nicotinic signaling in the down-regulation of cholinergic-induced anion secretion as well as the mechanism of the second phase of secretion to determine the second-phase effect of nicotinic signaling.

## C. Discussion

Using the non-differentiated enteroid monolayer system to determine the components involved in cholinergic-induced anion secretion we confirmed that chloride is the major anion involved when the basolateral potassium channel that drives chloride flux is inhibited resulted in inhibition of the initial peak of carbachol induced $I_{sc}$. There is some data supporting the presence of an apical potassium channels in the rat colon and a rat small intestinal cell line IEC-18, but its role in cholinergic anion secretion in the small intestine has not been observed until now[144,145]. This finding indicates that we are missing an entire component to our understanding of the regulation of the chloride secretion, adding a new consideration to both basic and clinical understanding of the chloride secretory pathway.

It was also determined that both CFTR and CaCC class transporters are involved in the apical efflux of chloride in response to mixed cholinergic signaling. When the physiological response is broken down into muscarinic and nicotinic components, it was observed that muscarinic-induced signaling results in a primarily CaCC-mediated efflux as inhibition of CFTR has no effect on $I_{sc}$ when only the muscarinic pathway was activated. Interestingly, there is a secondary pathway where CFTR was partially activated, but only when the CaCCs were inhibited. Only by inhibiting both anion channels was the initial peak abolished after muscarinic stimulation. These two findings together indicate that nicotinic signaling is activating CFTR.

Since there are many isoforms of CaCCs, the two most likely candidates were screened for mRNA expression in the monolayer system. In the mouse jejunal tissue, TMEM16F was shown by genetic knock-down to be involved in anion secretion while TMEM16A performed the same function in the mouse colon[113–115,146]. Both CaCCs were shown to be functionally linked to CFTR and involved in the regulation of chloride secretion via calcium signaling. In the jejunal monolayer system, both isoforms were expressed, with *Tmem16F* being the more highly expressed isoform, in non-differentiated

monolayers this isoform was expressed at similar levels as *Cftr*. However, as both isoforms show mRNA expression, and protein measurements are made difficult by the lack of useful antibodies and the multi-membrane spanning domain nature of the channels, future genetic knock-down is the next best method to assess which isoform is involved in our system.

These two classes of chloride channel are regulated by two interconnected signaling pathways; CFTR is regulated by phosphorylation by PKA—a cAMP dependent enzyme—while CaCCs are true to their name and regulated by increases in $[Ca^{2+}]_i$. The activation of only CaCCs by muscarinic signaling and both by cholinergic signaling indicates that the nicotinic pathway may be regulating cross-talk between intracellular calcium and cAMP signaling.

As both muscarinic and nicotinic receptors are known to increase $[Ca^{2+}]_i$, we were interested in determining 1) where the potential cross-talk occurs relative to the increase in intracellular calcium and 2) if there was a quantifiable increase in $[Ca^{2+}]_i$ in cholinergic-stimulated monolayers compared to ones stimulated by bethanechol alone. Control Caco-2 monolayers expressing both the M3 receptor and the cytosolic calcium sensor GCaMP6s showed bethanechol stimulated calcium release was not altered by the co-application of nicotine, and nicotine alone was not sufficient to stimulate a detectable increase in calcium in this system. This is unexpected as the nicotinic receptors are commonly considered ligand-gated cation channels, though specific subunits modify the exact selectivity for calcium and determining the specific composition of each channel is difficult due to endogenous heterogeneity and the difficulty in detecting small differences between subunit isoforms[91–95,147]. As we did not observe a synergistic increase in calcium upon nicotinic stimulation compared to muscarinic alone as expected, we concluded that the nicotinic receptors could not be acting through their channel function to increase $I_{sc}$, but through a new, poorly described receptor-mediated signaling pathway. Based on our observations regarding nicotinic activation of CFTR and literature indicating nicotinic-induced $I_{sc}$ in mouse trachea is sensitive to the PKA inhibitor H-89, we hypothesize that nicotinic receptors could be directly increasing cAMP in response to nicotine and carbachol[148,149]. This effect could possibly be mediated through $G_s$ signaling based on recent data demonstrating that alpha 7 receptors are capable of binding and activating $G_q$ in neurons[150,151].

Recent data has shown that nicotinic signaling in the rat colonic epithelium is mediated through PKC to regulate the $Na^+/K^+$-ATPase rather than through cation conductance[101,148]. While the pump is not the rate-limiting step in generating potassium current, it does generate electrical current as a result of electrogenic exchange of 3 sodium ions for 2 potassium. This helps maintain the electrical state of the cell and provide some driving force for chloride secretion, even if it's not the primary protein involved in that function. Links between nicotinic ligand-gated cation channels and non-channel related functions are a very new concept, thus little is known about the signaling mechanisms involved[150–152]. However, we can agree that signaling independent of the nicotinic receptor's ion transport capabilities is involved as our own data demonstrates a lack of cation-mediated effect through nicotinic signaling relating to chloride secretion.

Intracellular calcium is known to be the major signal mediating cholinergic-induced anion secretion and barring a nicotinic contribution, the muscarinic-induced release of ER calcium stores into the cytosol is the primary contributor. Knowing this, chelation of intracellular calcium with membrane permeable BAPTA-AM was hypothesized to abolish cholinergic- and muscarinic-induced $I_{sc}$ as our understanding of the pathway resulting in cholinergic anion secretion depends on the increase in cytosolic calcium. Surprisingly, BAPTA-AM only partially reduced $I_{sc}$ in CCh and BCh stimulated monolayers. Validation of the BAPTA-AM conditions using calcium imaging in Caco-2 M3R/GCaMP6s monolayers indicated that this residual $I_{sc}$ is not due to incomplete chelation, but rather it is likely the result of a pathway activated upstream of ER release of calcium stores.

As intracellular calcium is at least partially involved in regulation of cholinergic secretion and the cAMP pathway needs to be activated to in turn activate CFTR in the presence of nicotinic signaling, it stands to reason that nicotinic signaling may regulate a protein or enzyme involved in calcium-to-cAMP crosstalk. The adenylyl cyclases are a family of enzymes that catalyzes the ATP to cAMP reaction. Many of isoforms are calcium sensitive and of the three isoforms known to be calcium activated[129,132], only AC8 had detectable expression in the mouse jejunal monolayers. Very little is known about AC8, but it has been shown to be activated by extracellular calcium entering the cell via the CRAC channels of the SOCE

pathway[124–127,130,131,153]. As a result, analysis of the contribution of extracellular calcium on cholinergic secretion was the next step.

There are links in the literature tying ACs to anion secretion, ACs to extracellular calcium, and extracellular calcium to anion secretion. We hypothesized that part of the nicotinic regulatory mechanism of muscarinic chloride secretion involved nicotinic regulation of the extracellular calcium (SOCE) pathway. In overexpression systems, AC8 has been shown to be activated by CRAC-mediated calcium entry to generate cAMP and induce chloride secretion[124–128,130,131,153,154]. SOCE has also been implicated in a broader way in secretion in a few other tissues such as the sweat gland and salivary gland[122,123,155–157]. Store-operated calcium entry (SOCE) is a mechanism by which depletion of ER calcium levels leads to dimerization and re-localization of ER membrane protein and calcium sensor STIM1. These dimers bind to the plasma membrane calcium channel ORAI1, allowing extracellular calcium to enter the cytosol[135–142]. In sweat glands, a polarized, secretory epithelium with many of the same mechanisms regulating chloride secretion observed in the intestinal epithelium, SOCE is an apical process with a role in chloride secretion[123].

However, in practice extracellular calcium only had a moderate effect on maximum $I_{sc}$ in the jejunal monolayers and only loss of the basolateral pool of calcium had an effect at all. This indicated that 1) chelation was incomplete, 2) SOCE is basolateral rather than apical in the intestinal epithelium, or 3) SOCE was uninvolved. SOCE has not been investigated thoroughly in the intestinal epithelia, but there is some data indicating a basolateral calcium pool being involved in SOCE in this population[143]. Interestingly, though it has not been linked to SOCE directly, the role of serosal calcium in intestinal secretory function is not a new concept, though molecular identities and functions that have since been identified need to be linked to the previously described observations[30–32].

While extracellular calcium had very little effect on the first phase of the $I_{sc}$ response, chelating calcium from the basolateral pool completely abolished the second phase of secretion. This data reinforces the observations made using the potassium channel inhibitor, separating cholinergic anion secretion by not only potassium channel localization, but also by calcium source.

Unexpectedly, the second phase also showed that stimulation with carbachol after inhibition with either of the chloride channel inhibitors resulted in a faster return to baseline and reduced total secretion quantified as AUC, while monolayers stimulated with bethanechol were unaffected indicating that nicotinic signaling also has a role in the second phase. Based on the fact that the presence of nicotinic signaling reduced total secretion and decreased the time it took to return to baseline, it is possible that nicotinic signaling is involved in the down-regulation of cholinergic anion secretion.

Further studies of the contributions of the apical potassium channel, basolateral calcium pool, or nicotinic signaling to the second-phase and/or down-regulation of cholinergic anion secretion would be performed using agonists and antagonists of the known down-regulation pathways, such as EGFR as the most upstream activator and select downstream targets such as PI3K, ERK, and p38 which are involved in several independent pathways of downregulation of cholinergic secretion.

This novel two phase paradigm for cholinergic signaling brings up more questions than it answers, but at the same time demonstrates how a system or function we believe we completely understand may in fact be far more complicated and have hidden contributors.

# VII. Co-culture of mouse jejunal enteroids with the enteric neurons and glial cells of the sub-mucosal plexus (SMP)

## A. Background

Interconnected biological systems are constantly influencing each other in order to maintain homeostasis. Under normal, homeostatic conditions, cells do not function at either their minimum or maximum capacity; whether the function is cell growth and division, secretion, absorption, tone, or signaling. This allows for the cells and systems to respond to stress or environmental stimulus. This responsiveness is necessary for organisms which do not exist in a static equilibrium, but instead flux between states: fed and fasting, resting and active, healthy and ill. The cells of the enteric nervous system, present in the sub-mucosal plexus and the cells of the intestinal epithelia have been shown to exert such reciprocal communication; neurotransmitters secreted from the epithelia, such as serotonin, act on the neurons to stimulate neuronal transmitters, which then alter epithelial function.

Current models of the intestine focus on the extremes of isolated cell populations or entire tissues. Isolating cultures completely removes the constant, modulating effects of other cell populations but allows for systematic interrogation of a specific cell type in a highly controlled environment. Whole tissue or whole organism work has multiple cell populations involved, making it difficult to determine which cell populations and/or signals are responsible for a specific response. It becomes a complicated question of which comes first, the chicken or the egg, only there is on the order of tens—if not hundreds—of potential components.

There are pathologies in the gut which affect more than just the intestinal epithelial cells. Up to half of the secretion from major diarrheal disease models, such as cholera and rotavirus, involve the contributions of the ENS[16,158,167–175,159–166]. Without understanding how both the neuronal and epithelial cell populations influence each other, a part of the pathophysiology of diarrhea and potential treatment remains unaddressed. We proposed to put together two defined models to better understand whole intestinal physiology and disease.

Intestinal enteroids are cultures derived from the crypts of adult intestine which maintain the capability to proliferate and differentiate into the various intestinal cell populations, including goblet cells, enteroendocrine cells, and enterocytes[9,52,53,55,176]. These cultures can be expanded indefinitely without becoming cancerous and used to assay various functions. Similarly, the sub-mucosal plexus (SMP) neurospheres used in culture are derived from the SMP of an adult mouse and consist of the neuroglial precursor stem cells, enteric nerves, and enteric glia[65,66]. These cultures can also be expanded, differentiated, and assayed for function[65,66,177,178]. Culturing these primary, adult derived neurons and glia with isolated intestinal epithelia will offer a tool to enhance the collective understanding of these two populations, how they affect each other *in vivo*, and model a more complex intestinal system[178–183].

## B. Results

### 1. Established SMP cultures can persist in enteroid-permissive conditions

Sub-mucosal plexus cells were isolated from adult *Wnt1cre:tdTomato* mouse (in which all neural crest-derived populations are *tdTomato*+) small intestine and purified by magnetic sorting for the CD45- negative fraction to remove contaminating immune cells from the culture. Resulting neurospheres were grown in suspension in stem cell medium containing growth factors EGF, FGF, and GDNF (SCM+GF) to proliferate for one week before being plated adherently on coverslips coated with 50% diluted Matrigel in neuron differentiation media (stem cell medium, SCM) for 5-7 days. Isolated small intestinal mouse SMP neurospheres, plated adherently and allowed to differentiate before being transferred to enteroid-permissive conditions as published by Sato et al[9,11,55,184] were able to grow equally as well as cultures that remained in neural differentiation media (SCM) (**Methods**). Cultures plated in the presence of mouse jejunum enteroids showed no morphological difference to those in Sato media alone or cultures remaining in SCM. Enteroids and SMP cultured on coated coverslips without the other population served as negative controls.

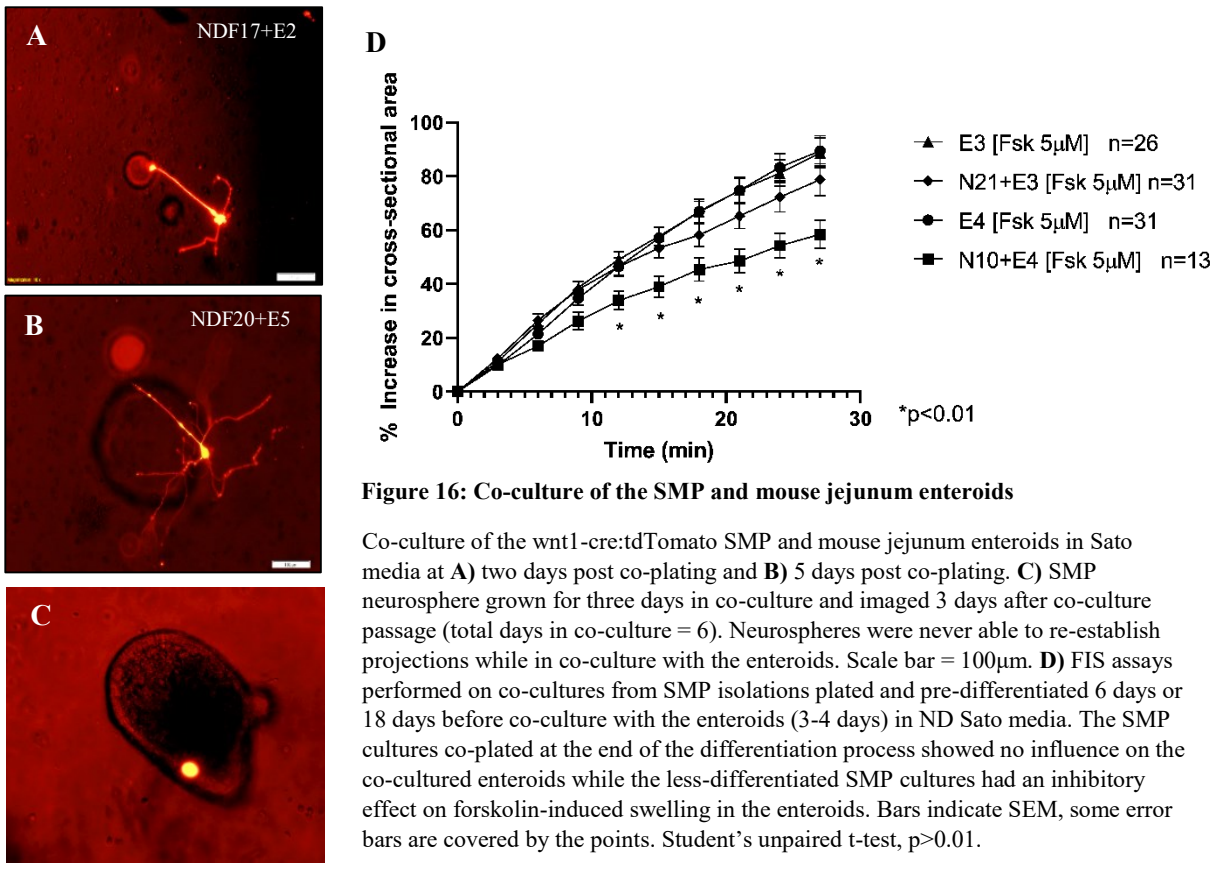


**Figure 16: Co-culture of the SMP and mouse jejunum enteroids**

Co-culture of the wnt1-cre:tdTomato SMP and mouse jejunum enteroids in Sato media at **A)** two days post co-plating and **B)** 5 days post co-plating. **C)** SMP neurosphere grown for three days in co-culture and imaged 3 days after co-culture passage (total days in co-culture = 6). Neurospheres were never able to re-establish projections while in co-culture with the enteroids. Scale bar = 100μm. **D)** FIS assays performed on co-cultures from SMP isolations plated and pre-differentiated 6 days or 18 days before co-culture with the enteroids (3-4 days) in ND Sato media. The SMP cultures co-plated at the end of the differentiation process showed no influence on the co-cultured enteroids while the less-differentiated SMP cultures had an inhibitory effect on forskolin-induced swelling in the enteroids. Bars indicate SEM, some error bars are covered by the points. Student's unpaired t-test, $p>0.01$.

Unfortunately, though the cultures grew well together over time (**Figure 16A, B**), the co-culture system has a limited lifespan due to the limitations of the 3D enteroid culture. Without breaking open and passaging the enteroids to remove dead cell debris from the mouse enteroid cultures, the enteroids have a maximum culture lifespan of approximately one week in standard conditions. When passaged as a co-culture, both cell populations persisted. However, the SMP population lost all projections and was unable to regenerate them to the same extent under culture conditions despite survival of the population (**Figure 16C**). It was eventually determined, that while the enteroid-permissive condition was permissive to neuronal survival and growth, it was not enough to *initiate* differentiation and neuronal projections as neurospheres plated directly in Sato media likewise were unable to produce neuronal processes, though the cells neither died nor proliferated. As such, future co-culture protocol includes at minimum a five day pre-differentiation period for the neurons once they are plated adherently before being co-cultured with the enteroids. SMP cultures at five days started to display small projections and co-plating with the

enteroids did not prevent further development. The co-cultures themselves then have a limited lifespan of 3-5 days before cell death begins to overtake the enteroids and affect the SMP culture. For consistency, most physiological assays of the SMP and co-cultures were performed 2-3 days after co-culture.

While the enteroids are maintained in a proliferative state throughout the culture lifespan, the SMP neurons are undergoing a long differentiation process. The normal differentiation protocol for the SMP cultures is 21-24 days in SCM. Based on imaging of SMP cultures grown side-by-side in SCM and Sato media, the Sato media appears to support the continued differentiation of the SMP with and without the presence of the enteroids. Whether this steady differentiation process has an effect on the co-culture system was investigated with a pair of FIS assays performed on co-cultures that were co-plated at the earliest possible time point (N6) and the latest (N18). It was shown that the older SMP cultures did not exert an effect on the forskolin-induced secretion of the enteroids while the younger cultures do appear to have a basal suppressive effect on forskolin-induced [5μM] enteroid secretion (**Figure 16D**). Additionally, the younger SMP cultures were more motile, actively moving and generating processes towards nearby enteroids—most notable in the processes reaching across z-planes—while the older SMP cultures did not demonstrate any morphological or motor changes in response to enteroids plated nearby or even directly on top of the SMP, remaining steadfastly within the original z-plane and networks (**data not shown**). As a result, most experiments were performed with SMP cultures that were 7-14 days pre-differentiated.

## 2. SMP effects on enteroid secretion depends on the differentiation status of the SMP culture when co-cultured

Basal functions of the epithelial barrier such as transport have been shown to be subject to modulation by the ENS[171,173,192,174,185–191]. However, specifics of function such as effects on basal or stimulated secretion and specific transmitter effects vary between segments and species.

The primary transport assay of the 3D co-cultures is the FIS assay[12,13,20,67,68]. In short, 3D enteroids have a closed, ‘inside-in’ morphology. Luminal secretion thus increases the volume of the

enteroid. This change in volume can be observed post-stimulation (ex. 5μM Fsk) and imaged using any imaging system that supports live cell time-lapse imaging, though an incubation chamber for longer studies may be necessary as well. The increase in cross-sectional area over time of each enteroid is then measured, normalized, and averaged to produce a summary of basal and stimulated chloride secretory function.

The presence of the SMP in co-culture with the enteroids for two days prior to the FIS assay showed no significant effect on basal behavior of the enteroids pre-stimulation (**Figure 16D)**. The basal activity of the SMP in these conditions has neither a stimulatory nor inhibitory effect on basal secretory behavior of the enteroids. The SMP culture was not affected in any way beyond the signaling of the enteroid culture, showing that at baseline and under initial co-culture conditions, enteroids have the same secretory behavior over time with and without the SMP.

Stimulation with forskolin caused chloride secretion that resulted in a significant increase in cross-sectional area of enteroids cultured in Sato media both with and without the SMP for 3-4 days. The forskolin-induced response was significantly reduced in the presence of SMP cultures that were not fully differentiated at the time of co-culture. This may be a result of 1) the aged SMP cultures may not signal as strongly and the weaker signal is not detected by the enteroids, 2) the aged SMP cultures have a different signaling profile, or 3) the aged SMP cultures are not plastic enough to respond to the enteroids and establish the required connections to signal properly. Observations of plated SMP cultures with and without the enteroids indicate that plasticity may at least partially explain the difference, as 'young' SMP cultures plated with enteroids exhibit extensive, 3D branching patterns when within an undefined distance of an enteroid that paired 'young' SMP cultures plated without enteroids do not. 'Aged' SMP cultures do not exhibit much 3D branching over the same period of time, regardless of the presence or absence of the enteroids. This can be observed using an inverted microscope where SMP cultures either reside entirely in a single plane or branch off into the z-direction dependent upon proximity to enteroids (**Figure 16B vs Figure 17A**).

## 3. 2-Dimensional co-culture Conditions

Due to the inability of enteroids grown in Sato media to generate monolayers, a different media condition (minimal media) was generated that permitted mouse enteroids to be grown to confluence on Transwell filters (**Table 1, Figure 1, Figure 2)**. Due to limitations of the 3D co-culture model, designing a 2D co-culture model was a logical next step once the mouse enteroids were able to be grown as confluent monolayers.

Attempting to culture the SMP in the monolayer media condition led to loss of SMP viability within 14 hours (**Figure 17B**). Subsequent re-building of the previously successful media condition (Sato) using permutations of the removed components, gave rise to four combinations that led to SMP culture survival longer than 72 hours (**Figure 18C-F**). These four conditions were then tested for monolayer permissiveness, where two of the four conditions formed confluent monolayers within ten days while the other two conditions did not (**Figure 18G**). The two conditions that were deemed monolayer-permissive, minimal media +Gastrin and SB202190 or +NGF, were then further investigated.

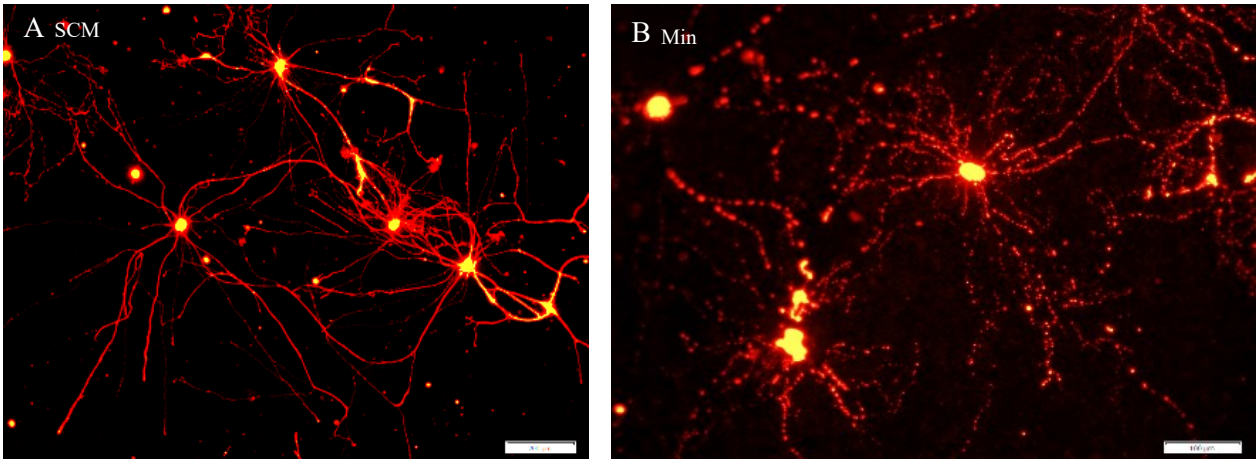


**Figure 17: Monolayer permissive conditions are not sufficient to support SMP culture survival**

SMP Neurons grown in **A)** SCM for 6 days (scale bar = 200µm) and **B)** 14 hours post-condition switch to the monolayer-permissive minimal media (scale bar = 100µm).

## 4. Effects of enteroid media composition on SMP culture identity

While determining the effect on secretory function of the different media conditions, the effect of those conditions on the differentiation of the SMP was also being investigated. In particular, the effect of the media condition on the sub-type of SMP neurons in culture. To do this, SMP cultures were grown in either of the two monolayer permissive conditions (+GS and +N) and then stained for either choline-acetyltransferase (ChAT) or vasoactive intestinal peptide (VIP), markers of the two most prominent

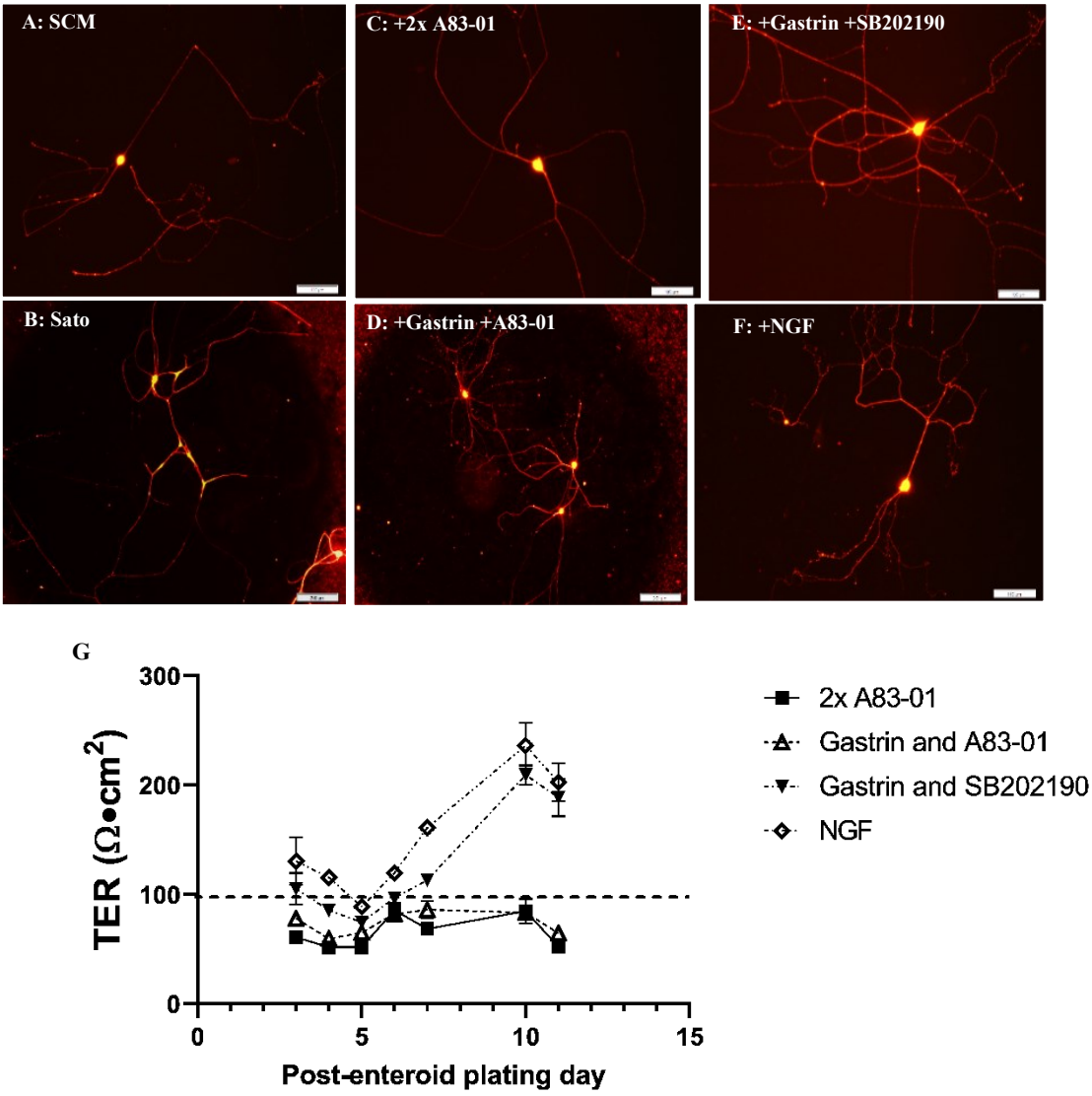


**Figure 18: Determination of 2D co-culture permissive conditions**

**A-F)** SMP cultures that survived 72 hours in culture after media was changed to the indicated conditions. Scale bar A, D-F = 100µM, B-C = 200µm. **G)** TER of enteroid monolayers plated in SMP-permissive conditions. The dotted line indicates approximate TER of confluent monolayers. SEM indicated by error bar, may be covered by individual points.

neural sub-populations of the SMP. Together, these two markers should account for almost all of the SMP neurons, are almost mutually exclusive markers, and in the mouse SMP, VIP should stain 50-60% of all neurons while ChAT stains 40-50%[174,193,194].

After 6 days pre-differentiation and 3 days in either of the monolayer-permissive media conditions, it was determined that the SMP cultures co-expressed far more ChAT and VIP than expected in both conditions (**Figure 19A and B**). The discrepancy in ChAT and VIP expressing populations in culture versus published observations in tissue led us to question 1) the specificity of the antibodies and 2) the possibility of artificial select by culture conditions as our findings indicated that almost 100% of the SMP populations we had in culture co-expressed ChAT and VIP when the two markers should be mutually exclusive.

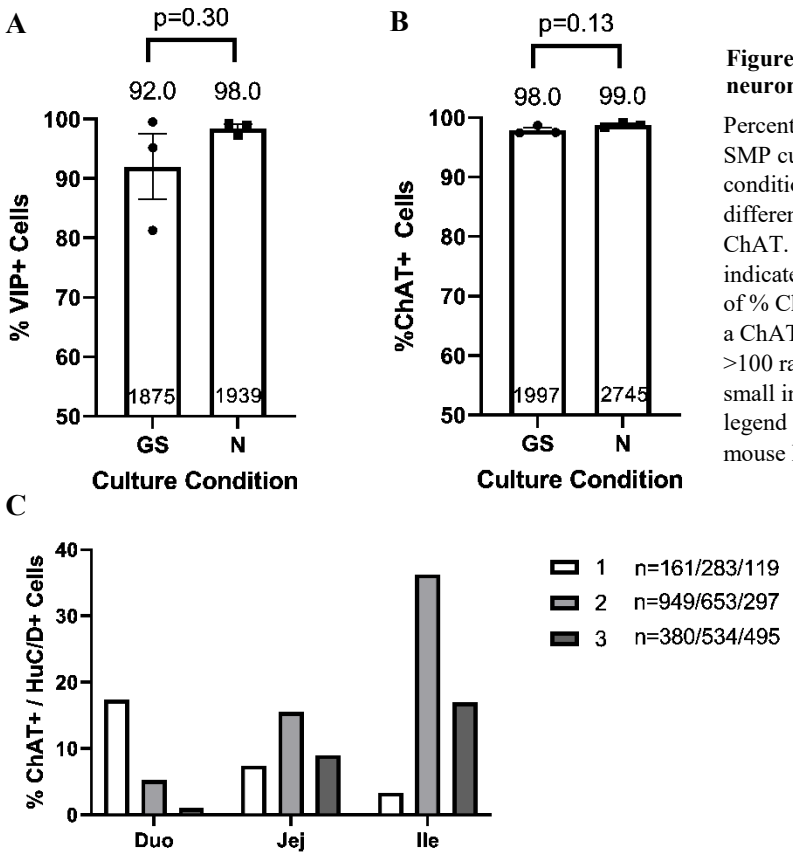


**Figure 19: Summary of ChAT expressing neurons in the SMP**

Percent of specific neuron sub-populations in SMP cultures grown in the indicated media condition for 3 days after 6 days of pre-differentiation and stained for **A)** VIP and **B)** ChAT. Number of cells counted (Hoescht+) is indicated at the base of each bar. **C)** Summary of % ChAT expression in HuC/D+ neurons in a ChAT-tdTomato transgenic mouse line. >100 random fields per mouse across all three small intestinal segments. n indicated in the legend is the number of cells counted per mouse Duo/Jej/Ile.

## 5. ChAT+ neurons in mouse small intestinal tissue

To determine whether this discrepancy with the literature was true or due to non-specific antibody staining, we isolated tissue from all three small intestinal segments from 3 adult littermate ChAT-cre:tdTomato mice and stained with the well characterized pan-neuronal marker antibody HuC+HuD before counting the number of ChAT+ neurons in the mouse tissue. Surprisingly, the SMP showed greater similarity in the sections from the same mouse than across sections between littermates, though there were no significant differences in any of the populations of neurons examined (**Figure 19C**). More importantly, the transgenic ChAT marker was expressed in far fewer of the neurons than the antibody in culture showed, preliminary culture of ChAT-tdTomato neurospheres in monolayer-permissive conditions with the addition of Calcien Green-AM to indicate live cells indicated that ChAT expression was not as prevalent as the antibody indicated in previous cultures (**data not shown**) leading to the conclusion that both antibodies were likely non-specific as they gave similar results in culture and the results of the culture analysis were artificially high rather than artificial selection in culture for a co-expressing sub-type. Due to continued technical difficulties in staining with the ChAT and VIP antibodies, the final composition of the SMP cultures remains unknown, but due to the variability in mouse tissue expression (**Figure 21C**), it is likely that variability in culture will have less of an effect on epithelial function than believed unless an entire sub-population is completely missing.

## 6. ChAT+ epithelial cells

The use of the ChAT-tdTomato mouse to generate clear ChAT+ populations for imaging led to the unexpected observation of a rare, ChAT+ epithelial cell population. The rarity of the population led us to hypothesize that the population was either the CHGNA expressing enteroendocrine population or the DCLK1 expressing tuft cell population. Both populations serve sensory and communication purposes but have distinct morphologies, expression profiles, and functions[69,78,200–204,79–81,195–199]. Cryo sections from

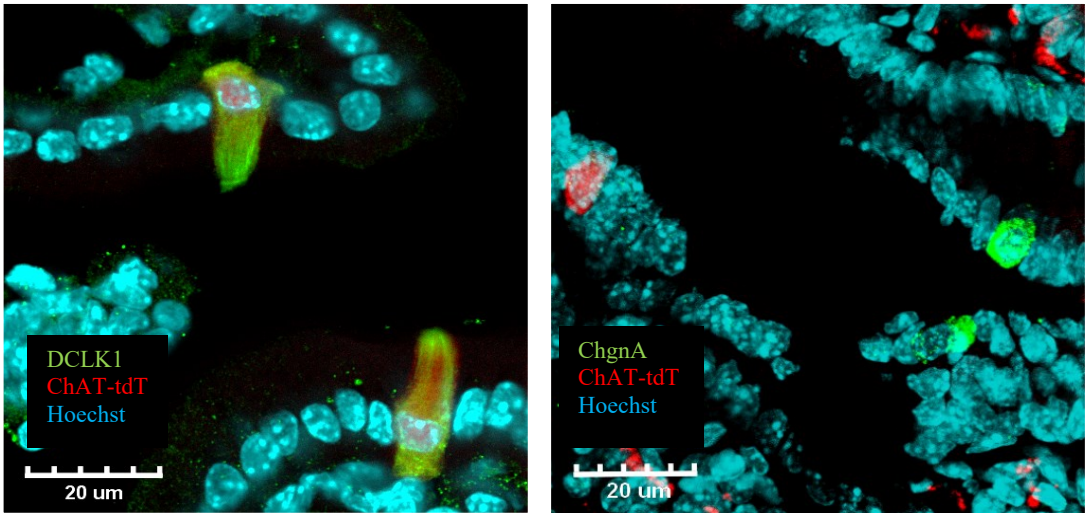


**Figure 20: Epithelial ChAT**

Epithelial ChAT (red) is expressed in A) Tuft (green, DCLK1+) cells, not B) Enteroendocrine (green, ChgnA+) cells in the mouse jejunum. Adult ChAT-tdTomato jejunum. Nuclear marker Hoescht (cyan). Scale bar=20μm

ChAT-tdTomato mouse jejunum were stained with either the EEC marker CHGNA or the Tuft cell marker DCLK1 and imaged. We found that ChAT-tdTomato expression could be found in the same cells that stained positively for DCLK1 and independent of CHGNA, indicating that the ChAT+ population was tuft cells (**Figure 20**). A literature search confirmed the presence of this ChAT+ epithelial population by both imaging using an even more extensive array of Tuft cell and Enteroendocrine cell markers and single-cell RNAseq[97,203,204]. The ChAT+ population persisted in enteroid and monolayer culture, with *Chat* being expressed in both ND and DF cultures by qRT-PCR and matching our previous observation of the tuft cell marker *Dclk1* being expressed in both ND and DF cultures.

## 7. FIS Assay in SMP permissive conditions

As there was no conclusive, significant difference observed in the two SMP-permissive media conditions in regards to SMP identity using the methods we tested, we proceeded to test for a possible functional influence of the media conditions on the FIS assay. In initial experiments, basal behavior was unaffected and forskolin [5μM]-induced swelling exhibited a significant increase in cross-sectional area regardless of the conditions used or the presence of the SMP (**Figure 21A).** There is what appears to trending decrease in the forskolin-induced response in enteroids cultured minimal media+NGF with the

SMP compared to the +GS+SMP co-culture condition or in NGF without the SMP present (NGF+SMP: 26.31% ± 5.51% vs GS+SMP: 42.16% ± 4.6% and NGF-SMP: 40.87% ± 6.17%), but it does not reach significance, likely due to the small n of the experiment.

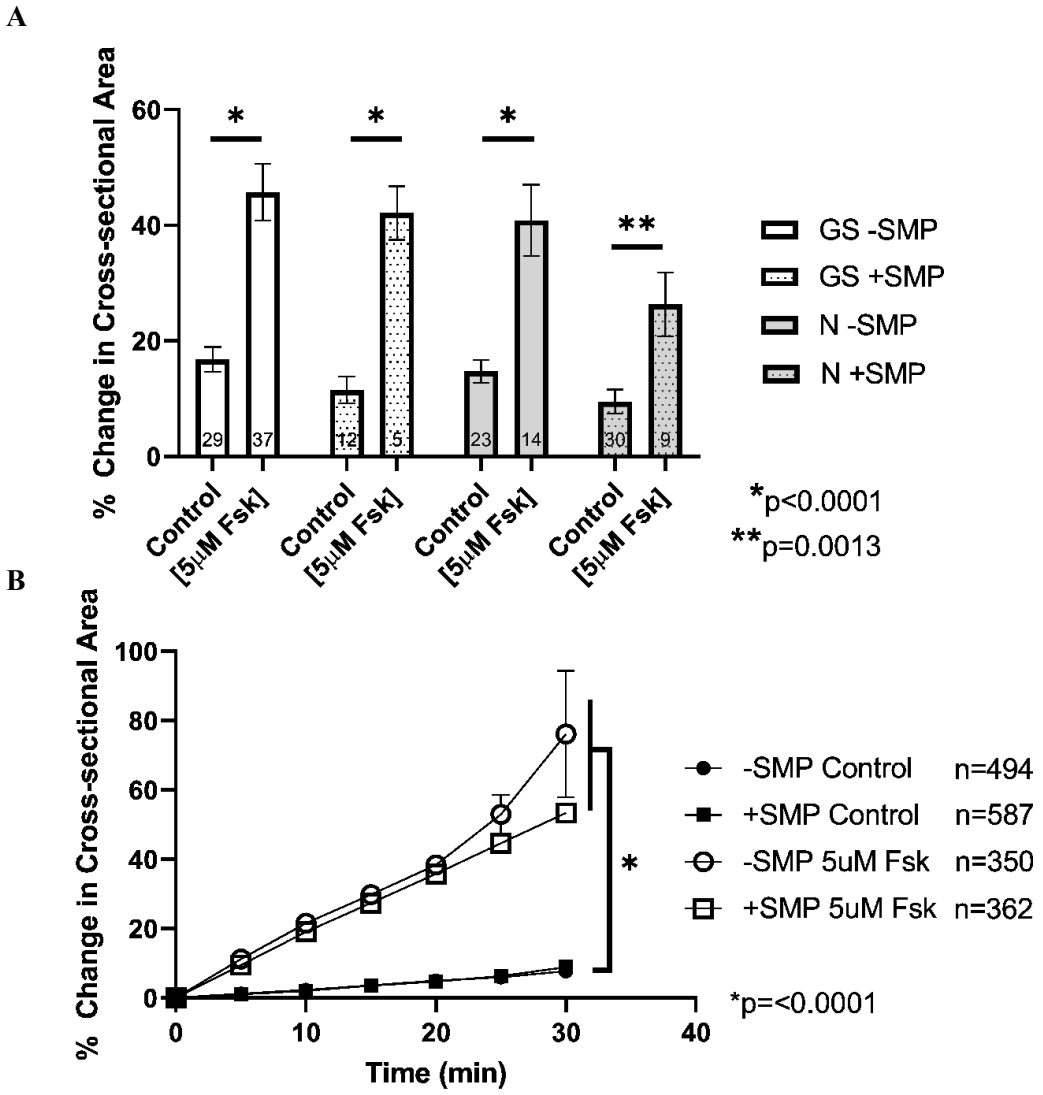


**Figure 21: Secretory behavior in co-culture permissive conditions**

**A)** Preliminary FIS assay using enteroids co-plated for 2 days with or without the SMP (N10+E2) in either media +Gastrin and SB202190 or +NGF normalized to the area of the enteroid at t=0 for control and post-forskolin [5μM] addition to account for normal variation in enteroid size. Forskolin induced a significant increase in cross-sectional area in all conditions. **B)** Expanded FIS assay using enteroids co-plated for 2 days with or without the SMP (N10+E2) in +GS media condition normalized to the area of the enteroid at t=0 for control and t=0 when forskolin is added to account for normal variation in enteroid size. Enteroids respond with a significant increase in cross-sectional area in response to forskolin ($p<0.0001$) regardless of the presence of the SMP or not, and there is no difference between responses in the cultures that were co-plated with the SMP and the enteroids plated alone. The SMP also has no effect on basal secretory behavior of the enteroids without stimulation by forskolin. Error bars depicting the SEM and points may overlap.

Due to the apparent trending decrease in FIS in the +NGF+SMP co-cultures and the fact that the +GS condition is almost identical to the Sato condition (minus one component) while the +NGF condition is more dis-similar (minus three components and plus one new component), we decided to do a more extensive test with the GS condition to confirm the secretory behavior of the co-culture. As expected based on previous observations, in a larger population the presence or absence of the SMP had no effect on FIS in the enteroids (**Figure 21B**). Continued use of the +NGF condition would have required complete re-characterization of the enteroid cultures. Though it is interesting that something about the

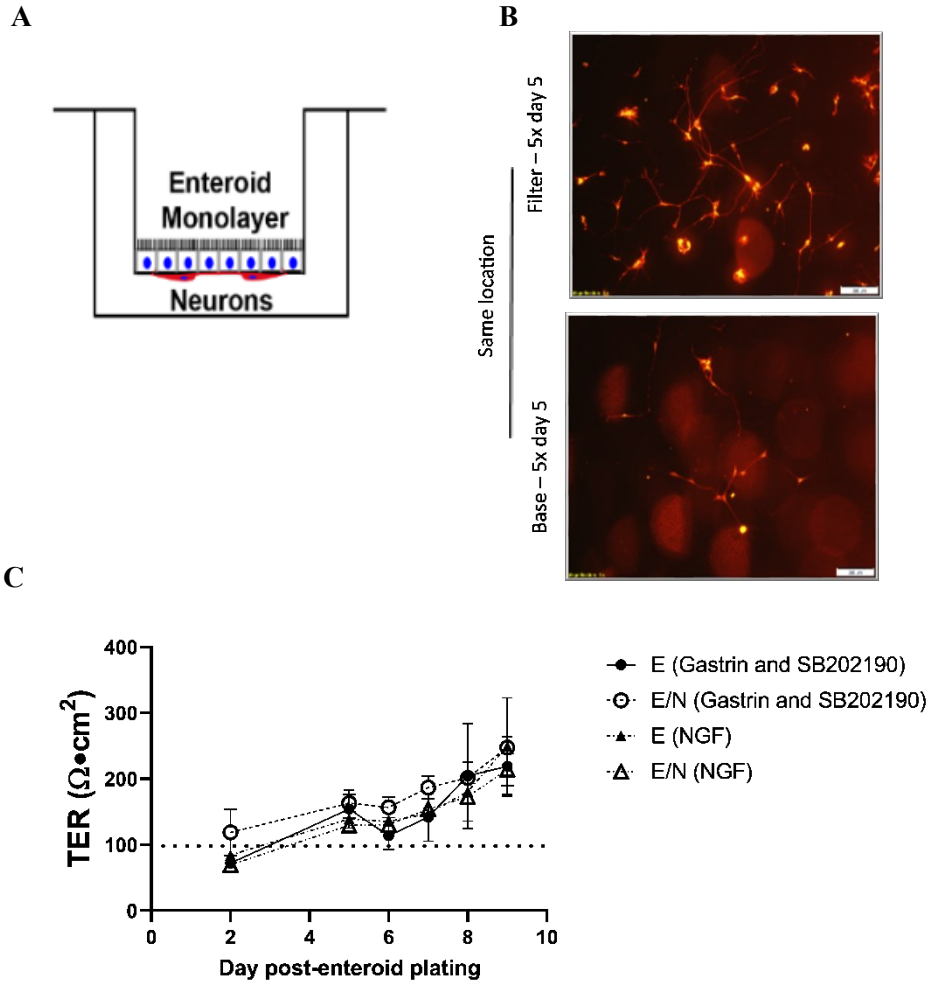


**Figure 22: Mouse enteroid/ENS 2D Co-culture model**

**A)** Cartoon schematic of the proposed co-culture system. **B)** Images of the base of the Transwell filter and the base of the well immediately below the same location five days post-seeding. Scale bar = 200µm. **C)** Average TER of mouse jejunum enteroids seeded on dual-coated Transwell filters with or without the SMP in the two permissive conditions. The dotted line indicates when monolayers are approximately confluent. SEM indicated by error bars, bars may be covered by individual points.

+NGF culture condition changed either the SMP population, the enteroid population, or both to lead to a possible effect on anion secretion, determining the cause of this effect was beyond the scope of this project.

## 8. Assembly of 2D co-culture system

Once conditions permissible to all components of the proposed co-culture system were determined, the next step was to attempt assembly of the culture. Since the SMP culture required pre-differentiation, and mouse enteroids were shown to be incapable of growing to confluence when seeded on the inverse of the Transwell filter (**data not shown**), SMP cultures were seeded on the bottom of Transwell filters that had been pre-coated on the top with 200μg/mL rat tail collagen type 1 (for the enteroids) and double coated with 1mg/mL rat tail collagen I and 20μg/mL fibronectin on the bottom (for the SMP). After adhering to the inverted filter for 45 minutes-1hour at 37°C, the filters were gently flipped into pre-warmed (37°C) SCM and allowed to differentiate.

Both the filter and the base of the well were imaged over several days to determine the efficiency of SMP adherence to the filter over time (**Figure 22B**). After differentiating 7 days, mouse jejunum enteroids were seeded in either of the two permissive media conditions (+GS and +NGF) and TER was monitored (**Figure 22C**). As there was no difference in TER or in the time for the monolayers to become confluent regardless of the condition used or the presence of the SMP (**Figure 22**), the decision was made to focus on the +GS condition for future experiments. As there were no observed functional differences in the metrics we were interested in, it was decided to test the more-similar condition to reduce the amount of re-characterization necessary.

## 9. 2-Dimensional co-culture of the ENS with mouse jejunum enteroids: SMP behavior

Once culture conditions and protocol permitted successful co-culture of the ENS and mouse jejunum enteroids, the question of SMP behavior on the Transwell filters was addressed. In particular, do

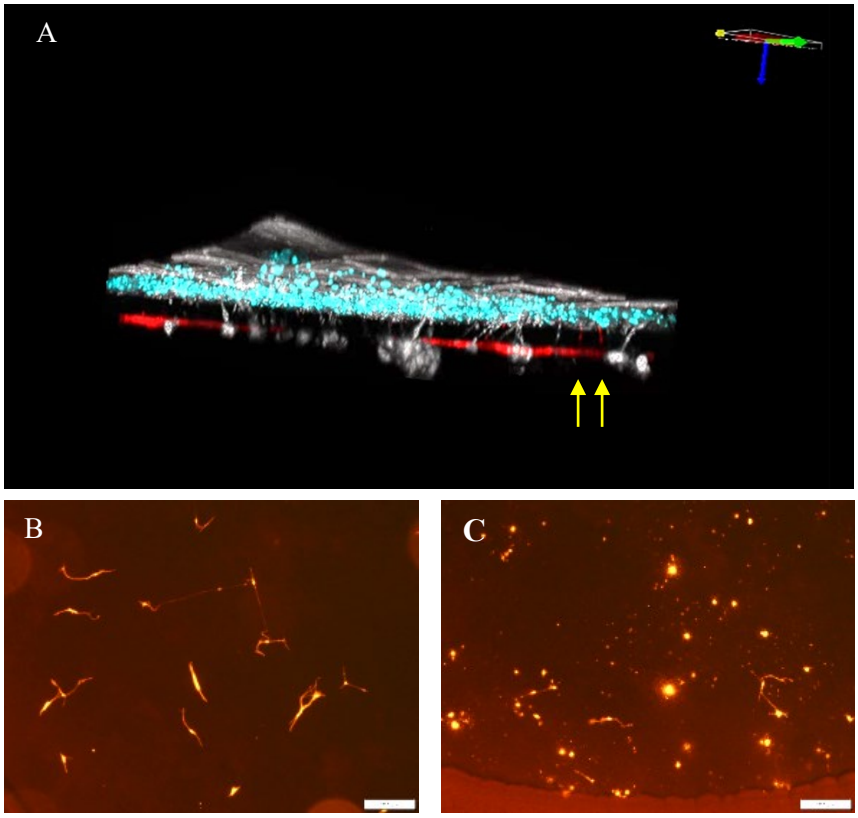


**Figure 23: Influence of co-culture arrangement on neural morphology**

**A)** SMP neural projections 'reach' towards enteroid monolayers on a volumetric rendering of a z-stack obtained on confocal. Arrows indicate neural projection 'reaching' across the Transwell filter. Image of the SMP 3 days post-enteroid plating in +GS on **B)** on the opposite side of the Transwell filter and **C)** on the same side of the Transwell filter. SMP cells in direct contact with the enteroids have largely begun to lose projections within three days of co-culture while the SMP cells on the inverse side of the filter from the enteroids remain stable. Scale bar = 200µm.

the SMP neuron projections reach through the filter pores towards the epithelial monolayer or does the filter remain as 'dead space'?

Two experiments were done to address these questions. First, co-cultures plated on 1.0µm pore Transwell filters (Millipore)--to better facilitate neural 'reaching' if it does occur—were plated and grown to confluence before being fixed and imaged for any slender projections extending into the 10µm thick filter. While not common, in multiple locations on several filters, projections did indeed reach through the pores towards the monolayer (**Figure 23A**).

The second experiment was to plate the enteroid monolayer in direct contact to the SMP culture, similar to how the 3D cultures were generated, but without the layer of Matrigel in between the two populations. Direct plating of the enteroids on the SMP led to rapid loss of projections from a majority of

the cells of the SMP culture that never recovered (**Figure 23B, C**). So while the neural projections do indeed reach towards the epithelial layer through the Transwell fitler, plating the SMP in direct contact with the epithelia is detrimental to SMP survival. The final co-culture protocol consisted of SMP plated on the bottom of a double-coated Transwell filter with the enteroids plated on the single coated top after 5-7 days predifferentiation and transfer to the +GS medium condition until TER was determined to be confluent.

It is interesting to note that co-culture with the enteroids appears to have an effect on the survival and lifespan of the SMP cultures. Though there are no SMP only controls in the co-culture conditions, it is known that SMP cultures in the normal SMP differentiation condition (SCM) have a culture lifespan of about 22-24 days before the majority of the culture is dead/dying. In monolayer co-culture experiements, it was observed that neurons are still morphologically healthy at SMP culture day 34 (co-cultured with enteorid monolayers for 27 days). This unexpected finding is definitely a benefit for future studies of the co-culture as the 24-day lifespan of the SMP is no longer a limiting factor and investigation into the cause of SMP persistence may also help SMP research by both allowing the SMP to be cultured for longer and offering insight in to physiological signaling between the two populations and the SMP survival pathways.

## 10. The presence of the SMP in 2D co-culture leads to an increase in stimulated short-circuit current ($I_{sc}$)

Mouse jejunal enteroid monolayers plated in +GS medium concurrently with enteroids co-plated with the SMP on the bottom side of the filter on SMP differentiation day 7 (E15 v N22+E15) were mounted in an Ussing Chamber/Voltage Clamp to assess electrogenic ion transport. Previous FIS assays indicated that the SMP had no effect on either basal or stimulated secretion when cross-sectional area of the 3D enteroids was used as the metric. This was in contrast to the literature describing a strong influence of the ENS on intestinal secretion after exposure to several different agonists, including diarrheal diseases.

Basal $I_{sc}$ appears to be increased in the co-cultures compared to passage and age matched enteroid-only monolayers (0.36μA/cm$^2$ vs 4.18 ± 1.63μA/cm$^2$) but data is inconclusive without a greater number of samples (**Figure 24B**). Similarly, stimulation with 5μM forskolin appears to cause an increase in peak $I_{sc}$ (8.11μA/cm$^2$ vs 15.20 ± 2.60μA/cm$^2$, **Figure 24C**) that does not seem to fully resolve after the addition of $CFTR_{inh}$-172 [20μM] (determined as the average of the last ten time points recorded; -0.18μA/cm$^2$ vs 2.67 ± 1.15μA/cm$^2$), indicating that the presence of the SMP may be activating CaCCs

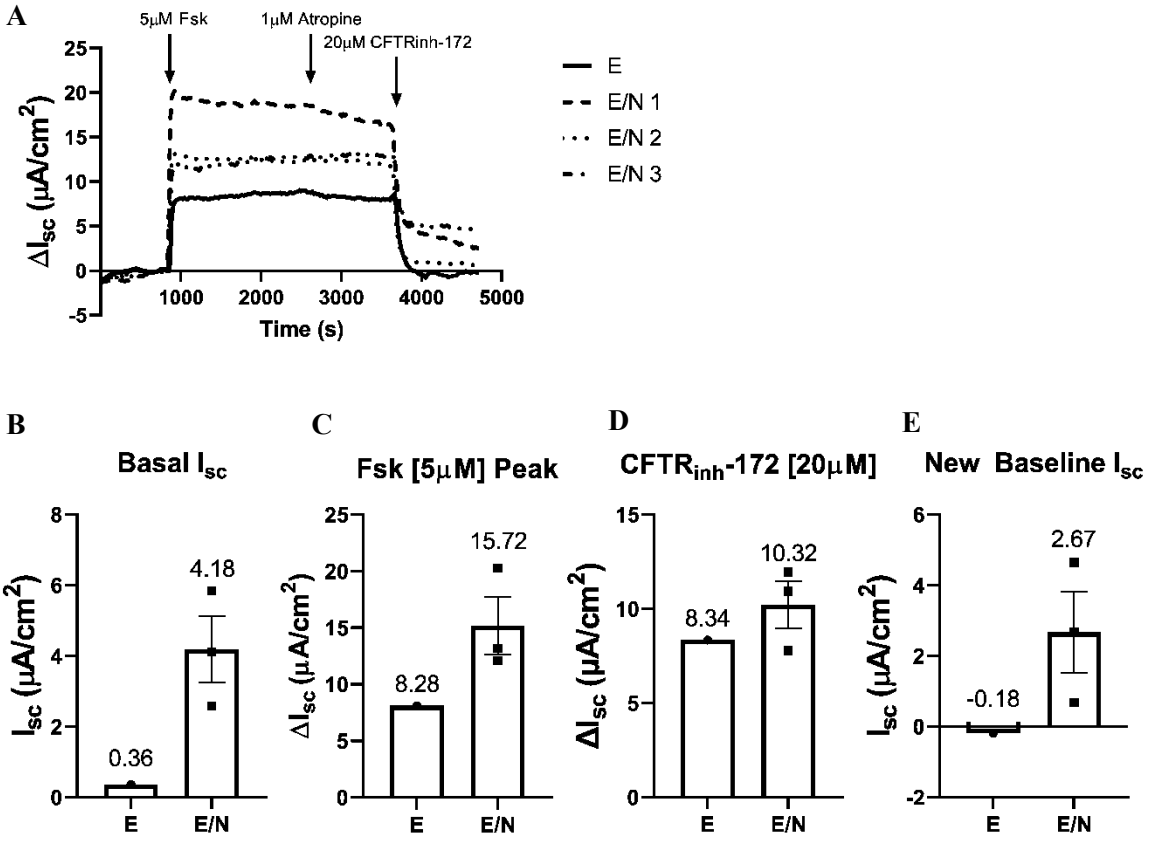


**Figure 24: Co-culture with the SMP appears to increase Forskolin-induced $I_{sc}$**

**A)** Short-circuit current traces of three co-cultures and one control culture and B) Average maximum peak in response to stimulation with 5μM Fsk. Co-culture with the SMP appears to increase stimulated Isc in response to 5μM forskolin. Atropine has no effect on forskolin-induced Isc post-stimulation with Fsk and the inhibitor CFTRinh-172 inhibits Fsk-induced Isc. **B)** The basal $I_{sc}$ exhibited in both control and co-cultured monolayers. Baseline secretion was determined as the average of the ten time points immediately prior to addition of forskolin divided by the area of the monolayer. **C)** Max peak $I_{sc}$ after forskolin [5μM] stimulation in both control and co-cultured enteroid monolayers. **D)** The difference in the average $I_{sc}$ of ten time points 200s after the addition of $CFTR_{inh}$-172 compared to the average of ten time points immediately prior to CFTR inhibitor addition. The drop in $I_{sc}$ in the control monolayer is about equal to the Fsk-induced increase while the reduction in co-cultured monolayers is less. **E)** Average of the final ten time indicates that inhibition of CFTR is not enough to return $I_{sc}$ to baseline in monolayers co-cultured with the SMP. Bars represent mean ± SEMs. p-values not calculated due to limited number of experiments; n=1.

during secretion (**Figure 24D**). The late addition of atropine had no apparent effect on the stimulated current or the resolution of Fsk-induced $I_{sc}$, showing that the increase in forskolin-induced secretion is not due to SMP release of acetylcholine.

Overall, the addition of the SMP culture appears to have increased the short-circuit current ($I_{sc}$) in response to forskolin [5μM] in a manner similar to tissue behavior as documented in the literature, this is in contrast to the observations made using the FIS assay in 3D co-cultures in the same media condition. Whether this is due to the longer co-culture time for the monolayers (15 days opposed to 2-4 days) or some other factor we do not yet know and investigation fell beyond the scope of this project.

## C. Discussion

The inclusion of the SMP component of the ENS in culture jointly with the epithelial enteroids demonstrates not only that the two cultures can persist together in appropriately permissive conditions, but also that there is a functional influence exerted on the epithelia by the presence of the SMP. The development of this co-culture method opens the door to more physiologically accurate studies of both intestinal function and pathophysiology. Though its composition appears to be highly variable, it is without doubt that the SMP plays an important role in monitoring and influencing the intestinal epithelia.

The variability in tissue samples taken across the entirety of the small intestine and the technical problems with antibody staining limits the characterization of the SMP component of the current model which is an unfortunate limitation that may require single cell sequencing to ultimately address if the immunofluorescence capabilities remain limiting. Despite this major, unresolved component, the SMP cultures were able to exert a modulatory influence on the enteroid monolayers with relatively small numbers. Further optimization of the SMP isolation and culturing techniques is undoubtedly required to get a better measure of the scope of functional coupling the two systems undergo, but even this initial method is able to demonstrate a functional effect on anion secretion similar to that observed in intestinal tissues exposed to neuronal inhibitors and a known secretogogue. This system then, provides a first step that proves the concept of these systems' capabilities to grow and function together long term.

The preliminary ion transport data acquired in the monolayers does offer insight to intestinal physiology already. The co-culture demonstrates an increase in baseline $I_{sc}$, indicating a role of the SMP in baseline secretion resulting in higher basal $I_{sc}$ in the presence of the SMP. Determining whether this is a permanent change due to the long-term co-culture or short-term change maintained by constant signaling remains unknown but investigation will offer insight to the differences in development and identify in culture versus tissue models.

Like in tissues, there is an increase in forskolin-induced $I_{sc}$ indicating a role of the SMP in cAMP-induced $I_{sc}$ but there is also the fact that the CFTR inhibitor 172 did not fully abolish the Fsk-induced $I_{sc}$ in the co-culture model. Thus the SMP facilitates not only a potential increase in CFTR-mediated current, but it is likely that a second pathway is activated in the presence of the SMP. The identity of this pathway can be determined by testing the effects of other inhibitors such as the CaCC inhibitor A01 on Fsk-induced $I_{sc}$ in the co-cultures. The lack of a significant effect by atropine indicates that whatever signaling is responsible for the SMP effect on forskolin-stimulated secretion, it is not likely to be SMP release of acetylcholine.

Another interesting thing about this experiment is that as far as we know, forskolin does not on its own stimulate paracrine signaling from the neurons. That is, forskolin itself does not stimulate neuronal secretion to signal to the epithelium which then causes an increase in $I_{sc}$. Thus the SMP effect on epithelial secretion is caused by either 1) basal SMP signaling behavior and effects on the epithelium or 2) a secondary signal from the epithelium being released in response to forskolin and having an effect on the SMP half of the culture which then signals back to the enteroids to change secretory behavior.

As forskolin does not itself stimulate neuronal signaling, a follow up experiment using a stimulus that targets the SMP culture resulting in an SMP-induced effect on the epithelium is still required. The difficulty in designing such an experiments is the diversity of the intestinal epithelium. Even the ND enteroid cultures may be able to sense and respond to most of the agonists known to cause a neuronal response that results in signaling that could stimulate ion transport, so an alternative readout may be necessary to demonstrate linear SMP-to-epithelium signaling.

While data is only preliminary, it is promising that the monolayer co-cultures closely mimic tissue behavior in these initial tests. Should the co-culture system behave as expected, we would expect not only forskolin-induced secretion to be increased, but application of secretory pathogens and toxins, such as cholera toxin and rotavirus, to co-cultures should also result in higher $I_{sc}$ compared to enteroid monolayers alone. From there, the model could be used to study the pathology of secretory diseases, identification of pharmacological treatments for disease, or even the basal physiology of the SMP-epithelium cross-talk.

Despite requiring further optimization, the system shows promise as a tool to further characterize intestinal physiology and pathophysiology, as even this non-optimized system displays the characteristic increase in anion secretion in preliminary experiments. This proves its use in further studying diseases that have a neuronal component modulating pathophysiology such as diarrhea.

Should further characterization indicate the co-culture system as an acceptable replacement, studies of the SMP-epithelium cross-talk in physiology and pathophysiology will be possible without the confounding factors of immune and muscular populations present in the tissue. As demonstrated earlier in this work, the presence of additional populations and the assumptions made because of them can mask important physiology, leading to inaccurate conclusions and perpetuated misunderstanding of physiology. These assumptions can then influence or even limit clinical applications, our understanding of disease, or the investigation of pharmacological targets.

# VIII. Final Comments

The enteroid culture system has a wealth of potential in moving forward studies of epithelial biology, but it—like any other model—has its flaws and drawbacks. Here we attempted to address several of those limitations to create a more physiological model and in the process, observed and began to define entirely new aspects to a process previously considered understood.

The confirmation of a previously defined differentiation protocol in addition to the modified non-differentiation conditions provides a more polarized system than previously defined for the mouse enteroids. This system can be used to separate the crypt and villus populations for studies of differentiation, regeneration, transport, infection, and other physiological functions. The intestinal crypt and villus display distinct functional behaviors, and being able to reproducibly culture the two systems is an important ability that the mouse enteroid community lacked for many years.

The second development described significantly increases the usability of the mouse enteroid system by defining a reproducible method for generating confluent monolayer cultures of the mouse enteroids. Previously, studies were limited to what assays could be performed in the 3D enteroid cultures, and the stochastic nature of these cultures for many metrics such as gradients for nutrient, infection, or drug exposure to the enteroids made analysis of the resulting data difficult in some cases. Even physical considerations such as greater stiffness of the Matrigel matrix surrounding enteroids earlier in the culture life or enteroids being located more interior in the Matrigel dome compared to enteroids plated towards the edge of a culture brought up questions about the variability and significance of assays like the FIS assay where greater stiffness will likely expert a greater force suppressing the swelling used as a metric for secretion, this introduces an unquantified variable to FIS analysis that is ill-defined. To reduce variability in results and expand the potential applications of the system, monolayers will be a powerful tool.

Enteroid monolayers proved their usefulness when control experiments both recapitulated findings observed in intestinal tissues, but also revealed a previously undefined aspect of cholinergic-

induced secretion hidden by the standard protocols used to separate epithelial function from residual neuronal input. The system proved its usefulness as a strictly epithelial system, offering greater understanding of epithelial biology separate from the underlying populations, something important for not only understanding the system in health, but also necessary for untangling the course of infection and disease and ensuring that the proper populations are targeted for treatment. There are many basal and pathological functions of the intestinal epitheliumio in response to cholinergic signaling, calcium signaling, and apparently the combination of the two. Not only has the enteroid monolayer system identified a series of new pathways and signaling applications, but it provides a platform for further investigation.

The novel two phase paradigm for cholinergic signaling proposed brings up more questions than it answers, but at the same time demonstrates how a system or function we believe we completely understand may in fact be far more complicated and have hidden contributors. This is important to recognize not only for the contribution to basic science of correcting a misunderstood signaling pathway, but the widespread use of the muscarinic pathway to induce secretion in secretory epithelia may indicate a more widespread application of the nicotinic contribution in other secretory cell types as well. The pathways previously uncharacterized may be masking disease mechanisms or potential therapeutic targets. There may be genetic variation that was having previously unexplainable effects. If we as medical professionals do not understand how the body functions when healthy, it is impossible to adequately diagnose, study, or treat disease. That there are widespread assumptions regarding cholinergic-induced secretion, potentially in more secretory systems than the intestine alone, reveals an oversight in epithelial biology that could later influence clinical applications.

The previously undefined nicotinic component to cholinergic intestinal secretion opens the door to identification of not only potential disease and therapeutic targets in the intestine, but also raises the question of muscarinic secretion in other secretory systems. Even more broadly, there is now the question of if other muscarinic functions throughout the body are possibly regulated by nicotinic signaling or if

there are other nicotinic functions such as the newly described signaling capabilities of the nicotinic receptors.

Further expanding the enteroid system as a co-culture model including the sub-mucosal plexus of the enteric nervous system offers another new model for the study of health and disease. It is known that there are diarrheal diseases with strong ENS components that epithelia-only models can not address either when studying the course of disease or developing treatment. Generating and characterizing a culture system that incorporates the SMP populations with the enteroid monolayers and demonstrating a preliminary functional influence of the co-culture compared to enteroid monocultures offers a promising solution to this limitation. The largest drawback is the time intensive protocol to generate the primary SMP cultures and the contributing factor of the harsh protocol meaning that several mice are needed to isolate enough cells for a single set of experiments.

Overall, the development and characterization of both the monolayer culture and the co-culture system strengthens the enteroid system by expanding potential assay methods and allowing for additional questions to be addressed.

# IX. References


1. Takahashi K, Yamanaka S. Induction of Pluripotent Stem Cells from Mouse Embryonic and Adult Fibroblast Cultures by Defined Factors. *Cell*. 2006;126(4):663-676. doi:10.1016/j.cell.2006.07.024
2. Takahashi K, Tanabe K, Ohnuki M, et al. Induction of pluripotent stem cells from adult human fibroblasts by defined factors. *Cell*. 2007;131(5):861-872. doi:10.1016/j.cell.2007.11.019
3. Okita K, Nakagawa M, Hyenjong H, Ichisaka T, Yamanaka S. Generation of mouse induced pluripotent stem cells without viral vectors. *Science (80- )*. 2008;322(5903):949-953. doi:10.1126/science.1164270
4. Ueda T, Yamada T, Hokuto D, et al. Generation of functional gut-like organ from mouse induced pluripotent stem cells. *Biochem Biophys Res Commun*. 2010;391(1):38-42. doi:10.1016/j.bbrc.2009.10.157
5. Spence JR, Mayhew CN, Rankin SA, et al. Directed differentiation of human pluripotent stem cells into intestinal tissue in vitro. *Nature*. 2011;470(7332):105-109. doi:10.1038/nature09691
6. Barker N, Van Es JH, Jaks V, et al. Very long-term self-renewal of small intestine, colon, and hair follicles from cycling Lgr5+ve stem cells. *Cold Spring Harb Symp Quant Biol*. 2008;73(Soriano 1999):351-356. doi:10.1101/sqb.2008.72.003
7. Barker N, Clevers H. Leucine-Rich Repeat-Containing G-Protein-Coupled Receptors as Markers of Adult Stem Cells. *Gastroenterology*. 2010;138(5):1681-1696. doi:10.1053/j.gastro.2010.03.002
8. Barker N, van Es JH, Kuipers J, et al. Identification of stem cells in small intestine and colon by marker gene Lgr5. *Nature*. 2007;449(7165):1003-1007. doi:10.1038/nature06196
9. Sato T, Vries RG, Snippert HJ, et al. Single Lgr5 stem cells build crypt-villus structures in vitro without a mesenchymal niche. *Nature*. 2009;459(7244):262-265. doi:10.1038/nature07935
10. Barker N, Huch M, Kujala P, et al. Lgr5(+ve) stem cells drive self-renewal in the stomach and build long-lived gastric units in vitro. *Cell Stem Cell*. 2010;6. doi:10.1016/j.stem.2009.11.013
11. Clevers H. Modeling Development and Disease with Organoids. *Cell*. 2016;165(7):1586-1597.

doi:10.1016/j.cell.2016.05.082

12. Dekkers JF, Wiegerinck CL, de Jonge HR, et al. A functional CFTR assay using primary cystic fibrosis intestinal organoids. *Nat Med*. 2013;19(7):939-945. doi:10.1038/nm.3201

13. Dekkers JF, Berkers G, Kruisselbrink E, et al. Characterizing responses to CFTR-modulating drugs using rectal organoids derived from subjects with cystic fibrosis. *Sci Transl Med*. 2016;8(344):344ra84. doi:10.1126/scitranslmed.aad8278

14. Ettayebi K, Crawford SE, Murakami K, et al. Replication of human noroviruses in stem cell-derived human enteroids. *Science (80- )*. 2016;353(6306):1387-1393. doi:10.1126/science.aaf5211

15. In J, Foulke-Abel J, Zachos NC, et al. Enterohemorrhagic Escherichia coli Reduces Mucus and Intermicrovillar Bridges in Human Stem Cell-Derived Colonoids. *Cell Mol Gastroenterol Hepatol*. 2016;2(1):48-62. e3. https://www.ncbi.nlm.nih.gov/pmc/articles/PMC4740923/pdf/main.pdf.

16. Camilleri M, Nullens S, Nelsen T. Enteroendocrine and neuronal mechanisms in pathophysiology of acute infectious diarrhea. *Dig Dis Sci*. 2012;57(1):19-27. doi:10.1007/s10620-011-1939-9

17. Wang X, Yamamoto Y, Wilson LH, et al. Cloning and variation of ground state intestinal stem cells. *Nature*. 2015;522(7555):173-178. doi:10.1038/nature14484

18. Wilson SS, Tocchi A, Holly MK, Parks WC, Smith JG. A small intestinal organoid model of non-invasive enteric pathogen-epithelial cell interactions. *Mucosal Immunol*. 2015;8(2):352-361. doi:10.1038/mi.2014.72

19. Zhang YG, Wu S, Xia Y, Sun J. Salmonella-infected crypt-derived intestinal organoid culture system for host-bacterial interactions. *Physiol Rep*. 2014;2(9):e12147. doi:10.14814/phy2.12147

20. Zomer-van Ommen DD, Pukin A V, Fu O, et al. Functional Characterization of Cholera Toxin Inhibitors Using Human Intestinal Organoids. *J Med Chem*. 2016;59(14):6968-6972. doi:10.1021/acs.jmedchem.6b00770

21. Saxena K, Blutt SE, Ettayebi K, et al. Human Intestinal Enteroids: a New Model To Study Human Rotavirus Infection, Host Restriction, and Pathophysiology. *J Virol*. 2016;90(1):43-56.

doi:10.1128/JVI.01930-15

22. Foulke-Abel J, In J, Kovbasnjuk O, et al. Human enteroids as an ex-vivo model of host-pathogen interactions in the gastrointestinal tract. *Exp Biol Med*. 2014;239(9):1124-1134. doi:10.1177/1535370214529398

23. Pilowsky PM, Farnham MMJ, Fong AY. *Stimulation and Inhibition of Neurons*. Springer; 2013.

24. Foulke-Abel J, In J, Yin J, et al. Human Enteroids as a Model of Upper Small Intestinal Ion Transport Physiology and Pathophysiology. *Gastroenterology*. 2016;150(3):638-649 e8. doi:10.1053/j.gastro.2015.11.047

25. Yin Y, Bijvelds M, Dang W, et al. Modeling rotavirus infection and antiviral therapy using primary intestinal organoids. *Antivir Res*. 2015;123:120-131. doi:10.1016/j.antiviral.2015.09.010

26. Heo I, Dutta D, Schaefer DA, et al. Modelling Cryptosporidium infection in human small intestinal and lung organoids. *Nat Microbiol*. 2018;3(7):814-823. doi:10.1038/s41564-018-0177-8

27. Rao MC. Physiology of electrolyte transport in the gut: Implications for disease. *Compr Physiol*. 2019;9(3):947-1023. doi:10.1002/cphy.c180011

28. Hardcastle PT, Eggenton J. The effect of acetylcholine on the electrical activity of intestinal epithelial cells. *BBA - Biomembr*. 1973;298(1):95-100. doi:10.1016/0005-2736(73)90013-8

29. Browning JG, Hardcastle J, Hardcastle PT, Redfern JS. Localization of the effect of acetylcholine in regulating intestinal ion transport. *J Physiol*. 1978;281(1):15-27. doi:10.1113/jphysiol.1978.sp012406

30. Donowitz M, Asarkof N. Calcium dependence of basal electrolyte transport in rabbit ileum. *Am J Physiol*. 1982;243(1).

31. Donowitz M, Fogel R, Battisti L, Asarkof N. The neurohumoral secretagogues carbachol, substance P and neurotensin increase Ca++ influx and calcium content in rabbit ileum. *Life Sci*. 1982;31(18):1929-1937. doi:10.1016/0024-3205(82)90031-5

32. Hardcastle J, Hardcastle PT, Noble JM. The involvement of calcium in the intestinal response to secretagogues in the rat. *J Physiol*. 1984;355(1):465-478. doi:10.1113/jphysiol.1984.sp015432

33. Dharmsathaphorn K, McRoberts JA, Mandel KG. A human colonic tumor cell line that maintains vectorial electrolyte transport. *Am J Physiol - Gastrointest Liver Physiol*. 1984;9(2). doi:10.1152/ajpgi.1984.246.2.g204

34. Dharmsathaphorn K, Mandel KG, Masui H, McRoberts JA. Vasoactive intestinal polypeptide-induced chloride secretion by a colonic epithelial cell line. Direct participation of a basolaterally localized Na+,K+,Cl- cotransport system. *J Clin Invest*. 1985;75(2):462-471. doi:10.1172/JCI111721

35. McRoberts JA, Beuerlein G, Dharmsathaphorn K. Cyclic AMP and Ca2+-activated K+ transport in a human colonic epithelial cell line. *J Biol Chem*. 1985;260(26):14163-14172.

36. Mandel KG, Dharmsathaphorn K, McRoberts JA. Characterization of a cyclic AMP-activated Cl- transport pathway in the apical membrane of a human colonic epithelial cell line. *J Biol Chem*. 1986;261(2):704-712.

37. Mandel KG, McRoberts JA, Beuerlein G. Ba2+ inhibition of VIP- and A23187-stimulated Cl- secretion by T84 cell monolayers. *Am J Physiol - Cell Physiol*. 1986;250(3 (19/3)):486-494. doi:10.1152/ajpcell.1986.250.3.c486

38. Reinlib L, Mikkelsen R, Zahniser D, Dharmsathaphorn K, Donowitz M. Carbachol-induced cytosolic free Ca2+ increases in T84 colonic cells seen by microfluorimetry. *Am J Physiol - Gastrointest Liver Physiol*. 1989;257(6). doi:10.1152/ajpgi.1989.257.6.g950

39. Wong SME, Lindeman RP, Parangi S, Chase HS. Role of calcium in mediating action of carbachol in T84 cells. *Am J Physiol - Cell Physiol*. 1989;257(5). doi:10.1152/ajpcell.1989.257.5.c976

40. Barrett KE. Positive and negative regulation of chloride secretion in T84 cells. *Am J Physiol - Cell Physiol*. 1993;265(4 34-4). doi:10.1152/ajpcell.1993.265.4.c859

41. Wong SME, Tesfaye A, Debell MC, Chase HS. Carbachol increases basolateral K+ conductance in T84 cells: Simultaneous measur of cell [Ca] and gk explore calcium's role. *J Gen Physiol*. 1990;96(6):1271-1285. doi:10.1085/jgp.96.6.1271

42. Kachintorn U, Vajanaphanich M, Traynor-Kaplan AE, Dharmsathaphorn K, Barrett KE. Activation by calcium alone of chloride secretion in T84 epithelial cells. *Br J Pharmacol*. 1993;109(2):510-517. doi:10.1111/j.1476-5381.1993.tb13599.x

43. Hirota CL, McKay DM. Cholinergic regulation of epithelial ion transport in the mammalian intestine. *Br J Pharmacol*. 2006;149(5):463-479. doi:10.1038/sj.bjp.0706889

44. Dharmsathaphorn K, Pandol SJ. Mechanism of chloride secretion induced by carbachol in a colonic epithelial cell line. *J Clin Invest*. 1986;77(2):348-354. doi:10.1172/JCI112311

45. Hirota CL, McKay DM. M 3 muscarinic receptor-deficient mice retain bethanechol-mediated intestinal ion transport and are more sensitive to colitis . *Can J Physiol Pharmacol*. 2006;84(11):1153-1161. doi:10.1139/y06-068

46. Lindeman RP, Chase HS. Protein kinase C does not participate in carbachol's secretory action in T84 cells. *Am J Physiol - Cell Physiol*. 1992;263(1 32-1). doi:10.1152/ajpcell.1992.263.1.c140

47. Uribe JM, Keely SJ, Traynor-Kaplan AE, Barrett KE. Phosphatidylinositol 3-kinase mediates the inhibitory effect of epidermal growth factor on calcium-dependent chloride secretion. *J Biol Chem*. 1996;271(43):26588-26595. doi:10.1074/jbc.271.43.26588

48. Keely SJ, Uribe JM, Barrett KE. Carbachol stimulates transactivation of epidermal growth factor receptor and mitogen-activated protein kinase in T84 cells: Implications for carbachol-stimulated chloride secretion. *J Biol Chem*. 1998;273(42):27111-27117. doi:10.1074/jbc.273.42.27111

49. Chang N, Uribe JM, Keely SJ, Calandrella S, Barrett KE. Insulin and IGF-I inhibit calcium-dependent chloride secretion by T84 human colonic epithelial cells. *Am J Physiol - Gastrointest Liver Physiol*. 2001;281(1 44-1):129-137. doi:10.1152/ajpgi.2001.281.1.g129

50. Keely SJ, Barrett KE. p38 mitogen-activated protein kinase inhibits calcium-dependent chloride secretion in T84 colonic epithelial cells. *Am J Physiol - Cell Physiol*. 2003;284(2 53-2):339-348. doi:10.1152/ajpcell.00144.2002

51. Riedl J, Flynn KC, Raducanu A, et al. Lifeact mice for studying F-actin dynamics. *Nat Methods*. 2010;7(3):168-169. doi:10.1038/nmeth0310-168

52. Clevers JC, Sato T, Huch OM, WOUTER RK. Culture media for stem cells. 2012. https://www.google.com/patents/WO2012168930A2?cl=en.

53. Sato T, Clevers H. Primary mouse small intestinal epithelial cell cultures. *Methods Mol Biol*. 2013;945:319-328. doi:10.1007/978-1-62703-125-7_19

54. Sato T, Clevers H. SnapShot: Growing Organoids from Stem Cells. *Cell*. 2015;161(7):1700-1700 e1. doi:10.1016/j.cell.2015.06.028

55. Sato T, Stange DE, Ferrante M, et al. Long-term expansion of epithelial organoids from human colon, adenoma, adenocarcinoma, and Barrett's epithelium. *Gastroenterology*. 2011;141(5):1762-1772. doi:10.1053/j.gastro.2011.07.050

56. Heijmans J, van Lidth de Jeude JF, Koo BK, et al. ER stress causes rapid loss of intestinal epithelial stemness through activation of the unfolded protein response. *Cell Rep*. 2013;3(4):1128-1139. doi:10.1016/j.celrep.2013.02.031

57. Noel G, Baetz NW, Staab JF, et al. A primary human macrophage-enteroid co-culture model to investigate mucosal gut physiology and host-pathogen interactions. *Sci Rep*. 2017;7:45270. doi:10.1038/srep45270

58. Kozuka K, He Y, Koo-McCoy S, et al. Development and Characterization of a Human and Mouse Intestinal Epithelial Cell Monolayer Platform. *Stem Cell Reports*. 2017;9(6):1976-1990. doi:10.1016/j.stemcr.2017.10.013

59. Lebovitz RM, Takeyasu K, Fambrough DM. Molecular characterization and expression of the (Na+ + K+)-ATPase alpha-subunit in Drosophila melanogaster. *EMBO J.* 1989;8(1):193-202. doi:10.1002/j.1460-2075.1989.tb03364.x

60. Bonner C, Kerr-Conte J, Gmyr V, et al. Inhibition of the glucose transporter SGLT2 with dapagliflozin in pancreatic alpha cells triggers glucagon secretion. *Nat Med*. 2015;21(5):512-517. doi:10.1038/nm.3828

61. Jurysta C, Nicaise C, Cetik S, Louchami K, Malaisse WJ, Sener A. Glucose transport by acinar cells in rat parotid glands. *Cell Physiol Biochem*. 2012;29(3-4):325-330. doi:10.1159/000338487

62. Yin J, Tse C-MM, Avula LR, et al. Molecular Basis and Differentiation-Associated Alterations of Anion Secretion in Human Duodenal Enteroid Monolayers. *Cmgh*. 2018;5(4):591-609. doi:10.1016/j.jcmgh.2018.02.002

63. Ehlert FJ, Pak KJ, Griffin MT. Muscarinic Agonists and Antagonists: Effects on Gastrointestinal Function. In: Fryer AD, Christopoulos A, Nathanson NM, eds. *Muscarinic Receptors*. Berlin, Heidelberg: Springer Berlin Heidelberg; 2012:343-374. doi:10.1007/978-3-642-23274-9_15

64. Zachos NC, Alamelumangpuram B, Lee LJ, Wang P, Kovbasnjuk O. Carbachol-mediated endocytosis of NHE3 involves a clathrin-independent mechanism requiring lipid rafts and Cdc42. *Cell Physiol Biochem*. 2014;33(3):869-881. doi:10.1159/000358659

65. Becker L, Kulkarni S, Tiwari G, Micci MA, Pasricha PJ. Divergent fate and origin of neurosphere-like bodies from different layers of the gut. *Am J Physiol Gastrointest Liver Physiol*. 2012;302(9):G958-65. doi:10.1152/ajpgi.00511.2011

66. Becker L, Peterson J, Kulkarni S, Pasricha PJ. Ex vivo neurogenesis within enteric ganglia occurs in a PTEN dependent manner. *PLoS One*. 2013;8(3):e59452. doi:10.1371/journal.pone.0059452

67. Vijftigschild LA, Berkers G, Dekkers JF, et al. beta2-Adrenergic receptor agonists activate CFTR in intestinal organoids and subjects with cystic fibrosis. *Eur Respir J*. 2016;48(3):768-779. doi:10.1183/13993003.01661-2015

68. Dekkers JF, Gogorza Gondra RA, Kruisselbrink E, et al. Optimal correction of distinct CFTR folding mutants in rectal cystic fibrosis organoids. *Eur Respir J*. 2016;48(2):451-458. doi:10.1183/13993003.01192-2015

69. Cheng H. Origin, differentiation and renewal of the four main epithelial cell types in the mouse small intestine. II. Mucous cells. *Am J Anat*. 1974;141(4):481-501. doi:10.1002/aja.1001410404

70. Cheng H, Leblond CP. Origin, differentiation and renewal of the four main epithelial cell types in the mouse small intestine III. Entero-endocrine cells. *Am J Anat*. 1974;141(4):503-519.

71. Gunawardene AR, Corfe BM, Staton CA. Classification and functions of enteroendocrine cells of the lower gastrointestinal tract. *Int J Exp Pathol*. 2011;92(4):219-231. doi:10.1111/j.1365-

2613.2011.00767.x

72. Bellono NW, Bayrer JR, Leitch DB, et al. Enterochromaffin Cells Are Gut Chemosensors that Couple to Sensory Neural Pathways. *Cell*. 2017;170(1):185-198 e16. doi:10.1016/j.cell.2017.05.034

73. Cheng H. Origin, differentiation and renewal of the four main epithelial cell types in the mouse small intestine IV. Paneth cells. *Am J Anat*. 1974;141(4):521-535.

74. Sato T, Van Es JH, Snippert HJ, et al. Paneth cells constitute the niche for Lgr5 stem cells in intestinal crypts. *Nature*. 2011;469(7330):415-418. doi:10.1038/nature09637

75. Cheng H, Leblond CP. Origin, differentiation and renewal of the four main epithelial cell types in the mouse small intestine I. Columnar cell. *Am J Anat*. 1974;141(4):461-479.

76. Fre S, Huyghe M, Mourikis P, Robine S, Louvard D, Artavanis-Tsakonas S. Notch signals control the fate of immature progenitor cells in the intestine. *Nature*. 2005;435(7044):964-968. doi:10.1038/nature03589

77. Demitrack ES, Samuelson LC. Notch regulation of gastrointestinal stem cells. *J Physiol*. 2016;594(17):4791-4803. doi:10.1113/JP271667

78. von Moltke J, Ji M, Liang HE, Locksley RM. Tuft-cell-derived IL-25 regulates an intestinal ILC2-epithelial response circuit. *Nature*. 2016;529(7585):221-225. doi:10.1038/nature16161

79. Gerbe F, Sidot E, Smyth DJ, et al. Intestinal epithelial tuft cells initiate type 2 mucosal immunity to helminth parasites. *Nature*. 2016;529(7585):226-230. doi:10.1038/nature16527

80. Herring CA, Banerjee A, McKinley ET, et al. Unsupervised Trajectory Analysis of Single-Cell RNA-Seq and Imaging Data Reveals Alternative Tuft Cell Origins in the Gut. *Cell Syst*. 2018;6(1):37-51 e9. doi:10.1016/j.cels.2017.10.012

81. Gerbe F, van Es JH, Makrini L, et al. Distinct ATOH1 and Neurog3 requirements define tuft cells as a new secretory cell type in the intestinal epithelium. *J Cell Biol*. 2011;192(5):767-780. doi:10.1083/jcb.201010127

82. Drummond CG, Bolock AM, Ma C, Luke CJ, Good M, Coyne CB. Enteroviruses infect human

enteroids and induce antiviral signaling in a cell lineage-specific manner. *Proc Natl Acad Sci U S A*. 2017;114(7):1672-1677. doi:10.1073/pnas.1617363114

83. Johnson K, Yin J, In JG, et al. Cholinergic-induced anion secretion in murine jejunal enteroids involves synergy between muscarinic and nicotinic pathways. *Am J Physiol Physiol*. 2020:321-330. doi:10.1152/ajpcell.00179.2020

84. Eglen RM. Muscarinic receptor subtypes in neuronal and non-neuronal cholinergic function. *Aut Autacoid Pharmacol*. 2006;26(3):219-233. doi:10.1111/j.1474-8673.2006.00368.x

85. Harrington AM, Peck CJ, Liu L, Burcher E, Hutson JM, Southwell BR. Localization of muscarinic receptors M1R, M2R and M3R in the human colon. *Neurogastroenterol Motil*. 2010;22(9):999-1008, e262-3. doi:10.1111/j.1365-2982.2009.01456.x

86. Kow RL, Nathanson NM. Muscarinic receptors become crystal clear Evolution after tumour spread. *Nature*. 2012;482:480-481.

87. Nathanson NM. Synthesis, trafficking, and localization of muscarinic acetylcholine receptors. *Pharmacol Ther*. 2008;119(1):33-43. doi:10.1016/j.pharmthera.2008.04.006

88. Goin JC, Nathanson NM. Subtype-specific regulation of the expression and function of muscarinic acetylcholine receptors in embryonic chicken retinal cells. *J Neurochem*. 2002;83(4):964-972. doi:10.1046/j.1471-4159.2002.01209.x

89. Nathanson NM. A multiplicity of muscarinic mechanisms: Enough signaling pathways to take your breath away. *Proc Natl Acad Sci U S A*. 2000;97(12):6245-6247. doi:10.1073/pnas.97.12.6245

90. Nathanson NM. Synthesis, trafficking, and localization of muscarinic acetylcholine receptors. *Pharmacol Ther*. 2008;119(1):33-43. doi:10.1016/j.pharmthera.2008.04.006

91. Fucile S. Ca2+ permeability of nicotinic acetylcholine receptors. *Cell Calcium*. 2004;35(1):1-8. doi:10.1016/j.ceca.2003.08.006

92. Ragozzino D, Fucile S, Giovannelli A, et al. Functional properties of neuronal nicotinic acetylcholine receptor channels expressed in transfected human cells. *Eur J Neurosci*.

1997;9(3):480-488. doi:10.1111/j.1460-9568.1997.tb01625.x

93. Fucile S. The distribution of charged amino acid residues and the Ca2+ permeability of nicotinic acetylcholine receptors: A predictive model. *Front Mol Neurosci*. 2017;10(May):1-10. doi:10.3389/fnmol.2017.00155

94. Lax P, Fucile S, Eusebi F. Ca2+ permeability of human heteromeric nAChRs expressed by transfection in human cells. *Cell Calcium*. 2002;32(2):53-58. doi:10.1016/S0143-4160(02)00076-3

95. Ragozzino D, Barabino B, Fucile S, Eusebi F. Ca2+ permeability of mouse and chick nicotinic acetylcholine receptors expressed in transiently transfected human cells. *J Physiol*. 1998;507(3):749-758. doi:10.1111/j.1469-7793.1998.749bs.x

96. Takahashi T, Shiraishi A, Murata J. The Coordinated Activities of nAChR and Wnt Signaling Regulate Intestinal Stem Cell Function in Mice. *Int J Mol Sci*. 2018;19(3). doi:10.3390/ijms19030738

97. Haber AL, Biton M, Rogel N, et al. A single-cell survey of the small intestinal epithelium. *Nature*. 2017;551(7680):333-339. doi:10.1038/nature24489

98. Neal KB, Bornstein JC. Mapping 5-HT inputs to enteric neurons of the guinea-pig small intestine. *Neuroscience*. 2007;145(2):556-567. doi:10.1016/j.neuroscience.2006.12.017

99. Takahashi T, Ohnishi H, Sugiura Y, et al. Non-neuronal acetylcholine as an endogenous regulator of proliferation and differentiation of Lgr5-positive stem cells in mice. *FEBS J*. 2014;281(20):4672-4690. doi:10.1111/febs.12974

100. Bader S, Diener M. Novel aspects of cholinergic regulation of colonic ion transport. *Pharmacol Res Perspect*. 2015;3(3):1-14. doi:10.1002/prp2.139

101. Bader S, Lottig L, Diener M. Stimulation of Na(+) -K(+) -pump currents by epithelial nicotinic receptors in rat colon. *Br J Pharmacol*. 2017;174(9):880-892. doi:10.1111/bph.13761

102. Summers AE, Whelan CJ, Parsons ME. Nicotinic acetylcholine receptor subunits and receptor activity in the epithelial cell line HT29. *Life Sci*. 2003;72(18-19):2091-2094. doi:10.1016/s0024-3205(03)00089-4

103. Qian J, Mummalaneni SK, Alkahtani RM, et al. Nicotine-induced effects on nicotinic acetylcholine receptors (nAChRs), Ca2+ and Brain-Derived Neurotrophic Factor (BDNF) in STC-1 cells. *PLoS One*. 2016;11(11):1-24. doi:10.1371/journal.pone.0166565

104. Hollenhorst MI, Lips KS, Kummer W, Fronius M. Nicotine-induced activation of soluble adenylyl cyclase participates in ion transport regulation in mouse tracheal epithelium. *Life Sci*. 2012;91(21-22):1009-1012. doi:10.1016/j.lfs.2012.06.027

105. Kurzen H, Berger H, Jäger C, et al. Phenotypical and molecular profiling of the extraneuronal cholinergic system of the skin. *J Invest Dermatol*. 2004;123(5):937-949. doi:10.1111/j.0022-202X.2004.23425.x

106. Albuquerque EX, Pereira EFR, Alkondon M, Rogers SW. Mammalian nicotinic acetylcholine receptors: From structure to function. *Physiol Rev*. 2009;89(1):73-120. doi:10.1152/physrev.00015.2008

107. Calandrella SO, Barrett KE, Keely SJ. Transactivation of the epidermal growth factor receptor mediates muscarinic stimulation of focal adhesion kinase in intestinal epithelial cells. *J Cell Physiol*. 2005;203(1):103-110. doi:10.1002/jcp.20190

108. Mroz MS, Keating N, Ward JB, et al. Farnesoid X receptor agonists attenuate colonic epithelial secretory function and prevent experimental diarrhoea in vivo. *Gut*. 2014;63(5):808-817. doi:10.1136/gutjnl-2013-305088

109. Keely SJ, Uribe JM, Barrett KE. Carbachol stimulates transactivation of epidermal growth factor receptor and mitogen-activated protein kinase in T84 cells: Implications for carbachol-stimulated chloride secretion. *J Biol Chem*. 1998;273(42):27111-27117. doi:10.1074/jbc.273.42.27111

110. Bader S, Lottig L, Diener M. Stimulation of Na+-K+-pump currents by epithelial nicotinic receptors in rat colon. *Br J Pharmacol*. 2017;174(9):880-892. doi:10.1111/bph.13761

111. Hartzell C, Putzier I, Arreola J. Calcium-activated chloride channels. *Annu Rev Physiol*. 2005;67:719-758. doi:10.1146/annurev.physiol.67.032003.154341

112. Pedemonte N, Galietta LJV. Structure and function of tmem16 proteins (anoctamins). *Physiol Rev*.

2014;94(2):419-459. doi:10.1152/physrev.00039.2011

113. Benedetto R, Ousingsawat J, Wanitchakool P, et al. Epithelial Chloride Transport by CFTR Requires TMEM16A. *Sci Rep*. 2017;7(1):1-13. doi:10.1038/s41598-017-10910-0

114. Benedetto R, Ousingsawat J, Cabrita I, et al. Plasma membrane–localized TMEM16 proteins are indispensable for expression of CFTR. *J Mol Med*. 2019:711-722. doi:10.1007/s00109-019-01770-4

115. Lee B, Hong GS, Lee SH, et al. Anoctamin 1/TMEM16A controls intestinal Cl− secretion induced by carbachol and cholera toxin. *Exp Mol Med*. 2019;51(8). doi:10.1038/s12276-019-0287-2

116. Suzuki J, Umeda M, Sims PJ, Nagata S. Calcium-dependent phospholipid scrambling by TMEM16F. *Nature*. 2010;468(7325):834-840. doi:10.1038/nature09583

117. Lhermusier T, Chap H, Payrastre B. Platelet membrane phospholipid asymmetry: From the characterization of a scramblase activity to the identification of an essential protein mutated in Scott syndrome. *J Thromb Haemost*. 2011;9(10):1883-1891. doi:10.1111/j.1538-7836.2011.04478.x

118. Kmit A, Van Kruchten R, Ousingsawat J, et al. Calcium-activated and apoptotic phospholipid scrambling induced by Ano6 can occur independently of Ano6 ion currents. *Cell Death Dis*. 2013;4(4):1-8. doi:10.1038/cddis.2013.135

119. Alvadia C, Lim NK, Mosina VC, Oostergetel GT, Dutzler R, Paulino C. Cryo-EM structures and functional characterization of the murine lipid scramblase TMEM16F. *Elife*. 2019;8:1-28. doi:10.7554/eLife.44365

120. Kunzelmann K, Nilius B, Owsianik G, et al. Molecular functions of anoctamin 6 (TMEM16F): A chloride channel, cation channel, or phospholipid scramblase? *Pflugers Arch Eur J Physiol*. 2014;466(3):407-414. doi:10.1007/s00424-013-1305-1

121. Ye W, Han TW, He M, Jan YN, Jan LY. Dynamic Change of Electrostatic Field in TMEM16F Permeation Pathway Shifts Its Ion Selectivity. *bioRxiv*. 2019:1-21. doi:10.1101/515569

122. Concepcion AR, Feske S. Regulation of epithelial ion transport in exocrine glands by store-

operated Ca2+ entry. *Cell Calcium*. 2017;63:53-59. doi:10.1016/j.ceca.2016.12.004

123. Concepcion AR, Yule DI, Feske S, et al. Store-operated Ca2+ entry regulates Ca2+-activated chloride channels and eccrine sweat gland function. 2016;126(11):4303-4318. doi:10.1172/JCI89056.Introduction

124. Cooper DMF. Store-operated Ca 2 + -entry and adenylyl cyclase. 2015;58:368-375.

125. Willoughby D, Everett KL, Halls ML, et al. Direct binding between Orai1 and AC8 mediates dynamic interplay between Ca 2+and cAMP signaling. *Sci Signal*. 2012;5(219):1-12. doi:10.1126/scisignal.2002299

126. Martin ACL, Willoughby D, Ciruela A, et al. Capacitative Ca2+ entry via Orai1 and Stromal Interacting Molecule 1 (STIM1) regulates adenylyl cyclase type 8 (Molecular Pharmacology (2009) 75, (830-842)). *Mol Pharmacol*. 2009;75(5):1248. doi:10.1124/mol.75.5.1248

127. Willoughby D, Wachten S, Masada N, Cooper DMF. Direct demonstration of discrete Ca2+ microdomains associated with different isoforms of adenylyl cyclase. *J Cell Sci*. 2010;123(1):107-117. doi:10.1242/jcs.062067

128. Cooper DMF, Tabbasum VG. Adenylate cyclase-centred microdomains. *Biochem J*. 2014;462(2):199-213. doi:10.1042/BJ20140560

129. Halls ML, Cooper DMF. Regulation by Ca2+-signaling pathways of adenylyl cyclases. *Cold Spring Harb Perspect Biol*. 2011;3(1):1-22. doi:10.1101/cshperspect.a004143

130. Willoughby D, Cooper DMF. Organization and Ca2+ regulation of adenylyl cyclases in cAMP microdomains. *Physiol Rev*. 2007;87(3):965-1010. doi:10.1152/physrev.00049.2006

131. Willoughby D, Cooper DMF. Ca2+ stimulation of adenylyl cyclase generates dynamic oscillations in cyclic AMP. *J Cell Sci*. 2006;119(5):828-836. doi:10.1242/jcs.02812

132. Cooper DMF. Regulation and organization of adenylyl cyclases and cAMP. *Biochem J*. 2003;375(3):517-529. doi:10.1042/BJ20031061

133. Fenton RA, Murali SK, Kaji I, et al. Adenylyl Cyclase 6 Expression Is Essential for Cholera Toxin-Induced Diarrhea. *J Infect Dis*. 2019;220(11):1719-1728. doi:10.1093/infdis/jiz013

134. Thomas A, Ramananda Y, Mun KS, Naren AP, Arora K. AC6 is the major adenylate cyclase forming a diarrheagenic protein complex with cystic fibrosis transmembrane conductance regulator in cholera. *J Biol Chem*. 2018;293(33):12949-12959. doi:10.1074/jbc.RA118.003378

135. Dehaven WI, Jones BF, Petranka JG, et al. TRPC channels function independently of STIM1 and Orai1. *J Physiol*. 2009;587(10):2275-2298. doi:10.1113/jphysiol.2009.170431

136. Feske S, Gwack Y, Prakriya M, et al. A mutation in Orai1 causes immune deficiency by abrogating CRAC channel function. *Nature*. 2006;441(7090):179-185. doi:10.1038/nature04702

137. Hogan PG, Rao A. Store-operated calcium entry: Mechanisms and modulation. *Biochem Biophys Res Commun*. 2015;460(1):40-49. doi:10.1016/j.bbrc.2015.02.110

138. Liou J, Kim ML, Won DH, et al. STIM is a Ca2+ sensor essential for Ca2+-store- depletion-triggered Ca2+ influx. *Curr Biol*. 2005;15(13):1235-1241. doi:10.1016/j.cub.2005.05.055

139. Putney JW. A model for receptor-regulated calcium entry. *Cell Calcium*. 1986;7(1):1-12. doi:10.1016/0143-4160(86)90026-6

140. Putney JW. Origins of the concept of store-operated calcium entry. *Front Biosci*. 2011;S3(1):980. doi:10.2741/202

141. Zhang SL, Yeromin A V., Zhang XHF, et al. Genome-wide RNAi screen of Ca2+ influx identifies genes that regulate Ca2+ release-activated Ca2+ channel activity. *Proc Natl Acad Sci U S A*. 2006;103(24):9357-9362. doi:10.1073/pnas.0603161103

142. Vig M, Peinelt C, Beck A, et al. CRACM1 is a plasma membrane protein essential for store-operated Ca2+ entry. *Science*. 2006;312(5777):1220-1223. doi:10.1126/science.1127883

143. Yang X, Wen G, Tuo B, et al. Molecular mechanisms of calcium signaling in the modulation of small intestinal ion transports and bicarbonate secretion. *Oncotarget*. 2018;9(3):3727-3740. doi:10.18632/oncotarget.23197

144. Basalingappa KM, Rajendran VM, Wonderlin WF. Characteristics of Kcnn4 channels in the apical membranes of an intestinal epithelial cell line. *Am J Physiol - Gastrointest Liver Physiol*. 2011;301(5):905-911. doi:10.1152/ajpgi.00558.2010

145. Perry MD, Rajendran VM, MacLennan KA, Sandle GI. Segmental differences in upregulated apical potassium channels in Mammalian colon during potassium adaptation. *Am J Physiol - Gastrointest Liver Physiol*. 2016;311(5):G785-G793. doi:10.1152/ajpgi.00181.2015

146. Lérias J, Pinto M, Benedetto R, et al. Compartmentalized crosstalk of CFTR and TMEM16A (ANO1) through EPAC1 and ADCY1. *Cell Signal*. 2018;44(November 2017):10-19. doi:10.1016/j.cellsig.2018.01.008

147. Fucile S, Renzi M, Lax P, Eusebi F. Fractional Ca2+ current through human neuronal α7 nicotinic acetylcholine receptors. *Cell Calcium*. 2003;34(2):205-209. doi:10.1016/S0143-4160(03)00071-X

148. Lottig L, Bader S, Jimenez M, Diener M. Evidence for metabotropic function of epithelial nicotinic cholinergic receptors in rat colon. *Br J Pharmacol*. 2019;176(9):1328-1340. doi:10.1111/bph.14638

149. Kumar P, Scholze P, Fronius M, Krasteva-Christ G, Hollenhorst MI. Nicotine stimulates ion transport via metabotropic β4 subunit containing nicotinic ACh receptors. *Br J Pharmacol*. 2020;177(24):5595-5608. doi:10.1111/bph.15270

150. King JR, Kabbani N. Alpha 7 nicotinic receptor coupling to heterotrimeric G proteins modulates RhoA activation, cytoskeletal motility, and structural growth. *J Neurochem*. 2016:532-545. doi:10.1111/jnc.13660

151. Kabbani N, Nichols RA. Beyond the Channel: Metabotropic Signaling by Nicotinic Receptors. *Trends Pharmacol Sci*. 2018;39(4):354-366. doi:10.1016/j.tips.2018.01.002

152. King JR, Ullah A, Bak E, Saleet Jafri M, Kabbani N. Ionotropic and metabotropic mechanisms of allosteric modulation of A7 nicotinic receptor intracellular calcium S. *Mol Pharmacol*. 2018;93(6):601-611. doi:10.1124/mol.117.111401

153. Lefkimmiatis K, Srikanthan M, Maiellaro I, Moyer MP, Curci S, Hofer AM. Store-operated cyclic AMP signalling mediated by STIM1. *Nat Cell Biol*. 2009;11(4):433-442. doi:10.1038/ncb1850

154. Tabbasum VG, Cooper DMF. Structural and Functional Determinants of AC8 Trafficking, Targeting and Responsiveness in Lipid Raft Microdomains. *J Membr Biol*. 2019;252(2-3):159-

172. doi:10.1007/s00232-019-00060-x

155. Ambudkar IS. Ca2+ signaling and regulation of fluid secretion in salivary gland acinar cells. *Cell Calcium*. 2014;55(6):297-305. doi:10.1016/j.ceca.2014.02.009

156. Ambudkar IS. Calcium signalling in salivary gland physiology and dysfunction. *J Physiol*. 2016;594(11):2813-2824. doi:10.1113/JP271143

157. Ambudkar I. Calcium signaling defects underlying salivary gland dysfunction. *Biochim Biophys Acta - Mol Cell Res*. 2018;1865(11):1771-1777. doi:10.1016/j.bbamcr.2018.07.002

158. Fung C, Koussoulas K, Unterweger P, Allen AM, Bornstein JC, Foong JPP. Cholinergic Submucosal Neurons Display Increased Excitability Following in Vivo Cholera Toxin Exposure in Mouse Ileum. *Front Physiol*. 2018;9:260. doi:10.3389/fphys.2018.00260

159. Balasuriya GK, Hill-Yardin EL, Gershon MD, Bornstein JC. A sexually dimorphic effect of cholera toxin: rapid changes in colonic motility mediated via a 5-HT3 receptor-dependent pathway in female C57Bl/6 mice. *J Physiol*. 2016;594(15):4325-4338. doi:10.1113/JP272071

160. Kordasti S, Sapnara M, Thomas EA, et al. Effects of cholera toxin on the potential difference and motor responses induced by distension in the rat proximal small intestine in vivo. *Am J Physiol - Gastrointest Liver Physiol*. 2006;290(5):G948-G958. doi:10.1152/ajpgi.00267.2005

161. Cassuto J, Siewert A, Jodal M, Lundgren O. The involvement of intramural nerves in cholera toxin induced intestinal secretion. *Acta Physiol Scand*. 1983;117(2):195-202. doi:10.1111/j.1748-1716.1983.tb07197.x

162. Cassuto J, Jodal M, Lundgren O. The effect of nicotinic and muscarinic receptor blockade on cholera toxin induced intestinal secretion in rats and cats. *Acta Physiol Scand*. 1982;114(4):573-577. doi:10.1111/j.1748-1716.1982.tb07026.x

163. Jodal M, Lundgren O. Nerves and cholera secretion. *Gastroenterology*. 1995;108(1):287-288. https://www.ncbi.nlm.nih.gov/pubmed/7806052.

164. Fung C, Ellis M, Bornstein JC. Luminal cholera toxin alters motility in isolated guinea-pig jejunum via a pathway independent of 5-HT3. *Front Neurosci*. 2010;4(SEP).

doi:10.3389/fnins.2010.0016210.1007/s10620-010-1164-y; Lundgren, O., Jodal, M., The enteric nervous system and cholera toxin-induced secretion (1997) Comp. Biochem. Physiol. A Physiol., 118, pp. 319-327; Mathias, J.R., Carlson, G.M., Bertiger, G., Martin, J.-L., Cohen, S., Migrating action potential complex of cholera: a possible prostaglandin-induced response (1977) Am. J. Physiol., 232, pp. G529-G534; Mathias, J.R., Nogueira, J., Martin, J.L., Carlson, G.M., Giannella, R.A., Escherichia coli heat

165. Sjoqvist A, Cassuto J, Jodal M, Lundgren O. Actions of serotonin antagonists on cholera-toxin-induced intestinal fluid secretion. *Acta Physiol Scand*. 1992;145(3):229-237. doi:10.1111/j.1748-1716.1992.tb09360.x

166. Jonsdottir IH, Sjoqvist A, Lundgren O, Thoren P. Somatic nerve stimulation and cholera-induced net fluid secretion in the small intestine of the rat: evidence for an opioid effect. *J Aut Nerv Syst*. 1999;78(1):18-23. https://www.ncbi.nlm.nih.gov/pubmed/10589819.

167. Lundgren O, Jodal M. The enteric nervous system and cholera toxin-induced secretion. *Comp Biochem Physiol - A Physiol*. 1997;118(2):319-327. doi:10.1016/S0300-9629(96)00312-X

168. Cedgard S, Hallback DA, Jodal M, Lundgren O, Redfors S. The effects of cholera toxin on intramural blood flow distribution and capillary hydraulic conductivity in the cat small intestine. *Acta Physiol Scand*. 1978;102(2):148-158. doi:10.1111/j.1748-1716.1978.tb06058.x

169. Nilsson O, Cassuto J, Larsson PA, et al. 5-Hydroxytryptamine and cholera secretion: A histochemical and physiological study in cats. *Gut*. 1983;24(6):542-548. doi:10.1136/gut.24.6.542

170. Camilleri M, Di Lorenzo C. Brain-gut axis: from basic understanding to treatment of IBS and related disorders. *J Pediatr Gastroenterol Nutr*. 2012;54(4):446-453. doi:10.1097/MPG.0b013e31823d34c3

171. Chambers JD, Bornstein JC, Sjövall H, Thomas EA. Recurrent networks of submucous neurons controlling intestinal secretion: A modeling study. *Am J Physiol - Gastrointest Liver Physiol*. 2005;288(5 51-5):G887-G896. doi:10.1152/ajpgi.00491.2004

172. Burns AJ, Roberts RR, Bornstein JC, Young HM. Development of the enteric nervous system and

its role in intestinal motility during fetal and early postnatal stages. *Semin Pediatr Surg*. 2009;18(4):196-205. doi:10.1053/j.sempedsurg.2009.07.001

173. Bornstein JC, Gwynne RM, Sjövall H. Enteric Neural Regulation of Mucosal Secretion. In: *Physiology of the Gastrointestinal Tract*. Vol 1. Elsevier Inc.; 2012:769-790. doi:10.1016/B978-0-12-382026-6.00027-0

174. Keast JR, Furness JB, Costa M. Investigations of Nerve Populations Influencing Ion-Transport That Can Be Stimulated Electrically, by Serotonin and by a Nicotinic Agonist. *Naunyn-Schmiedebergs Arch Pharmacol*. 1985;331(2-3):260-266. doi:Doi 10.1007/Bf00634247

175. Lundgren O, Peregrin AT, Persson K, Kordasti S, Uhnoo I, Svensson L. Role of the enteric nervous system in the fluid and electrolyte secretion of rotavirus diarrhea. *Science (80- )*. 2000;287(5452):491-495. doi:10.1126/science.287.5452.491

176. Mahe MM, Aihara E, Schumacher MA, et al. Establishment of Gastrointestinal Epithelial Organoids. *Curr Protoc Mouse Biol*. 2013;3(4):217-240. doi:10.1002/9780470942390.mo130179

177. Stamp LA, Gwynne RM, Foong JPP, et al. Optogenetic Demonstration of Functional Innervation of Mouse Colon by Neurons Derived From Transplanted Neural Cells. *Gastroenterology*. 2017;152(6):1407-1418. doi:10.1053/j.gastro.2017.01.005

178. Workman MJ, Mahe MM, Trisno S, et al. Engineered human pluripotent-stem-cell-derived intestinal tissues with a functional enteric nervous system. *Nat Med*. 2017;23(1):49-59. doi:10.1038/nm.4233

179. Toumi F, Neunlist M, Cassagnau E, et al. Human submucosal neurones regulate intestinal epithelial cell proliferation: Evidence from a novel co-culture model. *Neurogastroenterol Motil*. 2003;15(3):239-242. doi:10.1046/j.1365-2982.2003.00409.x

180. Schlieve CR, Fowler KL, Thornton M, et al. Neural Crest Cell Implantation Restores Enteric Nervous System Function and Alters the Gastrointestinal Transcriptome in Human Tissue-Engineered Small Intestine. *Stem Cell Reports*. 2017;9(3):883-896. doi:10.1016/j.stemcr.2017.07.017

181. Schlieve CR, Grikscheit TC. Created of Warm Blood and Nerves: Restoring an Enteric Nervous System in Organoids. *Cell Stem Cell*. 2017;20(1):5-7. doi:10.1016/j.stem.2016.12.012

182. Pochard C, Coquenlorge S, Jaulin J, et al. Defects in 15-HETE Production and Control of Epithelial Permeability by Human Enteric Glial Cells From Patients With Crohn's Disease. *Gastroenterology*. 2016;150(1):168-180. doi:10.1053/j.gastro.2015.09.038

183. Rao M, Rastelli D, Dong L, et al. Enteric Glia Regulate Gastrointestinal Motility but Are Not Required for Maintenance of the Epithelium in Mice. *Gastroenterology*. 2017;153(4):1068-1081 e7. doi:10.1053/j.gastro.2017.07.002

184. Kretzschmar K, Clevers H. Organoids: Modeling Development and the Stem Cell Niche in a Dish. *Dev Cell*. 2016;38(6):590-600. doi:10.1016/j.devcel.2016.08.014

185. Hao MM, Lomax AE, McKeown SJ, Reid CA, Young HM, Bornstein JC. Early development of electrical excitability in the mouse enteric nervous system. *J Neurosci*. 2012;32(32):10949-10960. doi:10.1523/JNEUROSCI.1426-12.2012

186. Foong JP, Parry LJ, Bornstein JC. Activation of neuronal SST(1) and SST(2) receptors decreases neurogenic secretion in the guinea-pig jejunum. *Neurogastroenterol Motil*. 2010;22(11):1209-1216, e317. doi:10.1111/j.1365-2982.2010.01566.x

187. Phillips TE, Phillips TH, Neutra MR. Regulation of intestinal goblet cell secretion. IV. Electrical field stimulation in vitro. *Am J Physiol*. 1984;247(6 Pt 1):G682-7. doi:10.1152/ajpgi.1984.247.6.G682

188. Bornstein JC, Furness JB. Correlated Electrophysiological and Histochemical-Studies of Submucous Neurons and Their Contribution to Understanding Enteric Neural Circuits. *J Auton Nerv Syst*. 1988;25(1):1-13. doi:Doi 10.1016/0165-1838(88)90002-1

189. Tixier E, Galmiche JP, Neunlist M. Intestinal neuro-epithelial interactions modulate neuronal chemokines production. *Biochem Biophys Res Commun*. 2006;344(2):554-561. doi:10.1016/j.bbrc.2006.03.159

190. Neunlist M, Toumi F, Oreschkova T, et al. Human ENS regulates the intestinal epithelial barrier

permeability and a tight junction-associated protein ZO-1 via VIPergic pathways. *Am J Physiol - Gastrointest Liver Physiol*. 2003;285(5 48-5):1028-1036. doi:10.1152/ajpgi.00066.2003

191. Van Landeghem L, Mahe MM, Teusan R, et al. Regulation of intestinal epithelial cells transcriptome by enteric glial cells: impact on intestinal epithelial barrier functions. *BMC Genomics*. 2009;10:507. doi:10.1186/1471-2164-10-507

192. Neunlist M, Aubert P, Bonnaud S, et al. Enteric glia inhibit intestinal epithelial cell proliferation partly through a TGF-β1-dependent pathway. *Am J Physiol - Gastrointest Liver Physiol*. 2007;292(1):231-241. doi:10.1152/ajpgi.00276.2005

193. Mongardi Fantaguzzi C, Thacker M, Chiocchetti R, Furness JB. Identification of neuron types in the submucosal ganglia of the mouse ileum. *Cell Tissue Res*. 2009;336(2):179-189. doi:10.1007/s00441-009-0773-2

194. Furness JB. Types of neurons in the enteric nervous system. *J Aut Nerv Syst*. 2000;81(1-3):87-96. https://www.ncbi.nlm.nih.gov/pubmed/10869706.

195. Kaji I, Kaunitz JD. Luminal chemosensing in the gastroduodenal mucosa. *Curr Opin Gastroenterol*. 2017;33(6):439-445. doi:10.1097/MOG.0000000000000396

196. Gerbe F, Legraverend C, Jay P. The intestinal epithelium tuft cells: specification and function. *Cell Mol Life Sci*. 2012;69(17):2907-2917. doi:10.1007/s00018-012-0984-7

197. Cheng X, Voss U, Ekblad E. Tuft cells: Distribution and connections with nerves and endocrine cells in mouse intestine. *Exp Cell Res*. 2018;369(1):105-111. doi:10.1016/j.yexcr.2018.05.011

198. Hoover B, Baena V, Kaelberer MM, Getaneh F, Chinchilla S, Bohorquez D V. The intestinal tuft cell nanostructure in 3D. *Sci Rep*. 2017;7(1):1652. doi:10.1038/s41598-017-01520-x

199. Howitt MR, Lavoie S, Michaud M, et al. Tuft cells, taste-chemosensory cells, orchestrate parasite type 2 immunity in the gut. *Science (80- )*. 2016;351(6279):1329-1333. doi:10.1126/science.aaf1648

200. Gronke K, Diefenbach A. Tuft cell-derived IL-25 activates and maintains ILC2. *Immunol Cell Biol*. 2016;94(3):221-223. doi:10.1038/icb.2016.10

201. Gerbe F, Jay P. Intestinal tuft cells: epithelial sentinels linking luminal cues to the immune system. *Mucosal Immunol*. 2016;9(6):1353-1359. doi:10.1038/mi.2016.68

202. Steele SP, Melchor SJ, Petri WA. Tuft Cells: New Players in Colitis. *Trends Mol Med*. 2016;22(11):921-924. doi:10.1016/j.molmed.2016.09.005

203. Porter AJ, Wattchow DA, Brookes SJ, Schemann M, Costa M. Choline acetyltransferase immunoreactivity in the human small and large intestine. *Gastroenterology*. 1996;111(2):401-408. https://www.ncbi.nlm.nih.gov/pubmed/8690205.

204. Schutz B, Jurastow I, Bader S, et al. Chemical coding and chemosensory properties of cholinergic brush cells in the mouse gastrointestinal and biliary tract. *Front Physiol*. 2015;6:87. doi:10.3389/fphys.2015.00087